DOCTORAATSPROEFSCHRIFT

2012 | Faculteit Wetenschappen

Development, modification and optimization of poly [1-(trimethylsilyl)-1-propyne] pervaporation membranes

Proefschrift voorgelegd tot het behalen van de graad van
Doctor in de Wetenschappen, Chemie, te verdedigen door:

Stan CLAES

Promotor: prof. dr. Marlies K. Van Bael
Copromotoren: dr. Roos Peeters
dr. Steven Mullens

D/2012/2451/1

universiteit hasselt

Members of the jury

Chairman of the jury

prof. dr. Jean Manca
Dean of the faculty of science, UHasselt

Promotor

prof. dr. Marlies K. Van Bael, UHasselt

Co-promotors

dr. Roos Peeters, XIOS Hogeschool Limburg
dr. Steven Mullens, VITO

Members of the jury

prof. dr. Frans H. J. Maurer, Lund University
prof. dr. Bart Van der Bruggen, KULeuven
prof. dr. Robert Carleer, UHasselt
dr. Alberto Figoli, ITM-CNR
dr. Heidi Van den Rul, Sirris

Acknowledgements

De afgelopen 4 jaar heb ik het geluk gehad vele hulpvaardige collega's en vrienden te ontmoeten die allen, al dan niet rechtstreeks, bijgedragen hebben tot het schrijven van deze thesis.

Als eerste wil ik graag mijn promotor prof. dr. Marlies Van Bael bedanken voor de leerrijke discussies en vergaderingen. Ook al zat ik als doctoraatstudent gestationeerd in de VITO te Mol en lag mijn onderwerp niet echt in jouw expertisedomein, toch hield jij een klare kijk op mijn onderzoek en hielp je actief mee bij het nalezen van publicaties, het vinden van geschikte analysetechnieken en daardoor het bewaken van de wetenschappelijke kwaliteit van dit werk.

De dagelijkse begeleiding viel dan weer op de schouders van mijn VITO begeleiders Lieven Gevers, Roger Leysen, Steven Mullens en Pieter Vandezande. Toen ik als groentje op VITO aankwam, Lieven, heb je mij op sleeptouw genomen en gedurende één jaar intensief gestuurd. Na je vertrek bij VITO, kwam Pieter Vandezande op het toneel. Pieter, jij had zelf net jouw doctoraat beëindigd en kreeg onmiddellijk de zware taak om mij te begeleiden. Maar je hebt dit uitstekend gedaan! Verder was er nog Roger Leysen, die als pater familias tot aan zijn pensioen een klare kijk had op het membraanonderzoek binnen VITO en waar ik altijd terecht kon met mijn vragen of problemen. In de voorbije 4 jaar was er één constante (of één iemand die het volgehouden heeft 4 jaar mijn begeleider te zijn), en dat was Steven Mullens. Jij kon als geen ander mij motiveren toch verder te gaan en net dat ietsje meer te doen dan normaal. Bedankt Steven, Pieter, Roger en Lieven voor jullie hulp!

Verder kon ik ook steeds beroep doen op mijn copromotor dr. Roos Peeters en bureaugenoot Kris voor het nalezen van de publicaties, posters en presentaties. Bedankt voor het ontcijferen van mijn teksten!

Naast de serieuze wetenschappelijke kennis die mij op VITO bijgebracht werd, is er in die 4 jaar ook veel afgelachen. Mijn eerste bureaugenoot Pieter Lens ontving me met open armen, en sloeg erin mij snel kennis te laten maken met het reilen en zeilen op VITO. Toen je onze onderzoeksgroep verliet, kwam Kris op jouw plaatsje zitten en nog later vervoegde Seppie onze rangen. Pieter, Kris en Seppie bedankt voor de leuke, ontspannende en leerrijke momenten op ons bureau!
Tijdens een doctoraat zit je natuurlijk ook veel in het labo, en daar kon ik dan weer rekenen op de kennis, vaardigheden en humor van Kenny, André, Bas, Raymond, Michel, Dirk, Willy, Myriam, Cédric, Jan, Gaby, Walter en Louis. Bedankt allemaal voor jullie hulp en de fijne momenten in het labo en koffielokaal!

Naast de collega's in Mol hebben ook andere slimme, aangename en hulpvaardige mensen mijn weg gekruist de afgelopen jaren.
First of all I would like to acknowledge prof. dr. Frans H. J. Maurer for the help with the PALS analysis, fruitful discussions and help with the publications. Together with Anna Andersson, you always helped me out if I had questions concerning PALS or other polymer related issues. I had a great time during my visits in Lund and really appreciated your hospitality! Tack så mycket!
Verder kon ik rekenen op de hulp van prof. dr. Robert Carleer, prof. dr. Peter Adriaensens, dr. Jan D'Haen, dr. Christopher De Dobbelaere en Alexander Riskin voor het uitvoeren van allerhande analyses en het interpreteren van data. Oprecht bedankt voor jullie samenwerking!
Ook wil ik alle collega doctoraatsstudenten van de onderzoeksgroep anorganische en fysische chemie bedanken voor de leuke kerstfeestjes en teambuildingdag. Al was ik zelden op de UHasselt aanwezig, toch kon ik indien nodig steeds op jullie hulp rekenen. Dikke merci allemaal!

De afgelopen 4 jaar was er op tijd en stond ook tijd voor ontspanning en daarvoor kon ik altijd terecht bij de 'homies', collega's van MaxHa! en muzikale vrienden van harmonie De Stoobanders. Iedereen bedankt!

Tot slot wil ik natuurlijk mijn ouders en familie bedanken voor de afgelopen jaren. Aangezien ik tijdens mijn doctoraat nog van de voordelen van hotel mama kon genieten, had ik extra tijd die ik goed kon gebruiken voor mijn onderzoek. Aangezien niet alles steeds rozengeur en maneschijn is tijdens een doctoraat, kwam ik ook wel eens zwijgzaam of nors thuis. Maar jullie konden als geen ander hiermee overweg en daarom enorm bedankt voor de steun de afgelopen 4 jaar! Nu ik als jongste van vier hotel mama weldra zal verlaten, wil ik jullie beiden ook nog bedanken voor de 26 jaren ten huize Salviastraat!

Verder wil ik ook mijn zussen, broer, schoonzus, schoonbroers en nichtjes bedanken voor de leuke momenten en het verdragen van mijn fratsen! Ciel & Dries, Wannes & Ellen, Tine & Filip, Griet, Nel en Fien bedankt en dat er nog veel mogen volgen!

Table of contents

Samenvatting

Dit doctoraatsonderzoek behandelt de ontwikkeling, modificatie en optimalisatie van poly[1-(trimethylsilyl)-1-propyne] (PTMSP) pervaporatie (PV) membranen. PV is een scheidingsproces dat gebruik maakt van een dens membraan dat als selectieve barrière dient voor de scheiding van vloeibare mengsels. PV wordt gezien als een energiezuinig alternatief voor conventionele distillatie in de scheiding van azeotropen, hittegevoelige producten of mengsels waarvan de kookpunten van de afzonderlijke componenten dicht bij elkaar liggen. In tegenstelling tot distillatie dient enkel de afgescheiden component verdampt te worden, waardoor het energieverbruik bij PV opmerkelijk lager ligt dan bij distillatie. De scheiding gebeurt voornamelijk op basis van affiniteit van de af te scheiden component voor het membraan en wordt geïnitieerd door middel van een partieel dampdrukverschil over het membraan.
Dehydratie van solventen met hydrofiele PV membranen is goed ontwikkeld en wordt reeds toegepast op industriële schaal. Voor het verwijderen van (vluchtige) organische componenten uit waterige mengsels door hydrofobe PV daarentegen, staan nog verschillende problemen grootschalige implementatie in de weg. Eén van deze problemen is de beperkte beschikbaarheid en prestatie van commerciële membranen. Dit onderzoek probeert deze leemte in te vullen door de ontwikkeling van een hoog doorlatend en selectief hydrofoob PV membraan.

Hierbij werd PTMSP als membraanvormend polymeer gekozen aangezien het een hydrofoob polymeer is dat gekend is omwille van zijn extreem hoog vrij volume en daarbij horende permeabiliteit in gasscheiding. In de literatuur werd al vaak gebruik gemaakt van PTMSP voor de ontwikkeling van hydrofobe PV membranen, maar de flux of permeabiliteit van deze dikke, dense membranen (30 – 200 µm) is relatief laag. Om het implementeren van deze PTMSP membranen in industriële processen mogelijk te maken, dient de permeabiliteit

verhoogd te worden zonder drastisch te moeten inboeten op de solvent/water selectiviteit.

Een eerste route die gevolgd werd voor het verhogen van de permeabiliteit is het inbrengen van silicadeeltjes die de pakking van de polymeerketens verstoren en daardoor het vrije volume vergroten. Eerder onderzoek wees uit dat hydrofobe silica erg geschikt is voor het vergroten van het vrije volume van PTMSP en dus leidt tot een verhoging van de permeabiliteit in gasscheiding. Dit doctoraatswerk toonde aan dat door inbouw van silica in een dens PTMSP membraan (~100 µm), de permeabiliteit tot 72 % verhoogd kan worden in de PV scheiding van een ethanol/water mengsel, met behoud van de selectiviteit.

In een tweede stap werd getracht het PTMSP membraan te verdunnen en aan te brengen op een poreuze drager. Deze poreuze drager geeft de dunne filmen extra mechanische stabiliteit en maakt het gebruik ervan in modules eenvoudiger. De permeabiliteit kan 25 keer verhoogd worden door het verdunnen van de membranen van 85 µm naar 1.5 µm. Deze stijging in permeabiliteit gaat echter gepaard met een verlaging van selectiviteit (van 24 naar 15). Maar deze lagere selectiviteit is nog steeds 2 keer hoger dan die van de commercieel beschikbare polydimethylsiloxaan (PDMS) membranen.

Hierna werd onderzocht wat het effect is van het verdunnen van de membranen in combinatie met het toevoegen van hydrofobe silica op de PV prestaties. Het verdunnen van de membranen en toevoegen van silica resulteert in een grote toename van de permeabiliteit (36 keer) en een daling van de selectiviteit ten opzichte van de ongevulde systemen (15 naar 13). Deze daling van de selectiviteit was het grootste voor de membranen met de hoogste silicabelading. Een te hoge silicabelading in deze dunne membranen zorgt voor een hogere kans op defecten en dus een bijhorende lagere selectiviteit.

Het onderzoek naar het verdunnen van de laagdikte en het inbrengen van silica resulteerde in membranen met een flux tussen 0.16 en 11.11 kg m^{-2} h^{-1} en ethanol/water scheidingsfactor tussen 12 en 24. Uitgaande van de PV scheidingsindex werd er een optimale flux/selectiviteit combinatie gevonden voor een membraan van 2.4 µm dik en gevuld met 25 gew.% silica. De permeabiliteit en selectiviteit van dit membraan lagen respectievelijk 7 en 5 keer hoger dan deze van het beste commerciële PDMS membraan.

Als alternatief voor het toevoegen van hydrofobe silica, werd een nabehandeling met superkritisch CO_2 ($skCO_2$) onderzocht. Van CO_2 is geweten dat het kan optreden als solvent voor verschillende polymeren, inclusief PTMSP. De invloed van een $skCO_2$ nabehandeling op het vrije volume en de PV prestaties werd onderzocht voor dense PTMSP membranen. Door het behandelen van PTMSP onder hoge druk en temperatuur kon het vrije volume drastisch verhoogd worden. Dit verhoogd vrije volume was bovendien reproduceerbaar, voldoende thermisch stabiel en had een geschatte relaxatietijd van 30 jaar. De toename in het vrije volume resulteerde bovendien in een stijging van de permeabiliteit en selectiviteit in de PV scheiding van een ethanol/water mengsel. Zo kon de permeabiliteit tot 76 % verhoogd worden, wat vergelijkbaar is met de permeabiliteitsverhoging bij toevoeging van de hoogste concentraties silica. Daarenboven werd een lichte toename in selectiviteit na de $skCO_2$ behandeling vastgesteld. Al deze eigenschappen samen maken de $skCO_2$ behandeling een beloftevol alternatief voor het toevoegen van hydrofobe silica. De combinatie van toevoeging van silicadeeltjes en vervolgens een $skCO_2$ behandeling op dit silica gevulde membraan gaf eveneens aanleiding tot een verbeterde membraanprestatie (permeabiliteitsstijging tot 23 % ten opzichte van onbehandeld membraan).

De relatief zwakke solventstabiliteit van PTMSP beperkt de toepasbaarheid van de membranen tot alcohol/water en andere minder agressieve solvent/water scheidingen. Door de PTMSP membranen met een bis(azide) te crosslinken kan de solventresistentie significant verbeterd worden, waardoor ze niet meer oplossen in bijvoorbeeld tolueen, een goed solvent voor PTMSP. In dit doctoraatsonderzoek werden twee verschillende crosslinkprocedures onderzocht, namelijk fotochemische crosslinking en thermische crosslinking. PTMSP membranen met verschillende bis(azide) concentraties werden op beide manieren gecrosslinkt en onderzocht met behulp van infrarood spectroscopie, ^{1}H-NMR relaxometrie, positron annihilatie levensduur spectroscopie, zwellingsmetingen en PV testen. De fotochemisch behandelde PTMSP membranen waren onvoldoende gecrosslinkt en ongewenste bijproducten werden gevormd, waardoor deze membranen ongeschikt zijn voor de scheiding

van agressieve mengsels. De thermisch behandelde PTMSP membranen waren wel voldoende gecrosslinkt en stabiel in verschillende agressieve solventen, zoals heptaan, tetrahydrufuraan (THF), methyl-*tert*-butyl ether en dichloormethaan. Hoewel de thermisch behandelde membranen duidelijk minder presteerden in de scheiding van een standaard ethanol/water mengsel, werden veelbelovende resultaten behaald in de scheiding van een agressiever THF/water mengsel. Zonder crosslinking is het gebruik van PTMSP membranen op een THF/water mengsel niet mogelijk. In vergelijking met twee commerciële PDMS membranen werd voor dit mengsel een vier keer hogere specific permeation rate met een vergelijkbare selectiviteit bekomen voor deze gecrosslinkte PTMSP membranen. Door de toegenomen solventstabiliteit kunnen deze gecrosslinkte PTMSP membranen nu in een breder gamma van processtromen ingezet worden.

Summary

The presented research handles the development, modification and optimisation of poly[1-(trimethylsilyl)-1-propyne] (PTMSP) pervaporation (PV) membranes. PV is a membrane-based separation process, which is seen as valuable alternative to conventional distillation for the separation of close-boiling point mixtures, azeotropes and heat-sensitive products. In contrast to distillation, only the minor component consumes the latent heat of evaporation, making PV an energy-friendly alternative. The separation in PV occurs by the selective interaction of the target component with the dense, non-porous membrane and is initiated by creating a partial vapour pressure gradient across the membrane which is practically achieved by applying a vacuum or sweep gas at the permeate side.

The dehydration of solvents by hydrophilic PV is a widely accepted technique and is readily available on industrial scale. For hydrophobic PV on the other hand, several issues hamper the large scale implementation thereof for the removal of volatile organic components from aqueous streams. One of the major issues is the limited availability of highly permeable and selective membranes, which was the motivation to initiate the presented research.

PTMSP is a hydrophobic polymer which exhibits the highest free volume fraction ever reported for polymers and renders highly permeable gas separation membranes. Although PTMSP is used for the manufacturing of PV membranes in literature, only dense free standing membranes with a thickness of 30 – 200 µm are reported. These thick unsupported membranes exhibit relatively low fluxes and therefore their performance should be drastically enhanced to render industrially relevant membranes.

A first route for the optimisation of these PTMSP membranes is the incorporation of inorganic silica particles to increase the high initial free volume even more and therefore positively affect the permeability. By incorporating 50 wt.% silica

in the PTMSP matrix a 72 % increase in permeability is observed in the separation of an ethanol/water mixture.
Secondly, the PTMSP layer was applied as thin film on top of a porous support to decrease the thickness of the selective top layer and thus increase the permeability. A 25 – fold increase in permeability and 1.5 – fold decrease in selectivity was observed upon decreasing the membranes from 85 to 1.5 μm.
Subsequently, the synergetic effect of adding hydrophobic silica and decreasing the top layer thickness was investigated. A wide range of membranes was prepared, with thicknesses ranging from 1.5 to 200 μm and silica filler loads of 0, 25 or 50 wt.%. In the pervaporative separation of an ethanol/water mixture, fluxes from 0.16 to 11.11 kg m^{-2} h^{-1} and separation factors between 12 and 24 were obtained. The optimal flux/selectivity combination was found for a 2.4 μm thick membrane containing 25 wt.% silica. The latter membrane exhibited a flux and accompanying ethanol/water separation factor which was respectively 7-fold and 5-fold higher than those of the best commercial membranes.

As alternative to the addition of hydrophobic silica, a supercritical CO_2 ($scCO_2$) treatment is considered. CO_2 is known to act as a plasticizer for a wide range of polymers, including PTMSP. Recent papers on the enlarging effect of $scCO_2$ on the free volume of common polymers, i.e. polystyrene, poly(lactic acid) and poly(ethylene naphtalate), attracted our attention and the effect of a $scCO_2$ treatment on the PV performance of PTMSP membranes was investigated. By treating PTMSP membranes with $scCO_2$ at high pressures and temperatures, the free volume cavities could be greatly enlarged. This $scCO_2$ enhanced free volume resulted in an improved permeability in PV. The 76 % increase of permeability obtained for PTMSP membranes treated at 24 MPa and 70 °C was comparable with the 72 % increase obtained by addition of 50 wt.% silica to PTMSP membranes. Moreover, the $scCO_2$ enlarged free volume had a relaxation time of approximately 30 years, good thermal stability and excellent reproducibility. The $scCO_2$ treatment is thus a valuable alternative to the incorporation of inorganic silica.
The combination of incorporation of silica particles and subsequent $scCO_2$ treatment did not reveal any synergistic effect. The effect of the $scCO_2$ on the

free volume even partially diminishes due to the increasing resistance to swelling by incorporating inorganic particles.

The relatively poor solvent stability of PTMSP membranes narrows their applicability to the separation of alcohols and less aggressive solvents (e.g. methyl ethyl ketone, ethyl acetate, …) from water. Crosslinking the PTMSP membranes with 3,3'-diazido-diphenylsulfone (CL) renders them insoluble in toluene, the solvent used to dissolve the uncrosslinked polymer. Both a photochemically and a thermally induced crosslinking method were investigated for PTMSP membranes containing 2.5, 5, 10 or 15 wt.% CL. The photochemically treated membranes were insufficiently crosslinked and unwanted by-products were formed, making them inappropriate for PV of more demanding solvent/water mixtures. The thermally treated membranes did render sufficiently crosslinked membranes which were insoluble in several demanding solvents, i.e. heptane, dichloromethane, methyl-*tert*-butyl ether and tetrahydrofuran (THF). Although thermal crosslinking did significantly influence the PV performance in ethanol/water separations, the crosslinked membranes performed well in the separation of THF from water. Compared to two commercial PDMS-based membranes, the thermally crosslinked PTMSP-CL (15wt.%) membranes exhibited a 4-fold higher specific permeation rate and comparable THF/water selectivity. By thermal crosslinking, the solvent stability of PTMSP membranes was successfully improved, thus extending their applicability range to more demanding feed streams.

Chapter 1

Pervaporation

1.1 Introduction

Pervaporation (PV), the contraction of permeation and evaporation, is a membrane process discovered by Philip Adolph Kober in 1917 in the course of some dialysis experiments. Kober reported the evaporation of water from an albumin/toluene solution through a tightly closed collodion bag at room temperature, indicating the presence of an extremely fine porosity, allowing vapour molecules to pass freely and prevent liquid to pass [1]. Until the late 1950's, no major progress was made in the field of PV, although few researchers published their findings on dehydration by PV [2,3].

In 1958 Binning *et al.,* assigned to the American Oil Company (Amoco), reported the use of PV for the separation of a ternary azeotrope of isopropanol-ethanol-water [4], being the start of several decades of dedicated research. From 1959 to 1961 more than 10 patents on PV were issued to Amoco [5], indicating the preliminary interest in and potential of PV in industry. The first commercial industrial dehydration PV unit was put into service in 1983 in Brazil by GFT (Germany), using polymeric membranes [6,7]. In contrast to polymeric membranes, the first large-scale dehydration PV unit using zeolite NaA membranes was operated almost 20 years later in 2001 in Japan [8].

Despite the promising results and realisations in the 1980's and the large number of published papers on PV membranes and processes in the last decades, the developments in PV technology stagnated and dehydration of organic solvents still remains the main industrial PV application [9].

Other applications like e.g. organic-organic separations [10], aroma recovery [11] and VOC removal from water [12] are rarely applied on industrial scale, despite their high potential. In the future, however, PV is believed to gain more industrial interest, due to the increasing energy costs, more stringent

environmental legislation and expected breakthroughs in membrane and process developments [9].

1.2 Membrane processes

A membrane process can be defined as a separation process which requires two bulk phases physically separated by a third phase, the membrane. The membrane is the interphase between these two phases and may comprise either a nonporous, or a nano-, micro- or macroporous solid of which the pores may be filled with a liquid phase or a gel [13]. A schematic representation of a basic membrane process is given in Figure 1.1. The separation is achieved because the membrane selectively transports the target component from the feed mixture to the permeate [14]. The transport mechanism and driving force for this selective transport can be diverse and depends on the type of membrane process.

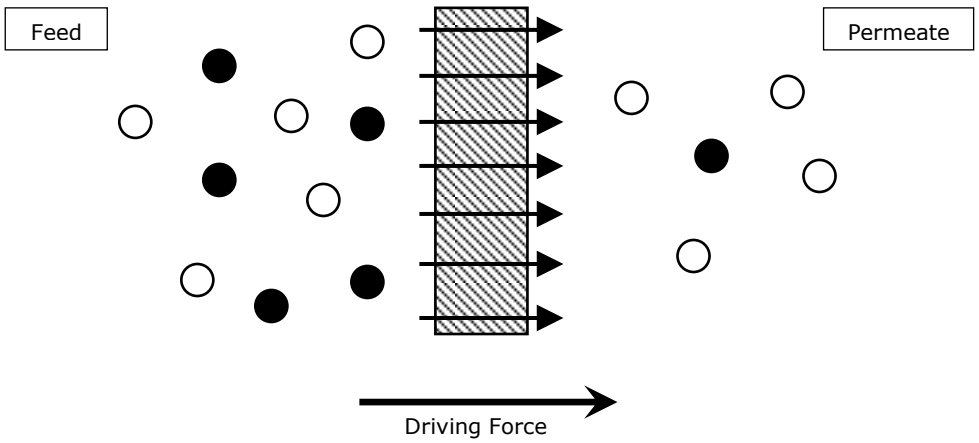

Figure 1.1: Schematic representation of a membrane process [14].

The different types of membrane processes can be classified according to their separation principle which is determined by the physical or chemical characteristics of the components to be separated [14]. The four main

physical/chemical properties of molecules relevant to membrane separations are:

1. **Size**: The separation occurs based on the size of the components, i.e. size sieving. (e.g. micro-, ultra- and nanofiltration)

2. **Vapour pressure**: Differences in vapour pressure of the components to be separated are the basis of separation. (e.g. membrane distillation)

3. **Affinity**: The target component selectively sorbs in the membrane, favouring its transport across the membrane. (e.g. gas separation and PV)

4. **Charge**: Based on opposite charges, ionic solutions are separated (e.g. electrodialysis)

Furthermore, membrane processes can be subdivided according to the driving forces required to initiate the separation. The different types of driving forces with corresponding membrane processes are listed in Table 1.1.

Table 1.1: Membrane processes classified according to their driving force [14].

Driving force		Membrane process
ΔP	pressure gradient	micro-, ultra-, nanofiltration and reverse osmosis
Δp	partial pressure gradient	gas separation, PV and vapour permeation
ΔE	electrical potential gradient	electrodialysis
Δc	concentration gradient	dialysis, membrane contactors
ΔT	temperature gradient	membrane distillation

It is beyond the scope of this thesis to thoroughly discuss all these different membrane processes, therefore the reader is referred to comprehensive books

[14-17]. Membrane research and engineering covers a wide range of areas, each of them requiring dedicated scientists or engineers. In the development of membrane processes, chemists, physicists, mathematicians and engineers are indispensable. While chemists can synthesise and modify materials or membranes, physicists and mathematicians are capable of modelling the transport mechanism. Engineers will optimise the final process by designing a membrane module/process, a pilot plant and even process simulation programs. These different aspects explain the multidisciplinarity of the teams involved with the development of new membrane technologies and their implementation in real industrial processes.

1.3 Principle of pervaporation

PV is a separation technique which involves the use of a non-porous polymeric or nanoporous inorganic membrane in contact with a liquid feed. The transport in PV is described in a single and unified way by the solution-diffusion model [18]. This model was formulated in the 19th century, based on the work of T. Graham (1829) [19], J. K. Mitchell (1831) [20] and S. von Wroblewski [21]. The transport in PV can be described with a three step mechanism [5]:

1. Selective **sorption** of the target component from the bulk feed in the membrane
2. (Selective) **diffusion** through the membrane
3. **Desorption** of the permeate in the vapour state at the downstream side of the membrane

The key feature in PV is thus the mass transfer of the target component through the membrane during which a phase transition from the liquid phase at the feed side to the vapour phase at the permeate side occurs. Basically, the transport through a PV membrane or the permeability (P) can be described in terms of the solubility (S) and the diffusivity (D) of the target component:

$$P = S \times D \qquad (1\text{-}1)$$

The solubility is a **thermodynamic** parameter, providing information on the amount of penetrant absorbed by the membrane under equilibrium conditions. The diffusivity, on the other hand, is a **kinetic** parameter indicating the transport rate of the penetrant [14].
The driving force in PV is the chemical potential (μ_i) gradient across the membrane [15,18] which is expressed as:

$$d\mu_i = RTd\ln(\gamma_i n_i) + v_i dp \qquad (1\text{-}2)$$

where γ_i is the activity coefficient, n_i the mole fraction ($\gamma_i n_i = a_i$), v_i the partial molar volume and p the pressure of component i, R the universal gas constant and T the absolute temperature.

The flux, J_i, of the target component i can be described by an equation similar to Fick's first law:

$$J_i = -L_i \frac{d\mu_i}{dx} \qquad (1\text{-}3)$$

where $d\mu_i/dx$ is the chemical potential gradient of the target component i across the membrane and L_i is a coefficient which describes the chemical potential proportionally with the flux.
Prior to defining the model of permeation in PV, some assumptions must be made. Firstly, the fluid and vapour on either side of the membrane are expected to be in equilibrium with the membrane material at the interface. Secondly, the solution-diffusion model assumes that the pressure within the membrane is uniform and that the chemical potential gradient across the membrane is expressed only as a concentration gradient [18]. Figure 1.2 represents a schematic diagram of the driving force gradients according to the solution-diffusion transport model.

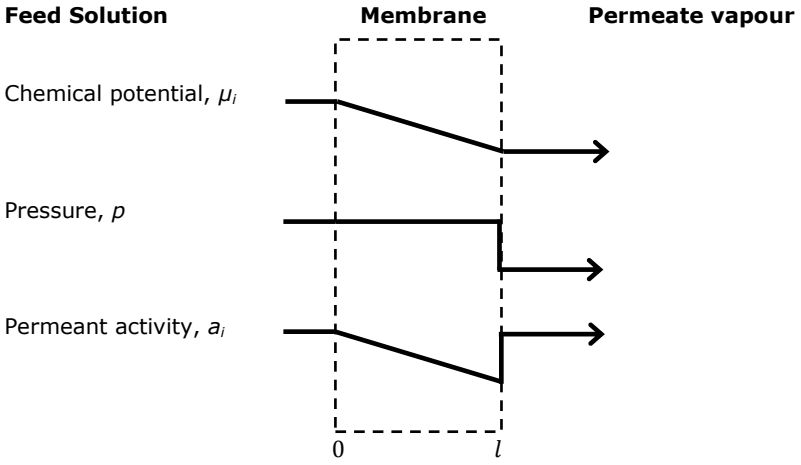

Figure 1.2: The driving force gradients for permeation through a dense membrane according to the solution-diffusion model [18].

At the feed side, two incompressible phases exist (the membrane and liquid) of which the volume does not change appreciably with pressure. Integrating equation 1-2 with respect to concentration and pressure then gives:

$$\mu_i = \mu_i^0 + RTln(\gamma_i n_i) + v_i(p - p_i^0) \tag{1-4}$$

where μ_i^0 is the chemical potential of the pure component i at a reference pressure p_i^0. For the equilibrium conditions at the liquid/membrane interface (0) at the feed side, the following equation can be written:

$$\overbrace{\mu_i^0 + RTln\left(\gamma_{i_0}^L n_{i_0}\right) + v_i\left(p_0 - p_{i_{sat}}\right)}^{\text{Liquid feed}} = \overbrace{\mu_i^0 + RTln\left(\gamma_{i_{0(m)}} n_{i_{0\,(m)}}\right) + v_i\left(p_0 - p_{i_{sat}}\right)}^{\text{Membrane}} \tag{1-5}$$

in which the subscript 0 denotes the liquid feed phase (Figure 1.2), $0(m)$ the liquid in the membrane at point 0 and the superscript L stands for liquid.

At the permeate gas/membrane interface, on the other hand, one side is a compressible gas of which the molar volume changes with pressure. By integrating Equation 1-2 and applying the ideal gas law, the following expression is obtained:

$$\mu_i = \mu_i^0 + RTln(\gamma_i n_i) + RT\ln\left(\frac{p}{p_i^0}\right) \tag{1-6}$$

To concede to the equilibrium conditions at the permeate gas/membrane interface, the following equation can be derived:

$$\overbrace{\mu_i^0 + RTln\left(\gamma_{i_l}^G n_{i_l}\right) + RT\ln\left(\frac{p_l}{p_{i_{sat}}}\right)}^{\text{Gaseous permeate}} = \overbrace{\mu_i^0 + RTln\left(\gamma_{i_{0(m)}} n_{i_{0\,(m)}}\right) + v_i\left(p_0 - p_{i_{sat}}\right)}^{\text{Membrane}} \tag{1-7}$$

At the permeate side interface l (Figure 1.2), the membrane phase is at the feed pressure as assumed by the solution-diffusion model, while the permeate phase is at a lower permeate pressure (vacuum). Since in an isothermal system the chemical potential consists of a pressure term and an activity term, as expressed by Equation 1-2, the activity in the permeate phase must be higher than the activity in the membrane phase to fulfil the equilibrium conditions. This is shown in Figure 1.2.

Taking into account all the equilibrium conditions of the solution-diffusion model, the component flux J_i can be derived as:

$$J_i = \frac{P_i^G}{l}\left(p_{i_0} - p_{i_l}\right) \tag{1-8}$$

where P_i^G represents the gas permeability coefficient, l the membrane thickness and $\left(p_{i_0} - p_{i_l}\right)$ the difference in partial vapour pressure of component i across the membrane, being the driving force for transport in PV. The extended

mathematical proof of this equation can be found in comprehensive textbooks [5,14,15] and review articles [18].

PV is often seen as a valuable alternative to or complementary technique to conventional distillation. In distillation the complete mixture to be separated has to be evaporated, which is highly energy-intensive. As energy-efficient alternative, PV has four important features making it less energy-consuming than its energy-obese brother, distillation.

1. In contrast to distillation where the entire feed is superheated, in PV, the membrane is chosen in such way that only the **minor component** (usually less than 10 wt.%) consumes the latent heat of vaporisation.
2. PV uses highly **selective membranes**, making the separation occur based on mutual affinity between the membrane and the penetrants, in contrast to distillation which is exclusively based on boiling point/vapour pressure differences.
3. PV can be carried out at **mild temperatures** which is particularly advantageous when heat-sensitive (bio-)molecules are present.
4. PV is performed in the **absence** of **additives** (e.g. entrainers), avoiding the need for extra recovery columns such as in extractive distillation.

Based on these four important features, PV demonstrates undeniable advantages over distillation, especially in the separation of heat-sensitive, close-boiling and azeotropic mixtures [22]. An azeotropic mixture consists of at least two liquids of which the composition in the vapour and liquid phase is identical. Therefore, azeotropic mixtures cannot be separated by conventional distillation. The boiling point of the azeotropic mixture can be either higher (negative azeotrope) or lower (positive azeotrope) than its individual components [23]. A well-known example of a positive azeotrope is a mixture containing 95.6 wt.% ethanol (EtOH) and 4.4 wt.% water (H_2O) (Figure 1.3).
If a mixture with a composition C_1, left from the azeotropic composition is distilled, it will boil at a temperature given by the liquid composition curve and produce a vapour with composition C_2. Reheating of the condensed vapour C_2

will result in a new vapour with composition C_3 (Figure 1.3). By repeating this boiling-condensing-reboiling sequence, finally the composition of the vapour and liquid will end up in the azeotropic point. This means that no pure EtOH can be obtained by conventional distillation. Pure H_2O is recovered in the boiling flask as the distillation residue, and an aqueous 95.6 wt.% EtOH mixture is obtained in the distillate (top of the fractionating column). Heating a mixture with a composition at the right-hand side of the azeotropic mixture will result in pure EtOH in the boiling flask and an aqueous 95.6 wt.% EtOH mixture in the distillate.

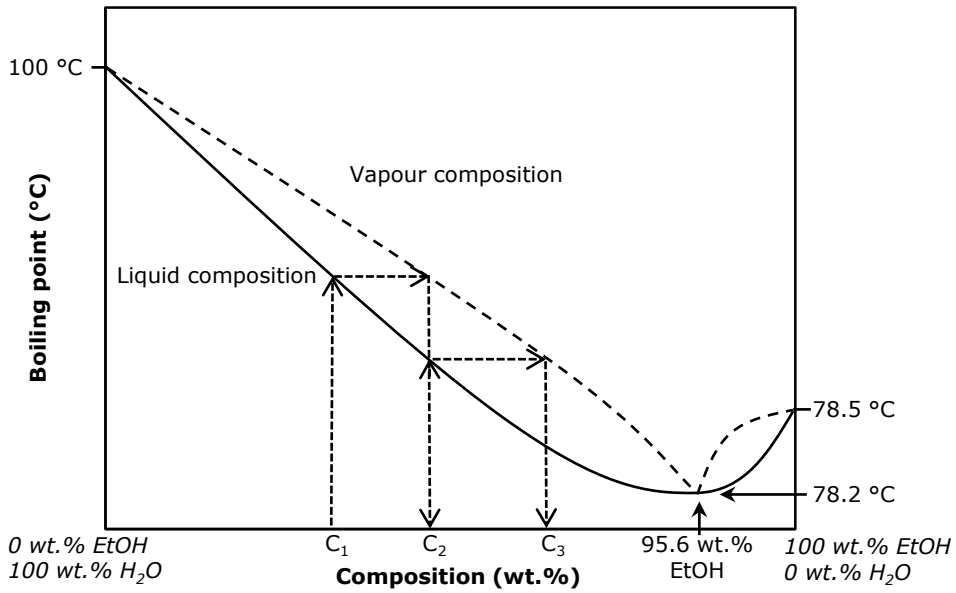

Figure 1.3: Boiling point as a function of the composition for an EtOH/H_2O mixture (positive azeotrope).

More sophisticated distillation techniques, such as pressure swing, vacuum or extractive distillation could be used to purify the mixture beyond the azeotropic point, but all of them require significantly more energy and/or rely on additives (e.g. entrainer) that must be recovered afterwards. PV, on the other hand, is not governed by the thermodynamics of the liquid-vapour equilibrium and can therefore break azeotropes as it predominantly relies on the selectivity of the

membrane. In the pervaporative dehydration of an EtOH (96 wt.%) / H_2O (4 wt.%) mixture at 40 °C, Uragami and co-workers reported a permeate composition of 98.9 wt.% H_2O and 1.1 wt.% EtOH [24]. This clearly demonstrates the strength of PV as the azeotrope is crossed at a mild temperature and without addition of entrainers.

1.4 Pervaporation membranes

Membrane selection in PV processes depends on the temperature and composition of the feed mixture (nature and concentration of liquids), the purification target and the aimed performance. A broad range of PV membranes can be used, both organic (polymeric) and inorganic (ceramic, zeolitic) in nature. Each type has its own specific pro's and contra's. Mixed matrix membranes, which comprise inorganic particles dispersed in a polymeric phase, combine the advantages of both materials.
Besides the differences in membrane material, PV membranes can be classified according to the character of the separation. Three main application types are usually distinguished:

- Dehydration of organic solvents
  → **Hydrophilic** membranes [25-27]
- Removal of organics from dilute aqueous solutions
  → **Hydrophobic** membranes [28-30]
- Organic-organic separations
  → **Organophilic** membranes [31-33]

Dehydration of organic solvents is the most widespread PV application and it is already industrially applied since 1983 [6,7]. Solvents can be dewatered with water selective **hydrophilic** membranes. These hydrophilic membranes are designed such that they have a high affinity for water, either by dipole-dipole interactions, hydrogen bonding or ion-dipole interactions [25-27]. A selection of polymeric and inorganic materials of which the use in the manufacturing of

hydrophilic PV membranes has been reported in literature, is presented in Table 1.2.

Table 1.2: Selection of polymeric and inorganic membrane materials used for manufacturing of hydrophilic, hydrophobic and organophilic PV membranes [25-33].

Hydrophilic	Hydrophobic	Organophilic
Cellulose	Polydimethylsiloxane	Poly(urethane)
Chitosan	Poly(urethane)	Methyl methacrylate
Poly(vinyl alcohol)	Poly(ether-block-amide)	Ethyl methacrylate
Poly(acrylic acid)	Nitrile-butadiene rubber	Benzoylchitosan
Polyamides	Styrene-butadiene rubber	Polyimide
Poly(ethyleneimine)	Poly[1-(trimethylsilyl)-1-propyne]	Poly(etherimide)
Polyaniline	Poly(tetrafluoroethylene)	Poly(tetrafluoroethylene)
Poly(acrylamide)	Polyoctylmethylsiloxane	
Sodium alginate	Polymer of intrinsic microporosity	
Polyimides		
Polyelectrolyte		
Silica	ZSM-5 zeolite	Zeolite X,Y
NaA zeolite	MEL zeolite	Mordenite
Zeolite T	Zeolite X	Silicalite

A vast amount of research has been performed on the development of polyvinyl alcohol (PVA) – based PV membranes [34-44], due to PVA's pronounced abrasion resistance, elongation, tensile strength, flexibility and excellent water perm-selective properties. It is therefore not surprising that the first commercial hydrophilic polymeric membranes manufactured by Sulzer Chemtech (Switzerland), formerly known as GFT, are based on PVA. These membranes were applied in the first industrial dehydration plant in Brazil [6,7]. For the inorganic membranes, such membrane material monopoly does not exist at present. Hydrophilic membranes based on zeolite types A and T are available from Mitsui (Japan) and Fraunhofer IKTS (Germany), while microporous silica membranes can be purchased from Pervatech (the Netherlands) [8,45]. Recently, ECN developed a new hydrophilic PV membrane HybSi®, which merges organic and inorganic fragments in a silica-based amorphous material [46-48].

This novel silica membrane with superior stability under acidic and hydrothermal conditions is now also manufactured and marketed by Pervatech.

Hydrophobic membranes rely on their ability to separate organic compounds from diluted aqueous mixtures. These membranes typically find application in the purification of waste waters, aroma recovery and *in situ* bio-alcohol recovery from fermentation broths. A list of used organic and inorganic hydrophobic membrane materials can be found in Table 1.2. Poly(dimethylsiloxane) (PDMS) - based membranes have found wide use [49-54] and are commercially available from Sulzer Chemtech (Switzerland), Pervatech (The Netherlands), SepraTek (South Korea) and Membrane Technology and Research, Inc (MTR, USA). Even though several PDMS membranes are available on the market, researchers are still trying to optimise PDMS-based membranes in terms of flux and selectivity, e.g. by incorporating inorganic porous or nonporous fillers, accounting for approximately 30-40 new research papers each year (since 2006).
Poly[1-trimethylsilyl)-1-propyne] (PTMSP) is another example of an extensively studied and promising polymer for the manufacturing of hydrophobic PV membranes [55-63]. However, PTMSP-based membranes are not yet commercially available.
So far, no real breakthrough of hydrophobic PV in industry has been achieved due to the combination of the complicated process design, the lack of highly selective and permeable membranes, the limited number of commercial membrane suppliers, and the biased competition with distillation plants that have been written down for several decades. New developments in membrane manufacturing are expected to enhance the industrial interest and applicability of hydrophobic PV in real processes.

The last category of PV membranes, the so-called target **organophilic** membranes, are applied in the separation of mixtures of two or more organic liquids [31-33]. Typically, they can be used in the separation of polar/non-polar, aromatic/aliphatic, aromatic/alicyclic and isomer mixtures. Industrial suppliers of target organophilic PV membranes are scarce, due to the complexity of the separation layer, which has to be tuned for almost each distinct application. A selection of materials that have been reported in relation with organophilic PV is

listed in Table 1.2 [29-33]. Sulzer Chemtech has reported two cases of industrial applications of organo-selective membranes, i.e. the separation of methanol from a methanol/methyl-*tert*-butyl ether mixture and the separation of EtOH from a mixture with ethyl-*tert*-butyl ether [31]. In Germany, PolyAn supplies molecular surface engineered (MSE) polymeric membranes which can be tailor-made for specific organic-organic separations [64]. MSE is a technique in which the pores of a porous membrane are "filled" with a functional polymer, rendering dense target organo-selective PV membranes.

The selection of new materials for the preparation of PV membranes is based mainly on three important requirements: (1) high chemical resistance, (2) respectable sorption capacity and (3) good mechanical strength. To estimate the compatibility of a specific membrane material with a certain feed stream mixture, solubility parameters and membrane polarity are the indices of interest [41]. Unfortunately, a highly selective and extremely permeable PV membrane, that could be successfully applied in several divergent feed streams, does not exist. For each application, the membrane has to be modified or tuned in order to obtain the best performance in the specific feed stream. Moreover, developing a novel PV membrane does not exclusively include the synthesis and optimization of novel membrane itself, but also up-scaling of the manufacturing process, module design and membrane sealing should be taken into account, without losing sight of the final membrane price. In view of this complexity, many ideas and promising developments don't make it any further than a screening PV test.

1.5 Applications

PV is a developing and promising membrane technology that can be used for various industrial applications. However, the optimal process design is unlikely to consist solely of PV. In many cases, a hybrid process combining PV with one or more other separation technologies, mostly distillation, is the most optimal solution from an economic point-of-view [65]. In this section, some typical applications of PV will be briefly discussed. At present, the major industrial

application still remains the dewatering of azeotropic or close boiling point mixtures [6-8,22,25-27] which will therefore be discussed first.

1.5.1 Dehydration of isopropyl alcohol

Isopropyl alcohol (IPA) is known to form a positive azeotrope with water at a ratio of 87 wt.% IPA and 13 wt.% H_2O. The boiling point of the azeotropic mixture is 80.4 °C, which is lower than the individual boiling points of IPA (82.5 °C) and H_2O (100 °C) [66]. If conventional distillation would be used to separate this mixture, the distillate would always consist of the azeotropic composition. Distilling a mixture with a composition left from the azeotropic point, as illustrated in Figure 1.3 for the EtOH/H_2O azeotrope, will result in pure water in the boiling flask and a mixture with the azeotropic composition in the distillate. Distilling a mixture with composition right from the azeotropic point, on the other hand, will result in pure IPA in the boiling flask and a mixture with the azeotropic composition in the distillate. As already discussed for the EtOH/H_2O mixture, special distillation techniques could be used to break the azeotrope, e.g. extractive or pressure swing distillation. However, these alternative distillation techniques are very energy intensive and extra distillation columns are required. A hybrid process based on PV and conventional distillation can be used to keep the operational costs within limits [65]. Van Hoof *et al.* [66] and Naidu *et al.* [67] have reported the economic evaluation of a hybrid PV-distillation setup for the purification of an IPA/H_2O mixture. Both authors report the beneficial effect of a PV unit coupled at the distillate outlet of the distillation column. Van Hoof *et al.* reported a decrease in total cost of approximately 49% and a decrease in energy consumption of 48% compared to azeotropic distillation [66]. Naidu *et al.* reported a comparable decrease in total cost of approximately 43% [67] for the hybrid PV-distillation process compared to azeotropic distillation, clearly demonstrating the potential of PV in dewatering of azeotropic solvent/water mixtures.

1.5.2 PV as tool to shift the chemical or bio-chemical equilibrium

A second application is the integration of PV with a chemical or bio-chemical reactor to control the equilibrium and therefore increase the product yield and substrate conversion. Two examples are shortly discussed below, one dealing

with esterification reactions and another with the fermentative production of bio-alcohols.

1.5.2.1 Esterification reactions facilitated by PV

Applying PV to shift chemical reaction equilibria is a relatively well developed area of membrane technology and has already found its way to industry [65]. A typical esterification involves the reaction between a carboxylic acid and an alcohol in the presence of a dehydrating agent (Fisher esterification).

$$RCO_2H + R'OH \leftrightarrow RCO_2R' + H_2O \quad (1\text{-}9)$$

By coupling PV to an esterification reaction, the produced water (or ester) can directly be removed, thereby shifting the reaction equilibrium towards higher production yields (le Châtelier). Research demonstrated the high potential of *in situ* PV in the removal of the formed water [68-70] or ester [71,72] from the reaction media. Tanaka *et al.* reported a conversion of almost 100 % after 8 hours using a zeolite T membrane coupled to the esterification reaction of acetic acid with EtOH. Without PV the conversion flattened out at the thermodynamic equilibrium (70 - 80 %) [72]. Sulzer Chemtech has meanwhile demonstrated this process at industrial scale [65].

1.5.2.2 *In situ* bio-butanol recovery

The increasing interest in the production of bio-alcohols as alternative for or additive to fossil fuels and as platform molecules for the synthesis of bio-chemicals, has led to a large number of papers on fermentation processes and the optimisation thereof, e.g. by improving the strain stability and chemical/thermal resistance of the bacteria [73-77]. One of the main bottlenecks of this process is the product toxicity and associated cell inhibition. Besides the optimisation of the fermentation itself, a facile and efficient recovery of the bio-alcohols from the broths would greatly improve the product yield, and thus boost the overall techno-economic feasibility and industrial applicability of these processes [75,76,78-82]. While most current industrial bio-alcohol plants rely on distillation techniques for the recovery of the produced alcohols after fermentation, membrane processes working at ambient conditions offer the

possibility to remove the alcohols from the broth during the fermentation. By coupling the fermentor to a hydrophobic PV unit, the bio-alcohol yield could be greatly improved since the inhibitory alcohols are continuously removed before toxic concentrations are reached in the broth [73,74,76]. Bio-butanol has gained a constantly increasing interest, since its energy content is higher compared to EtOH and it can be more easily blended with conventional gasoline. Liu *et al.* reported the influence of real acetone-butanol-EtOH (ABE) fermentation broths on the PV performance of PDMS/ceramic composite membranes [83]. The presence of inorganic salts in the ABE-fermentation broth increased the membrane selectivity, while adsorption of microbial cells to the membrane surface negatively influenced the PV performance [83]. Fadeev *et al.* reported the PV performance of dense toluene-cast PTMSP membranes in *in situ* butanol removal from of an ABE-fermentation broth [84]. Although a severe flux and selectivity decline over time was observed, at steady state conditions the PTMSP membranes still resulted in a 4-fold higher flux than commercial PDMS membranes at similar selectivities [84]. Several review articles express the potential of PV for *in situ* recovery of bio-butanol [73,74], bio-ethanol [28,76] or other organics produced from biomass by fermentation [30]. However, further improvements on the level of the bioconversion process and of the membrane are still needed to raise PV-assisted fermentation processes to an industrial scale.

1.6 State-of-the-art on the use of PTMSP membranes in PV

Since PTMSP will be used further in this work to synthesise PV membranes, its properties and characteristics are discussed and a short state-of-the-art of PTMSP-based membranes in PV is given.

1.6.1 Poly[1-(trimethylsilyl)-1-propyne]

PTMSP is a substituted polyacetylene that combines a rigid backbone chain with bulky trimethylsilyl side groups (Figure 1.4). The latter restrict rotational mobility and limit the ability of the polymer chains to closely pack. As a result of this inefficient chain packing and poor inter-chain cohesion, neat PTMSP is

understood to exhibit an extremely high free volume fraction and inherent nanoporosity [85]. Its free volume shows a bimodal distribution, with cavities having an average radius in the order of 0.3 and 0.5 nm according to the spherical cavity model [86]. It has been postulated that these small and larger cavities create a series of interconnected free volume pathways, thus giving PTMSP unique high-permeability characteristics [87]. Moreover, PTMSP exhibits a reverse-selective behavior in gas separation due to the fact that relatively large organic molecules adsorb on the walls of the free volume elements, thereby hampering the transport of smaller, permanent gases [88]. Thanks to its intrinsic nanoporosity, glassy nature (T_g > 300 °C) and pronounced hydrophobicity, PTMSP has received a lot of attention in literature as a promising membrane-forming material. Since Masuda synthesized the polymer for the first time in 1983 [89], PTMSP has been one of the most studied polymers for gas separation [15,86,90-95] and PV applications [15,22,28,55-63].

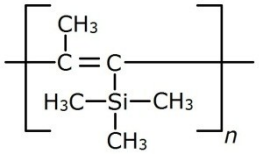

Figure 1.4: Chemical structure of PTMSP.

Despite PTMSP's intrinsic advantages [85,87,88], difficult polymer synthesis and membrane stability issues are impeding the up-scaling of the membrane manufacturing process. The polymerisation of PTMSP proceeds by the metathesis mechanism in which the propagating species is a metal carbene [85]. Besides the large amount of solvent needed to carry out the polymerisation and subsequently purify the formed PTMSP, its stability is strongly related to the polymerisation conditions. Several papers on the use of different catalysts, co-catalysts and solvents demonstrate the major role of the *cis-/trans*-configuration of the double bond in PTMSP's repeating unit [57,85,86,96]. In general, PTMSP synthesized with a $NbCl_5$ catalyst leads to more *cis*-functionalized double bonds, and therefore a more regular configuration, lower free volume and permeability. Moreover, the M_w and polydispersity (Pd = M_w/M_n < 2) is lower compared to the polymers synthesized

with the use of $TaCl_5$ (Pd > 2). The use of a $TaCl_5$ catalyst renders a polymer with high M_w, more irregular structure (*cis-/trans-*) and therefore higher free volume and permeability [85,96]. On the other hand, its stability in PV is lower than the $NbCl_5$ catalysed polymer [57]. The latter can be explained by its higher excess free volume which can relax more easily and lead to internal fouling, which can be particularly be significant in case small molecular weight impurities are present in the feed [85,96]. Overall, these stability problems can be divided in three aging phenomena: (1) physical aging, (2) chemical aging and (3) contamination (internal fouling). The latter is expected to be the predominant factor in the decrease of permeability in gas separation and especially PV [57,85,86]. Since internal fouling is a reversible process, membrane regeneration methods, in which the contaminants are removed out of the PTMSP membrane, are patented [97]. The chemical stability of PTMSP membranes to different vapours or solvents can be improved by crosslinking, as reported in literature [92,93,98-103].

1.6.2 PTMSP-based membranes in PV

Currently, research is still focused on unsupported (free standing), dense PTMSP membranes for gas separation [15,86,89-95], in which the term "dense" refers to the absence of pores in the membrane. Although PTMSP membranes are said to be non-porous, the free volume network serves as preferential transport pathway for the liquid, vapour or gas molecules. One could thus say that PTMSP has extremely small pores in the angstrom (Å) range.

While most research on PTMSP membranes is focused on gas separation applications [15,86,89-95], some academic research groups are active in the development of polyacetylene-based membranes for use in PV. Table 1.3 provides a literature overview of the synthesis of PTMSP membranes and their performance in PV.

One of the most active research groups in this field is A.V. Topchiev Institute of Petrochemical Synthesis (TIPS) in Moscow, which is part of the Russian Academy of Science. More precisely the Polymeric Membranes Laboratory (POLYMEM) and the Laboratory of Physico-Chemistry of Membrane Processes are involved with both the synthesis of PTMSP and PTMSP membranes and their use in the pervaporative separation of alcohol/water mixtures. TIPS focuses amongst

others on the synthesis and application of unsupported PTMSP membranes for removal of bio-alcohols from fermentation media (Table 1.3). A wide variety of catalyst/co-catalyst combinations have been used for the polymerisation of PTMSP and the influence thereof on the PV performance of synthetic and real fermentation media has been extensively studied [57,58,84,104,105]. PTMSP synthesized with a $NbCl_5$ or $TaCl_5$ catalyst and a Al(*i*-Bu)$_3$ co-catalyst resulted in membranes with stable performance during PV of a multicomponent ABE fermentation mixture. When $TaCl_5$/*n*-BuLi was used, however, severe flux decline and selectivity deterioration was observed [57]. The latter was ascribed to internal fouling, referring to contamination of the free volume with low molecular weight fermentation by-products. These impurities show high affinity for the membrane but have a low vapour pressure, thus blocking the free volume cavities and hindering the transport of the target component [58,84]. Despite the observed deterioration of both flux and selectivity, PTMSP membranes still performed significantly better than commercially available PDMS-based membranes [84].

Masuda and co-workers from the Department of Polymer Chemistry at Kyoto University (Japan) reported the PV performance of dense unsupported PTMSP membranes tested on various dilute aqueous streams containing organics (EtOH, acetone, acetonitrile and acetic acid) and at different operating conditions [63] (Table 1.3). The EtOH/H_2O separation factor decreased from 17 to 2.5 upon increasing the EtOH concentration in the feed from 10 to 85 wt.% and the specific permeation rate increased two magnitudes (10^{-3} → 10^{-1}). Upon decreasing the membrane thickness the EtOH/H_2O separation factor gradually decreased (22 → 15) and the specific permeation rate remained approximately unaffected (7×10^{-3} g m m^{-2} h^{-1}), indicating the inverse linear relationship between flux and membrane thickness [63]. Furthermore, separation factors up to 101 and 76, and corresponding specific permeation rates of 6.6×10^{-2} and 6.5×10^{-2} g m m^{-2} h^{-1} were obtained for feed streams containing acetonitrile and acetone. For acetic acid, the separation factor remained below 10 while the specific permeation rate ($\approx 7 \times 10^{-3}$ g m m^{-2} h^{-1}) was comparable with the EtOH/H_2O separations [63].

The University of Deusto (Bilbao, Spain) reported more than 10 years later again the influence of feed concentration, feed temperature, membrane thickness and

operation time on the PV performance of unsupported PTMSP membranes in the separation of EtOH/H_2O mixtures [55,56,59,60]. As reported by Masuda [63], an increase in EtOH feed concentration resulted in increased permeate fluxes and a decrease in EtOH/H_2O separation factor. Higher alcohol concentrations make the membrane swell more, thus facilitating the transport of both EtOH and H_2O molecules. With increasing temperature (38 – 75 °C), an increase in flux was reported, combined with an unaffected separation factor [56]. Reduction of the membrane thickness understandably increased the flux, but in contrast to Masuda [63], below 40 µm the increase deviated from linearity, meaning that further membrane thickness reduction below this critical value does not induce a proportional flux increase. Moreover, below 50 µm a drastic drop in separation factor was reported [56].
In the USA, the National Renewable Energy Laboratory reported in 1997 PV performance results of dense unsupported PTMSP membranes in EtOH/H_2O separations and in the recovery of bio-ethanol from fermentation broths [106]. A clear decrease in both flux and separation factor was observed for a EtOH/water model mixture containing 1.5 wt.% acetic acid, as well as for a real fermentation medium, and yeast-free and bacteria-free fermentation media [106].

While the above mentioned studies all focused on pure PTMSP membranes, without addition of inorganic particle, surface modifications or chemical modifications, these aspects have been investigated by others research groups.
The Department of Applied Chemistry at Meiji University (Tokyo) reported the PV performance of surface modified PTMSP membranes [61]. Asymmetric membranes consisting of a silica layer on top of a PTMSP membrane were prepared and used in the pervaporative separation of EtOH/H_2O mixtures [61] (Table 1.3). At high concentrations of the gel-type silica, a decrease in EtOH permselectivity was observed, that could be attributed to the "scalant" effect of the silica layer. Adding low concentrations of gel-type silica increased the specific permeation rate in the separation of mixtures containing more than 50 wt.% EtOH; at lower concentrations the effect was insignificant [61].
Uragami and co-workers reported the surface modification of PTMSP membranes by addition of a small amount of poly(fluoroacrylate)-*g*-poly(dimethylsiloxane)

(PFA-*g*-PDMS) to the casting solution. A clear difference in hydrophobicity between the air- and glass plate side was demonstrated by contact angle measurements. The performance of the hydrophobized membranes in the pervaporative separation of an EtOH/H_2O mixture is presented in Table 1.3 [107]. After the surface modification, the permeation rate decreased about 20 %, while the EtOH/H_2O separation factor increased with about 30 %.

The Membrane Laboratory at the Korean Institute of Science and Technology reported the synthesis of a hybrid PTMSP/PDMS membrane to prevent or retard physical aging of PTMSP. Firstly, PTMSP/PDMS membranes were prepared by semi-interpenetrating polymer networks, and secondly, PDMS was incorporated by sorption into the PTMSP membrane and subsequently crosslinked. The addition of PDMS stabilized the PV performance as a function of time, but the flux was drastically lower than the unmodified PTMSP membranes [62].

Nagase and co-authors reported several procedures to modify PTMSP membranes [108,109]. Firstly, PTMSP/PDMS graft membranes were tested in the separation of EtOH/H_2O mixtures. All membranes containing PDMS had a higher separation factor than the pure PTMSP membranes and a maximum (28.3) was reached for membranes containing 12 mol% PDMS. The specific permeation rate fluctuated with increasing PDMS content and both higher and lower values than for unmodified PTMSP membranes were obtained (Table 1.3) [108]. Secondly, PTMSP membranes were chemically modified by introducing fluoroalkyl groups. Addition of less than about 5 mol% of fluoroalkyl silylated units effectively enhanced the EtOH/H_2O separation factor, while higher concentrations caused a decrease in selectivity. Moreover, aqueous mixtures of tetrahydrofuran (THF), acetone, acetonitrile, dioxane and 2-propanol were efficiently separated (Table 1.3). The authors report that the co-polymer was soluble in THF and highly swollen in acetone and acetonitrile, but they claim that the membrane was not destroyed during the PV tests [109].

The reported fluxes and separation factors of dense PTMSP membranes in literature (Table 1.3) vary between 0.015 and 5 kg m^{-2} h^{-1} and 2 and 22, respectively.

These variations in PV performance can be explained by:

- The variations in polymer synthesis conditions, resulting in different polymer characteristics like M_w, *cis*- /*trans*- ratios, M_w distribution and degree of catalyst contamination.
- The variations in experimental conditions like e.g. temperature, feed composition and downstream pressure, which are known to influence the fluxes and separation factors of PTMSP membranes [55,56,63].

Altogether, these differences between the used materials and the experimental conditions make it extremely hard to compare data in literature. Therefore, a benchmark study is performed with commercially available membranes under exactly the same PV experimental conditions.

Table 1.3: Overview of literature data on PTMSP membrane synthesis and performance data in in PV.

Ref.	Topic	Temperature (°C)	Flux (kg m^{-2} h^{-1})	Separation factor
[84]	• dense unsupported • 16 µm • 20 g/l BuOH • $NbCl_5$	26	0.6	80
	• dense unsupported • 15 µm • 20 g/l BuOH • $TaCl_5$	23	0.4	147
	➔ Decline in flux as a function of time according: $y = At^{-b}$			
[104]	• dense unsupported • 22 µm • 0.3 – 6.0 wt.% BuOH • $TaCl_5$-Al(*i*-Bu)$_3$	25 – 70	0.1 – 2.1	41 - 78
[58]	• dense unsupported • 14-20 µm • 6 wt.% EtOH • $TaCl_5$-Al(*i*-Bu)$_3$	30	0.3	20
	• dense unsupported • 14-20 µm • EtOH (75 g/l) fermentation broth • $TaCl_5$-Al(*i*-Bu)$_3$	37	0.015	4
[57]	• dense unsupported • 15-25 µm • 6 wt.% EtOH • $TaCl_5$-Al(*i*-Bu)$_3$	30	0.34 – 0.44	15.1 – 19.9
	• dense unsupported • 14-20 µm • 6 wt.% EtOH • $TaCl_5$/n-BuLi		0.42 – 0.50	15.5 – 16.5
	• dense unsupported • 18-20 µm • 6 wt.% EtOH • $NbCl_5$		0.30 – 0.42	15.7 – 18.5

Ref.	Topic	Temperature (°C)	Flux (kg m^{-2} h^{-1})	Separation factor
[55]	• dense unsupported • 52-78 µm • 50 wt.% EtOH • $TaCl_5$	50 – 75	0.8 – 5.0	2 – 6
[56]	• dense unsupported • 100 µm • 10 wt.% EtOH • $TaCl_5$	38 – 75	0.037 – 0.450	8.5
	• dense unsupported • 15-175 µm • 10 wt.% EtOH • $TaCl_5$	75	0.15 – 1.05	4 – 11
	• dense unsupported • 48 µm • 10-70 wt.% EtOH • $TaCl_5$	50	0.5 – 4.0	2 – 16
[59] [60]	• dense unsupported • 100 µm • 10 wt.% EtOH • $TaCl_5$	75	0.5	12
[63]	• dense unsupported • 30 µm • $TaCl_5$ • 10 wt.% EtOH • 7 wt.% CH_3CN • 10 wt.% $(CH_3)_2CO$	30	 0.24 2.20 2.16	 17 101 76
[106]	• dense unsupported • 20 – 70 µm • 3-6 wt.% EtOH • $TaCl_5$	25	0.08 – 0.15	21 – 22
[61]	• unsupported • surface modified with silica • 83-146 µm • 10-90 wt.% EtOH	25	R = 0.005 – 0.040 g m m^{-2} h^{-1}	2 – 16
[107]	• unsupported • surface modified with PFA-*g*-PDMS • 10 wt.% EtOH • $TaCl_5$	40	0.6	20
[62]	• unsupported • PTMSP/PDMS • 5 wt.% EtOH • 32 µm • $TaCl_5$	30	0.02 – 0.8	1 - 18

Ref.	Topic	Temperature (°C)	Specific permeation rate (g m m^{-2} h^{-1})	Separation factor
[108]	• unsupported • PTMSP/PDMS • 7 wt.% EtOH • 30 – 50 µm • $TaCl_5$	30	2.05×10^{-4} - 2.42×10^{-3}	14.6 – 28.3
[109]	• unsupported • fluoroalkyl group • 30 – 50 µm • $TaCl_5$ • 6.9 wt.% EtOH • 6.5 wt.% THF • 6.5 wt.% acetone • 7.1 wt.% acetonitrile • 6.6 wt.% dioxane • 6.9 wt.% 2-propanol	50	 2.25×10^{-2} 1.63×10^{-1} 9.95×10^{-2} 8.95×10^{-2} 5.44×10^{-2} 2.95×10^{-2}	 21.3 77.0 61.0 57.7 24.5 24.6

However, several papers report the synthesis and application of PTMSP-based mixed matrix or organo-mineral membranes in gas separation [92,94,95,110]. These mixed matrix membranes comprise inorganic fillers embedded in a polymer matrix. The inorganic fillers can be either porous (zeolites, carbon molecular sieves) [111-113] or non-porous (silica, clays) [114,115]. Incorporation of the latter in a polymer matrix is known to affect several characteristics of the neat polymer. The mechanical, thermal and chemical stability can be altered, both the physical appearance and electrical conductivity can be changed and the flame retardancy can be improved. For the synthesis of PV membranes, the change in physical appearance by means of disturbance of the polymer chain configuration is the most interesting feature, but also the effects of filler incorporation on the thermal, chemical and mechanical resistance of PTMSP-based membranes are attractive.

Free volume changes in PTMSP due to incorporation of hydrophobic silica have been reported in literature [94,116]. It has been demonstrated that aggregates of the primary silica particles hinder the polymer chain packing and create mesopores of about 1.1 nm in the polymer matrix and hindered the polymer chain packing, resulting in an increase of the initial free volume cavity radius with about 8 % [116]. This increased free volume drastically enhanced the gas permeability, but decreased the reverse selectivity [94]. This thesis will focus on the effect of hydrophobic silica addition, and thus the enhanced free volume, on

the PV properties of PTMSP membranes. No papers on the use of PTMSP-based mixed matrix membranes in PV can be found in the open literature.

Although a significant number of papers has been published on the development of PTMSP-based membranes for application in PV [15,28,55-63,84,104], only dense, unsupported membranes with a thickness ranging from 14 to 175 µm have been prepared, of which the majority has been tested on EtOH/H_2O mixtures. As displayed in Table 1.3, the fluxes of these dense unsupported membranes are generally rather low in the pervaporation of aqueous EtOH mixtures (EtOH < 10 wt.%) and therefore not competitive with commercial PDMS-based hydrophobic membranes. This unfavourable flux clearly affects the economic feasibility of membrane up-scaling and thus impedes their implementation in large scale applications. To meet the requirements of the industry, the fluxes of these PTMSP-based membranes should be significantly enhanced, without affecting the selectivity. Unfortunately, a general target flux and selectivity cannot be set, since the envisaged performance highly depends on the specific case (feed composition, expected purity and throughput, etc.). Moreover, to estimate the optimal flux and selectivity for certain applications, detailed information of the process is needed, which is often hard to retrieve. Therefore the general objective of this thesis was to improve the performance of PTMSP-based membranes to make them perform better than commercial PDMS-based hydrophobic PV membranes, with a specific focus on ethanol/water separations. For the separation of a 5 wt% aqueous EtOH mixture at 30°C, Chovau and co-workers reported for the PERVAP 4060 (Sulzer Chemtech) and Pervatech PDMS (Pervatech) membrane a flux of 0.6 and 1 kg m^{-2} h^{-1}, and an accompanying EtOH/H_2O separation factor of 8.4 and 5.2, respectively [117]. As reference throughout this thesis, both commercial membranes were tested.

1.7 Scope

The Flemish Institute for Technological Research (VITO) has a history in PV research since the late nineties. Originally, the focus was on the dehydration of solvents with commercial membranes. In 2002, K. De Sitter started a PhD on the preparation of organo-mineral membranes by the incorporation of nanoparticles in high free volume polymers. While the main focus of the work was the application of unsupported PTMSP-silica and poly(4-methyl-2-pentyne)-silica membranes in gas separation, few screening tests already indicated the potential of these mixed membranes in PV.

The aim of this thesis was to thoroughly investigate the influence of the hydrophobic silica filler, membrane thickness and free volume on the PV performance of the membranes, and to study/improve the chemical stability of the membranes. A profound understanding of these effects should lead to the synthesis of an optimised, highly selective and/or highly permeable PV membrane which outclasses the commercially available PV membranes in the separation of alcohol/water mixtures.

Figure 1.5 shows a schematic presentation of the different aspects in this work and how they are linked to the main objective "Development, modification and optimisation of poly[1-(trimethylsilyl)-1-propyne] PV membranes".

Most polymeric membranes exhibit a trade-off between flux and selectivity. This means that a membrane could have a low flux in combination with a high separation factor or a higher flux in combination with a lower separation factor. In gas separation this trade-off is described by Robeson's Upper Limit [118,119]. In PV this trade-off is also present, but currently such systematic review has not been performed.

The first topic in this thesis was to **improve** the **flux/selectivity trade-off** of the current PTMSP-based membranes by altering their free volume. This was pursued by several routes, i.e. (1) addition of silica nanoparticles to the polymer matrix, (2) application of a thin defect-free selective PTMSP layer on top of a porous support, (3) post-treatment of the membrane under supercritical CO_2 conditions, or (4) a combination thereof. The second topic aims at **broadening** the **applicability** of the membranes by improving their solvent resistance. This

was achieved by crosslinking the membranes, which also improves the physical stability of the membranes.

The reported results are divided in four chapters.
Chapter 3 presents the influence of membrane thickness, hydrophobic silica and the combination thereof on the free volume and PV performance of dense and supported PTMSP membranes.
Chapters 4 and 5 presented supercritical carbon dioxide ($scCO_2$) as a novel technique to alter the flux/selectivity trade-off. The influence of the pressure and temperature of the $scCO_2$ treatment on the free volume properties and PV performance of the membranes is reported and long term and thermal stability measurements are performed. Finally the reproducibility of the novel treatment is discussed.
In Chapter 5 the combination of the silica filler and a subsequent $scCO_2$ treatment is investigated.
Chapter 6 focuses on the thermally or photochemically induced chemical crosslinking of PTMSP membranes, their characterisation and application in the separation of more demanding feed mixtures.
At the end of the thesis, general conclusions are made, accompanied with suggestions for further work.

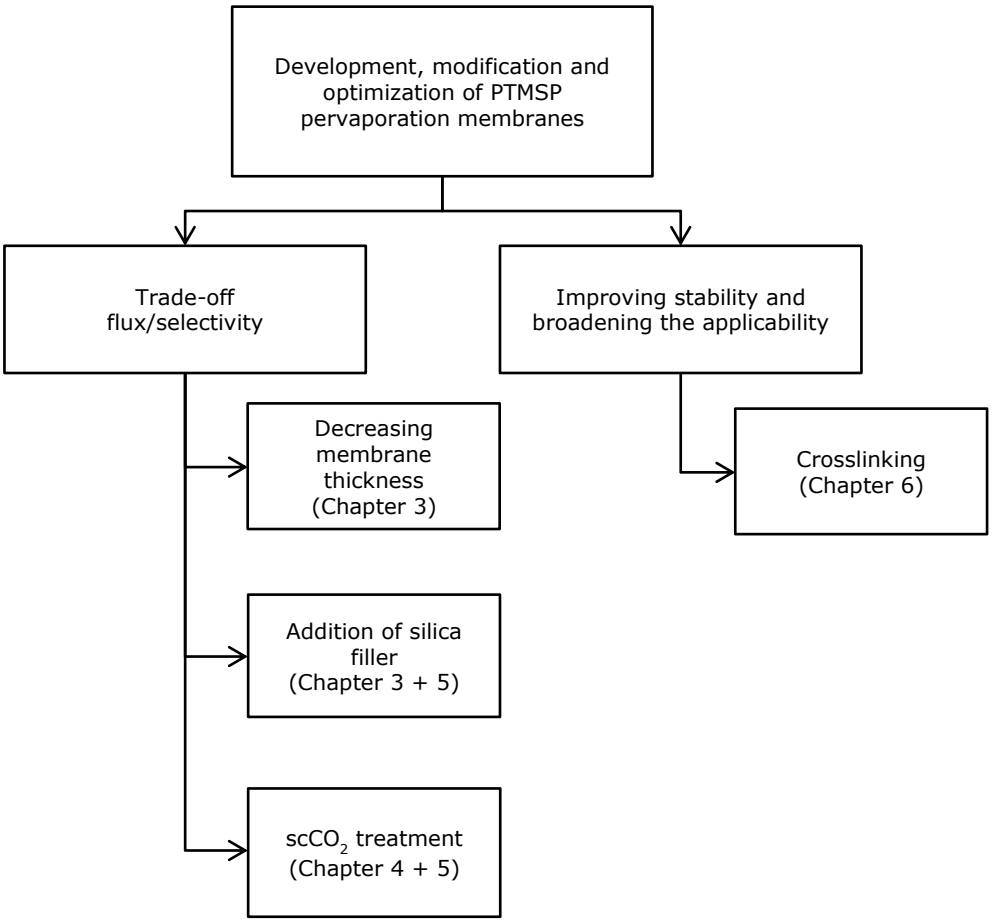

Figure 1.5: Schematic presentation of the different aspects in this work.

REFERENCES

[1] P. A. Kober, Pervaporation, perstillation and percrystallization, *J. Membr. Sci.* **100** (1995) 61 – 64.

[2] L. Farber, Applications of pervaporation, *Science* **82** (1935) 158.

[3] E. G. Heissler, A. S. Hunter, J. Sciliano, R. M. Treadway, Solute and temperature effects in the pervaporation of aqueous alcoholic solutions, *Science* **124** (1956) 77 – 79.

[4] R. C. Binning, R. J. Lee, J. F. Jennings, E. C. Martin, Separation of liquid mixtures by permeation, *ACS Div. Petroleum Chem. Preprints* **3** (1958) 131 – 141.

[5] H. L. Fleming, C. S. Slater, Pervaporation, In: W. S. W. Ho, K. K. Sirkar (Eds.), Membrane handbook, Van Nostrand Reinhold, New York, USA, 1992, pp. 103 – 159.

[6] H. E. A. Brüschke, State-of-art of pervaporation processes in the chemical industry, In: S. P. Nunes, K. V. Peinemann (Eds.), Membrane technology in the chemical industry, Wiley, Weinheim, Germany, 2003, pp. 127 – 172.

[7] A. H. Ballweg, H. E. A. Brüschke, W. H. Schneider, G. F. Tusel, Pervaporation membranes: an economical method to replace conventional dehydration and rectification columns in ethanol distilleries, *Paper at 5th International symposium on alcohol fuel technology*, Auckland, New Zealand, 1982.

[8] Y. Morigami, M. Kondo, J. Abe, H. Kita, K. Okamoto, The first large-scale pervaporation plant using tubular-type module with zeolite NaA membrane, *Sep. Purif. Technol.* **25** (2001) 251 – 260.

[9] A. Jonquières, R. Clément, P. Lochon, J. Néel, M. Dresch, B. Chrétien, Industrial state-of-the-art of pervaporation and vapour permeation in the western countries, *J. Membr. Sci.* **206** (2002) 87 – 117.

[10] M. S. K. Chen, G. R. Markiewicz, K. G. Venugopal, Development of membrane pervaporation TRIM^{TM} process for methanol removal from CH_3OH/MTBE/C_4 mixtures, AlChE, *Symp. Ser.* **85** (1989) 82 – 88.

[11] M. Catarino, A. Mendes, Non-alcoholic beer – a new industrial process, *Sep. Purif. Technol.* **79** (2011) 342 – 351.

[12] M. Peng, L. M. Vane, S. X. Liu, Recent advances in VOCs removal from water by pervaporation, *J. Hazard. Mater.* **B98** (2003) 69 – 90.

[13] W. S. W. Ho, K. K. Sirkar, Overview, In: W. S. W. Ho, L. L. Sirkar (Eds.), Membrane handbook, Van Nostrand Reinhold, New York, USA, 1992, pp. 1 – 15.

[14] M. Mulder, Basic principles of membrane technology, Kluwer Academic Publishers, 2nd edition, Dordrecht, The Netherlands, 1997.

[15] Y. Yampolskii, I. Pinnau, B. D. Freeman, Materials science of membranes for gas and vapor separation, John Wiley & Sons Ltd, Chichester, England, 2007.

[16] R. W. Baker, Membrane technology and applications, John Wiley & Sons Ltd, Chichester, England, 2004.

[17] W. S. W. Ho, L. L. Sirkar (Eds.), Membrane handbook, Van Nostrand Reinhold, New York, USA, 1992.

[18] J. G. Wijmans, R. W. Baker, The solution-difussion model: a review, *J. Membr. Sci.* **107** (1995) 1 – 21.

[19] T. Graham, On the absorption and dialytic separation of gases by colloid septa. Action of a septum of caoutchouc, *Philos. Mag.* **32** (1866) 401 – 420.

[20] J. K. Mitchell, On the penetrativeness of fluids, *J. Membr. Sci.* **100** (1995) 11 – 16.

[21] S. von Wroblewski, Ueber die natur der absorption der gase durch flussigkeiten unten hohen drucken, *Ann Physik u Chem* **8** (1879) 29 – 52.

[22] P. Shao, R. Y. M. Huang, Polymeric membrane pervaporation, *J. Membr. Sci.* **287** (2007) 162 – 179.

[23] A. B. Hadler, L. S. Ott, T. J. Bruno, Study of azeotropic mixtures with the advanced distillation curve approach, *Fluid Phase Equilib.* **281** (2009) 49 – 59.

[24] T. Uragami, H. Matsugi, T. Miyata, Pervaporation characteristics of organic – inorganic hybrid membranes composed of poly(vinyl alcohol-co-acrylic acid) and tetraethoxysilane for water ethanol separation, *Macromolecules* **38** (2005) 8440 – 8446.

[25] B. Bolto, M. Hoang, Z. Xie, A review of membrane selection for the dehydration of aqueous ethanol by pervaporation, *Chem. Eng. Process.* **50** (2011) 227 – 235.

[26] P. D. Chapman, T. Oliveira, A. G. Livingston, K. Li, Membranes for the dehydration of solvents by pervaporation, *J. Membr. Sci.* **318** (2008) 5 – 37.

[27] S. I. Semenova, H. Ohya, K. Soontarapa, Hydrophilic membranes for pervaporation: an analytical review, *Desalination* **110** (1997) 251 – 286.

[28] P. Peng, B. Shi, Y. Lan, A review of membrane materials for ethanol recovery by pervaporation, *Sep. Sci. Technol.* **46** (2011) 234 – 246.

[29] G. Busca, S. Berardinelli, C. Resini, L. Arrighi, Technologies for the removal of phenol from fluid streams: A short review of recent developments, *J. Hazard. Mater.* **160** (2008) 265 – 288.

[30] L. M. Vane, A review of pervaporation for product recovery from biomass fermentation processes, *J. Chem. Technol. Biotechnol.* **80** (2005) 603 – 629.

[31] B. Smitha, D. Sunhanya, S. Sridhar, M. Ramakrishna, Separation of organic-organic mixtures by pervaporation – a review, *J Membr. Sci.* **241** (2004) 1 – 21.

[32] J. P. G. Villaluenga, A. T. Mohammadi, A review on the separation of benzene/cyclohexane mixtures by pervaporation processes, *J. Membr. Sci.* **169** (2000) 159 – 174.

[33] F. Lipnizki, S. Hausmanns, P. K. Ten, R. W. Field, G. Laufenberg, Organophilic pervaporation: prospects and performance, *Chem. Eng. J.* **73** (1999) 113 – 129.

[34] M. L. Gimenes, L. Liu, X. S. Feng, Sericin/poly(vinyl alcohol) blend membranes for pervaporation separation of alcohol/water mixtures, *J. Membr. Sci.* **295** (2007) 71 – 79.

[35] V. S. Praptowidodo, Influence of swelling on water transport through PVA-based membrane, *J. Mol. Struct.* **739** (2005) 207 – 212.

[36] M. Rafik, A. Mas, M. F. Guimon, C. Guimon, A. Elharfi, F. Schulé, Plasma-modified poly(vinyl alcohol) membranes for the dehydration of ethanol, *Polym. Int.* **52** (2003) 1222 – 1229.

[37] W. Y. Chiang, Y. H. Lin, Properties of modified poly(vinyl alcohol) membranes prepared by the grafting of new polyelectrolyte copolymers for water–ethanol mixture separation, *J. Appl. Polym. Sci.* **86** (2002) 2854 – 2859.

[38] C. H. Lee, W. H. Hong, Influence of different degrees of hydrolysis of poly(vinyl alcohol) membrane on transport properties in pervaporation of IPA/water mixture, *J. Membr. Sci.* **135** (1997) 187 – 193.

[39] Y. M. Sun, T. L. Huang, Pervaporation of ethanol–water mixtures through temperature-sensitive poly(vinyl alcohol–g–*N*–isopropyacrylamide) membranes, *J. Membr. Sci.* **110** (1996) 211 – 218.

[40] E. Ruckenstein, L. Liang, Pervaporation of ethanol–water mixtures through polyvinyl alcohol-polyacrylamide interpenetrating polymer network membranes unsupported and supported on polyethersulfone ultrafiltration membranes: a comparison, *J. Membr. Sci.* **110** (1996) 99 – 107.

[41] E. Ruckenstein, L. Liang, Poly(acrylic acid)-poly(vinyl alcohol) semi- and interpenetrating polymer network pervaporation membranes, *J. Appl. Polym. Sci.* **62** (1996) 973 – 987.

[42] L. Liang, E. Ruckenstein, Polyvinyl alcohol - polyacrylamide interpenetrating polymer network membranes and their pervaporation characteristics for ethanol–water mixtures, *J. Membr. Sci.* **106** (1995) 167 – 182.

[43] A. Yamasaki, T. Iwatsubo, T. Masuoka, K. Mizoguchi, Pervaporation of ethanol/water through a poly(vinyl alcohol)/cyclodextrin (PVA/CD) membrane, *J. Membr. Sci.* **89** (1994) 111 – 117.

[44] Y. S. Kang, S. W. Lee, U. Y. Kim, Y. S. Shim, Pervaporation of water–ethanol mixtures through crosslinked and surface-modified poly(vinyl alcohol) membrane, *J. Membr. Sci.* **51** (1990) 215 – 226.

[45] S. Sommer, T. Melin, Performance evaluation of microporous inorganic membranes in the dehydration of industrial solvents, *Chem. Eng. Process.* **44** (2005) 1138 – 1156.

[46] H. L. Castricum, G. G. Paradis, M. C. Mittelmeijer-Hazeleger, R. Kreiter, J. F. Vente, J. E. ten Elshof, Tailoring the separation behavior of hybrid organosilica membranes by adjusting the structure of the organic bridging group, *Adv. Funct. Mater.* **21** (2011) 2319 – 2329.

[47] H. L. Castricum, R. Kreiter, H. M. van Veen, D. H. A. Blank, J. F. Vente, J. E. ten Elshof, High-performance hybrid pervaporation membranes with superior hydrothermal and acid-stability, *J. Membr. Sci.* **324** (2008) 111 – 118.

[48] H. L. Castricum, A. Sah, R. Kreiter, D. H. A. Blank, J. F. Vente, J. E. ten Elshof, Hybrid ceramic nanosieves: stabilizing nanopores with organic links, *Chem. Commun.* **9** (2008) 1103 – 1105.

[49] W. Liu, B. Li, R. Cao, Z. Jiang, S. Yu, G. Liu, H. Wu, Enhanced pervaporation performance of poly(dimethylsiloxane) membrane by incorporating titania microspheres with high silver ion loading, *J. Membr. Sci.* **378** (2011) 382 – 392.

[50] S. Chovau, A. Dobrak, A. Figoli, F. Galiano, S. Simone, E. Drioli, S. K. Sikdar, B. Van der Bruggen, Pervaporation performance of unfilled and filled PDMS membranes and novel SBS membranes for the removal of toluene from diluted aqueous solutions, *Chem. Eng. J.* **159** (2010) 37 – 46.

[51] A. Dobrak, A. Figoli, S. Chovau, F. Galiano, S. Simone, I. F. J. Vankelecom, E. Drioli, B. Van der Bruggen, Performance of PDMS membranes in pervaporation: Effect of silicalite fillers and comparison with SBS membranes, *J. Colloid Interface Sci.* **346** (2010) 254 – 264.

[52] S. Y. Li, R. Srivastava, R. S. Parnas, Separation of 1-butanol by pervaporation using a novel tri-layer PDMS composite membrane, *J. Membr. Sci.* **363** (2010) 287 – 294.

[53] I. Rutkiewicz, W. Kujawski, J. Namieśnik, Pervaporation of volatile organohalogen compounds through polydimethylsiloxane membrane, *Desalination* **264** (2010) 160 – 164.

[54] K. Okamoto, A. Butsuen, S. Tsuru, S. Nishioka, K. Tanaka, H. Kita, S. Asakawa, Pervaporation of water-ethanol mixtures through polydimethylsiloxane block-copolymer membranes, *Polym. J.* **I9** (1987) 747 – 756.

[55] C. López-Dehesa, J. A. González-Marcos, J. R. González-Valesco, Pervaporation of 50 wt.% ethanol-water mixtures with poly(1-trimethylsilyl-1-propyne) membranes at high temperatures, *J. Appl. Polym. Sci.* **103** (2007) 2843 – 2848.

[56] J. A. González-Marcos, C. López-Dehesa, J. R. González-Valesco, Effect of operation conditions in the pervaporation of ethanol-water mixtures with poly(1-trimethylsilyl-1-propyne) membranes, *J. Appl. Polym. Sci.* **94** (2004) 1395 – 1403.

[57] V. V. Volkov, A. G. Fadeev, V. S. Khotimsky, E. G. Litvinova, Y. A. Selinskaya, J. D. McMillan, S. S. Kelley, Effects of synthesis conditions on the pervaporation properties of poly[1-(trimethylsilyl)-1-propyne] useful for membrane bioreactors, *J. Appl. Polym. Sci.* **91** (2004) 2271 – 2277.

[58] A. G. Fadeev, S. S. Kelley, J. D. McMillan, Y. A. Selinskaya, V. S. Khotimsky, V. V. Volkov, Effect of yeast fermentation by-products on poly[1-(trimethylsilyl)-1-propyne] pervaporative performance, *J. Membr. Sci.* **214** (2003) 229 – 238.

[59] J. R. González-Valesco, C. López-Dehesa, J. A. González-Marcos, Pervaporation performance of PTMSP membranes at high temperatures, *J. Appl. Polym. Sci.* **90** (2003) 2255 – 2259.

[60] J. R. González-Valesco, J. A. González-Marcos, C. López-Dehesa, Pervaporation of ethanol-water mixtures through poly(1-trimethylsilyl-1-propyne) (PTMSP) membranes, *Desalination* **149** (2002) 64 – 65.

[61] S. Ulutan, T. Nakagawa, Separability of ethanol and water mixtures through PTMSP-silica membranes in pervaporation, *J. Membr. Sci.* **143** (1998) 275 – 284.

[62] Y. S. Kang, E. M. Shin, B. Jung, J. J Kim, Composite membranes of poly(1-trimethylsilyl-1-propyne) and poly(dimethylsiloxane) and their pervaporation properties for ethanol-water mixture, *J. Appl. Polym. Sci.* **53** (1994) 317 – 323.

[63] T. Masuda, M. Takatsuka, B. Z. Tang, T. Higashimura, Pervaporation of organic liquid - water mixtures through substituted polyacetylene membranes, *J. Membr. Sci.* **49** (1990) 69 – 83.

[64] H. Matuschewski, U. Schedler, MSE – modified membranes in organophilic pervaporation for aromatics/aliphatics separation, Desalination **224** (2008) 124 – 131.

[65] F. Lipnizki, R. W. Field, P. K. Ten, Pervaporation-based hybrid process: a review of process design, applications and economics, *J. Membr. Sci.* **153** (1999) 183 – 210.

[66] V. Van Hoof, L. Van den Abeele, A. Buekenhoudt, C. Dotremont, R. Leysen, Economic comparison between azeotropic distillation and different hybrid systems combining distillation with pervaporation for the dehydration of isopropanol, *Sep. Purif. Technol.* **37** (2004) 33 – 49.

[67] Y. Naidu, R. K. Malik, A generalized methodology for optimal configurations of hybrid distillation-pervaporation processes, *Chem. Eng. Res. Design* **89** (2011) 1348 – 1361.

[68] Q. Liu, Z. Zhang, H. Chen, Study on the coupling of esterification with pervaporation, *J. Membr. Sci.* **182** (2001) 173 – 181.

[69] Y. Zhu, H. Chen, Pervaporation separation and pervaporation-esterification coupling using crosslinked PVA composite catalytic membranes on porous ceramic plate, *J. Membr. Sci.* **138** (1998) 123 – 134.

[70] X. Feng, R. Y. M. Huang, Studies of a membrane reactor: Esterification facilitated by pervaporation, *Chem. Eng. Sci.* **51** (1996) 4673 – 4679.

[71] A. Hasanoğlu, Y. Salt, S. Keleşer, S. Dincer, The esterification of acetic acid with ethanol in a pervaporation membrane reactor, *Desalination* **245** (2009) 662 – 669.

[72] K. Tanaka, R. Yoshikawa, C. Ying, H. Kita, K. Okamoto, Application of zeolite membranes to esterification reactions, *Catal. Today* **67** (2001) 121 – 125.

[73] V. García, J. Päkkilä, H. Ojamo, E. Muurinen, R.L. Keiski, Challenges in biobutanol production: How to improve the efficiency, *Renew. Sust. Energy Rev.* **15** (2011) 964 – 980.

[74] M. Kumar, K. Gayen, Developments in biobutanol production: new insights, *Appl. Energy* **88** (2011) 1999 – 2012.

[75] H. Huang, H. Liu, Y.R. Gan, Genetic modification of critical enzymes and involved genes in butanol biosynthesis from biomass, *Biotechnol. Adv.* **28** (2010) 651 – 657.

[76] H. J. Huang, S. Ramaswamy, U. W. Tschirner, B. V. Ramarao, A review of separation technologies in current and future biorefineries, *Sep. Purif. Technol.* **62** (2008) 1 – 21.

[77] S. Bashir, S. Lee, Fuel ethanol-production from agricultural lignocellulosic feedstocks – a review, *Fuel Sci. Technol. Int.* **12** (1994) 1427 – 1473.

[78] K. Kraemer, A. Harwardt, R. Bronneberg, W. Marquardt, Separation of butanol from acetone-butanol-ethanol fermentation by a hybrid extraction-distillation process, *Comput. Chem. Eng.* **35** (2011) 949 – 963.

[79] W. Kaminski, E. Tomczak, A. Gorak, Biobutanol – production and purification methods, *Ecol. Chem. Eng. Sci.* **18** (2011) 31 – 37.

[80] K. Inokuma, J.C. Liao, M. Okamoto, T. Hanai, Improvement of isopropanol production by metabolically engineered Escherichia coli using gas stripping, *J. Biosci. Bioeng.* **110** (2010) 696 – 701.

[81] A. Converti, P. Perego, A. Lodi, G. Fiorito, M. Delborghi, G. Ferraiolo, In situ ethanol recovery and substrate recycling during continuous alcohol fermentation, *Bioprocess Eng.* **7** (1991) 3 – 10.

[82] W. J. Groot, M. C. H. den Reyer, T. B. de la Faille, R. G. J. M. van der Lans, K. C. A. M. Luyben, Integration of pervaporation and continuous butanol fermentation with immobilized cells. 1. Experimental results, *Chem. Eng. J. Biochem. Eng. J.* **46** (1991) B1 – B10.

[83] G. Liu, W. Wei, H. Wu, X. Dong, M. Jiang, W. Jin, Pervaporation performance of PDMS/ceramic composite membrane in acetone butanol ethanol (ABE) fermentation-PV coupled process, *J. Membr. Sci.* **373** (2011) 121 – 129.

[84] A. G. Fadeev, M. M. Meagher, S. S. Kelley, V. V. Volkov, Fouling of poly[-1-(trimethylsilyl)-1-propyne] membranes in pervaporative recovery of butanol from aqueous solutions and ABE fermentation broth, *J. Membr. Sci.* **173** (2000) 133 – 144.

[85] K. Nagai, T. Masuda, T. Nakagawa, B. D. Freeman, I. Pinnau, Poly[1-(trimethylsilyl)-1-propyne] and related polymers: synthesis, properties and functions, *Prog. Polym. Sci.* **26** (2001) 721 – 798.

[86] J. J. Bi, C. L. Wang, Y. Kobayashi, K. Ogasawara, A. Yamasaki, Effect of the casting solvent on the free-volume characteristics and gas permeability of poly[1-(trimethylsilyl)-1-propyne] membranes, *J. Appl. Polym. Sci.* **87** (2003) 497 – 501.

[87] G. Consolati, I. Genco, M. Pegoraro, L. Zangerighi, Positron annihilation lifetime (PAL) in poly[1-(trimethylsilyl)propyne] (PTMSP): Free volume determination and time dependence of permeability, *J. Polym. Sci. Part B: Polym. Phys.* **34** (1996) 357 – 367.

[88] I. Pinnau, L. G. Toy, Transport of organic vapors through poly(1-trimethylsilyl-1-propyne), *J. Membr. Sci.* **116** (1996) 199 – 206.

[89] T. Masuda, E. Isobe, T. Higashimura, K. Takada, Poly[1-(trimethylsilyl)-1-propyne] – a new high polymer synthesized with transition-metal catalysts and characterized by extremely high gas-permeability, *J. Am. Chem. Soc.* **105** (1983) 7473 – 7474.

[90] D. B. Knorr, L. S. Kocherlakota, R. M. Overney, Insight into reverse selectivity and relaxation behavior of poly[1-(trimethylsilyl)-1-propyne] by flux-lateral force and intrinsic friction microscopy, *J. Membr .Sci.* **346** (2010) 302 – 309.

[91] K. De Sitter, A. Andersson, J. D'Haen, R. Leysen, S. Mullens, F. H. J. Maurer, I. F. J. Vankelecom, Silica filled poly(4-methyl-2-pentyne) nanocomposite membranes: similarities and differences with poly(1-trimethylsilyl-1-propyne)-silica systems, *J. Membr. Sci.* **321** (2008) 284 – 292.

[92] S. D. Kelman, R. D. Raharjo, C. W. Bielawski, B. D. Freeman, The influence of crosslinking and fumed silica nanoparticles on mixed gas transport properties of poly[1-(trimethylsilyl)-1-propyne], *Polymer* **49** (2008) 3029 – 3041.

[93] S. D. Kelman, S. Matteucci, C. W. Bielawski, B. D. Freeman, Crosslinking poly(1-trimethylsilyl-1-propyne) and its effect on solvent resistance and transport properties, *Polymer* **48** (2007) 6881 – 6892.

[94] K. De Sitter, P. Winberg, J. D'Haen, C. Dotremont, R. Leysen, J. A. Martens, S. Mullens, F. H. J. Maurer, I. F. J. Vankelecom, Silica filled poly(1-trimethylsilyl-1-propyne) nanocomposite membranes: Relation between the transport of gases and structural characteristics, *J. Membr. Sci.* **278** (2006) 82 – 91.

[95] D. Gomes, S. P. Nunes, K. V. Peinemann, Membranes for gas separation based on poly(1-trimethylsilyl-1-propyne)-silica nanocomposites, *J. Membr. Sci.* **246** (2005) 13 – 25.

[96] A. Hill, S. J. Pas, T. J. Bastow, M. I. Burgar, K. Nagai, L. G. Toy, B. D. Freeman, Influence of methanol conditioning and physical aging on carbon spin-lattice relaxation times of poly(1-trimethylsilyl-1-propyne), *J. Membr. Sci.* 243 (2004) 37 – 44.

[97] A.G. Fadeev, M. M. Meagher, Poly(1-trimethylsilyl-1-propyne) regeneration process, US 6.423.119, 2002.

[98] L. Shao, J. Samseth, M. B. Hägg, Crosslinking and stabilization of nanoparticle filled poly(1-trimethylsilyl-1-propyne) nanocomposite membranes for gas separation, *J. Appl. Polym. Sci.* **113** (2009) 3078 – 3088.

[99] J. Peter, K. V. Peinemann, Multilayer composite membranes for gas separation based on crosslinked PTMSP gutter layer and partially crosslinked Matrimid® 5218 selective layer, *J. Membr. Sci.* **340** (2009) 62 – 72.

[100] S. D. Kelman, B. W. Rowe, C. W. Bielawski, S. J. Pas, A. J. Hill, D. R. Paul, B. D. Freeman, Crosslinking poly[1-(trimethylsilyl)-1-propyne] and its effect on physical stability, *J. Membr. Sci.* **320** (2008) 123 – 134.

[101] S. D. Kelman, R. D. Raharjo, C. W. Bielawski, B. D. Freeman, The influence of crosslinking and fumed silica nanoparticles on mixed gas transport properties of poly[1-(trimethylsilyl)-1-propyne], *Polymer* **49** (2008) 3029 – 3041.

[102] L. Shao, J. Samseth, M. B. Hägg, Crosslinking and stabilization of high fractional free volume polymers for gas separation, *Int. J. Greenh. Gas Control* **2** (2008) 492 – 501.

[103] J. Jia, G. L. Baker, Crosslinking of poly[1-(trimethylsilyl)-1-propyne] membranes using bis(aryl azides), *J. Polym. Sci. B: Polym. Phys.* **36** (1998) 959 – 968.

[104] A. G. Fadeev, Y. A. Selinskaya, S. S. Kelley, M. M. Meagher, E. G. Litvinova, V. S. Khotimsky, V. V. Volkov, Extraction of butanol from aqueous solutions by pervaporation through poly(1-trimethylsilyl-1-propyne), *J. Membr. Sci.* **186** (2001) 205 – 217.

[105] A. V. Volkov, V. V. Volkov, V. S. Khotimskii, Membranes based on poly[(1-trimethylsilyl)-1-propyne] for liquid-liquid separation, *Polym. Sci. Ser. A* **51** (2009) 1367 – 1382.

[106] S. L. Schmidt, M. D. Myers, S. S. Kelley, J. D. McMillan, N. Padukone, Evaluation of PTMSP membranes in achieving enhanced ethanol removal from fermentations by pervaporation, *Appl. Biochem. Biotech.* **63-65** (1997) 469 – 482.

[107] T. Uragami, T. Doi, T. Miyata, Control of permselectivity with surface modifications of poly[1-(trimethylsilyl)-1-propyne] membranes, *Int. J. Adhes. Adhes.* **19** (1999) 405 – 409.

[108] Y. Nagase, K. Ishihara, K. Matsui, Chemical modification of poly(substituted-polyacetylene) II. Pervaporation of ethanol/water mixture through poly(1-trimethylsilyl-1-propyne)/poly(dimethylsiloxane) graft copolymer membrane, *J. Polym. Sci. Part B: Polym. Phys.* **28** (1990) 377 – 386.

[109] Y. Nagase, K. Sugimoto, Y. Takamura, K. Matsui, Chemical modification of poly(substituted-polyacetylene) VI. Introduction of fluoroalkyl group into poly(1-trimethylsilyl-1-propyne) and the improved ethanol permselectivity at pervaporation, *J. Appl. Polym. Sci.* **43** (1991) 1227 – 1232.

[110] T. C. Merkel, B. D. Freeman, R. J. Spontak, Z. He, I. Pinnau, P. Meakin, A. J. Hill, Ultrapermeable, reverse-selective nanocomposite membranes, *Science* **296** (2002) 519 – 522.

[111] D. R. Paul, D. R. Kemp, The diffusion time lag in polymer membranes containing adsorptive fillers, *J. Polym. Sci Pol. Sym.* **41** (1973) 79 – 93.

[112] D. Q. Vu, W. J. Koros, S. J. Miller, Mixed matrix membranes using carbon molecular sieves: I. preparation and experimental results, *J. Membr. Sci.* **211** (2003) 311 – 334.

[113] E. Okumus, T. Gurkan, L. Yilmaz, Development of mixed-matrix membrane for pervaporation, *Separ. Sci. Technol.* **29** (1994) 2451 – 2473.

[114] S. G. Adoor, M. Sairam, L. S. Manjeshwar, K. V. S. N. Raju, T. M. Aminabhavi, Sodium montmorillonite clay loaded novel mixed matrix membranes of poly(vinyl alcohol) for pervaporation dehydration of aqueous mixtures of isopropanol and 1,4-dioxane, *J. Membr. Sci.* **285** (2006) 182 – 195.

[115] L. Wang, X. Han, J. Li, X. Zhan, J. Chen, Hydrophobic nano-silica/polydimethylsiloxane membrane for dimethylcarbonate-methanol separation via pervaporation, *Chem. Eng. J.* **171** (2011) 1035 – 1044.

[116] P. Winberg, K. De Sitter, C. Dotremont, S. Mullens, I. F. J. Vankelecom, F. H. J. Maurer, Free volume ad interstitial mesopores in silica filled poly(1-trimethylsilyl-1-propyne) nanocomposites, *Macromolecules* **38** (2005) 3766 – 3782.

[117] S. Chovau, S. Gaykawad, A. J. J Straathof, B. Van der Bruggen, Influence of fermentation by-products on the purification of ethanol from water using pervaporation, *Bioresource Technol.* **102** (2011) 1669 – 1674.

[118] L. M. Robeson, Correlation of separation factor versus permeability for polymeric membranes, *J. Membr. Sci.* **62** (1991) 165 – 185.

[119] L. M. Robeson, The upper bound revisited, *J. Membr. Sci.* **320** (2008) 390 – 400.

Chapter 2

Experimental methods

2.1 Introduction

This chapter discusses the used materials and experimental membrane preparation and characterization methods. Only the most frequently used characterization techniques are described, more sporadically used techniques will be discussed separately in each chapter. Firstly, several polymer characterization techniques are discussed, i.e. (1) Gel Permeation Chromatography (GPC), (2) X-ray Fluorescence (XRF) Spectroscopy and (3) rheology measurements. Next, the membrane characterisation techniques applied in this work are discussed, i.e. (4) Scanning Electron Microscopy (SEM), (5) Positron Annihilation Lifetime Spectroscopy (PALS) and (6) PV tests.

2.2 Materials

The selection of membrane-forming materials is extremely important and has to fit the application to obtain a good performance in the envisaged application. In this section it is motivated why PTMSP is chosen as selective polymer and why hydrophobic silica is used as filler material.

2.2.1 PTMSP

In Chapter 1, the chemical structure (Figure 1.4) and peculiar properties of PTMSP have already been discussed. The main reason for selecting PTMSP as PV membrane material is its extremely **high free volume fraction** that can be attributed to the bulky trimethylsilyl-side groups and the stiff main chain, rendering membranes with extremely high gas/vapour permeabilities [1]. Furthermore, PTMSP is a **hydrophobic** polymer with a water contact angle of

80-90° [2] and is thus suitable for the manufacturing of hydrophobic PV membranes. Finally, PTMSP shows a **high solubility** in common solvents (e.g. toluene, cyclohexane and tetrahydrofuran) and **mechanically stable membranes** can be formed by solution casting [1]. For each newly received polymer batch, the molecular weight (M_w) and amount of residual catalyst are determined by GPC and XRF, respectively. The viscosity of the suspensions is measured for each composition and polymer batch.

2.2.2 Hydrophobic silica

The free volume fraction of the PTMSP matrix can be further increased by the incorporation of hydrophobic silica particles, increasing the permeability even more [3-6]. Hydrophobic silica, Cab-O-Sil TS-530, was purchased from Cabot (Germany). By treating the fumed silica with hexamethyldisilazane, many of the surface hydroxyl groups are replaced by trimethylsilyl groups, making the silica extremely hydrophobic (Figure 2.1). The silica powder has a B.E.T. surface area of 225 $m^2\ g^{-1}$ and a specific gravity of 2.2 g cm^{-3}, and exists as aggregates with an average length of 0.2-0.3 μm.

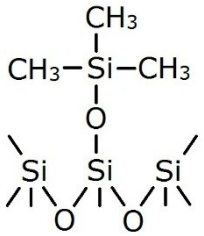

Figure 2.1: Surface chemistry of Cab-O-Sil TS-530.

2.3 Membrane preparation

Throughout this thesis, two different preparation methods are used for the manufacturing of PTMSP-based PV membranes. Both procedures use toluene-based suspensions. The first method is applied for the preparation of unsupported dense PTMSP(-silica) membranes, the second for the manufacturing of supported thin film membranes.

2.3.1 Polymer suspensions

Toluene-based polymer(-silica) suspensions were prepared according to De Sitter *et al.* [3-5]. Pure PTMSP solutions were prepared by dissolving the desired amount of polymer in toluene. After magnetically stirring the polymer solution for 4 days and measuring the viscosity, the homogeneous PTMSP solution can be either poured in a Petri dish to obtain a dense unsupported membrane, or applied as a thin film on a porous support using a tape-casting process (Figure 2.2).

The preparation of PTMSP-silica suspensions, on the other hand, involved an extra step to disperse the silica particles in the solvent. A precisely measured amount of silica was added to toluene and treated for 30 minutes in an ultrasonic bath from Branson (USA, MT-5210, 40 kHz - 185W). To this dispersion, PTMSP was added and the mixture was magnetically stirred for 4 days (Figure 2.2).

A clear distinction should be made between the silica concentrations in the polymer suspension and in the final membrane. For dry membranes the amount of silica is expressed on total solids basis (0, 2.5, 10, 20, 25 or 50 wt.%). The composition of the suspensions, on the other hand, takes into account the solvent. For example, a membrane containing 10 wt.% silica (c_{Si_m}), could be prepared from a polymer-silica suspension containing 97 wt.% toluene, 2.7 wt.% polymer (c_{P_s}) and 0.3 wt.% silica (c_{Si_s}).

$$c_{Si_m} = \frac{c_{Si_s}}{c_{Si_s} + c_{P_s}} \qquad (2\text{-}1)$$

The total solids concentration in the suspension varies between 3 and 10 wt.%, depending on the M_w and thus viscosity of the suspension.

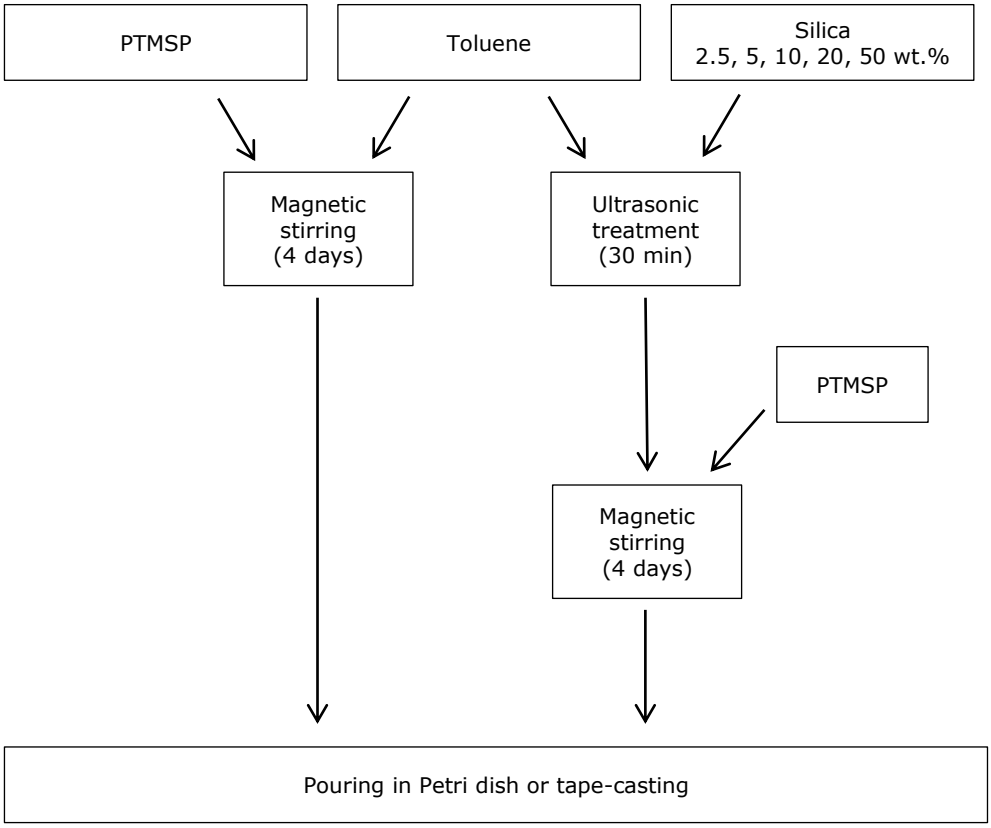

Figure 2.2: Schematic presentation of the membrane synthesis steps.

2.3.2 Unsupported membranes

Unsupported dense membranes were prepared by pouring the polymer solution or polymer-silica suspension in a Petri dish (d ≈ 9 cm), followed by a delayed evaporation under a glass bell for 10 days at room temperature. To remove the residual toluene, the membranes were then thermally treated in a vacuum oven at 70 °C for 1 h. Unsupported membranes with a thickness between 30 and 200 µm were obtained. The membrane thickness could be varied by changing the volume of suspension poured into the Petri dish.

2.3.3 Supported thin-film membranes

A widely used technique to decrease the thickness of polymer membranes is by applying it as a thin, selective layer on top of a porous support. The porous support is typically an ultrafiltration (UF) membrane of 100 – 500 µm thickness

and provides mechanical stability to the selective layer. The advantages of such **thin film composite (TFC) membranes** are the ability of optimising both layers independently and the possibility of applying extremely thin top layers. The separating layer can be as thin as a few hundreds of nanometres. Considering the importance of the support for the performance of TFC membranes, Chapter 3 discusses the properties of several porous support membranes that have been studied.

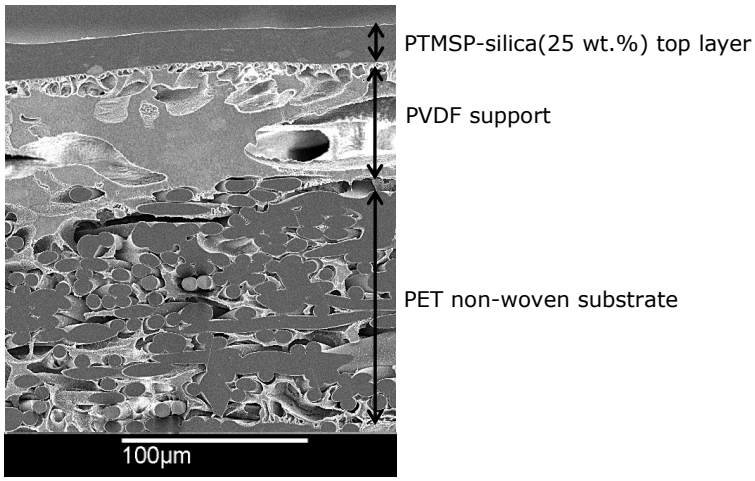

Figure 2.3: SEM (250 ×, 5.0 keV) image of the cross-section of a typical TFC membrane prepared in this work.

Figure 2.3 shows a SEM image of a typical TFC membrane prepared in this work. The SEM image displays a PTMSP-silica(25 wt.%) selective layer on top of a porous polyvinylidene fluoride (PVDF) supported membrane, which is in turn backed by a polyethylene terephthalate (PET) non-woven. The non-woven consists of a collection of PET fibres that are pressed together under heat, anchoring the fibres together and rendering an extremely mechanically stable and highly porous fabric. The surface of such non-woven substrate is however not sufficiently smooth to permit direct casting of a thin selective layer on top. Therefore, a porous PVDF membrane is applied on top of the non-woven by phase-inversion. In the latter process a polymer is controllably transformed from a liquid to a solid state, rendering membranes with a wide range of

morphologies depending on the used parameters [7]. In this work two different phase inversion processes are reported:

1. **Precipitation by solvent evaporation**: The polymer is dissolved in a volatile solvent, which is evaporated after tape-casting. This technique renders dense homogeneous membranes and is used in this work for the preparation of both unsupported PTMSP membranes (paragraph 2.3.2) and supported thin film PTMSP membranes.

2. **Immersion precipitation:** A polymer solution is cast as a thin film on top of a suitable support, after which the liquid film is immersed in a coagulation bath containing a nonsolvent. Pore formation and solidification of the film occur because of the exchange of solvent and nonsolvent. The porous support membranes of the PTMSP top layers are prepared by this technique. Various membrane morphologies can be obtained by changing the preparation parameters, such as the composition of the casting solution (polymer concentration, solvent type, possible additives, etc.) and of the coagulation bath.

All phase inversion processes are based on the same thermodynamic principles. The starting point is always a thermodynamically stable polymer solution which is subjected to demixing. Figure 2.4 shows the phase diagram of a ternary phase inversion system subjected to instantaneous demixing. The thermodynamically stable solution corresponding to composition point 1 is cast on a support and immersed in a coagulation bath, which contains the non-solvent. Almost instantaneously ($t < 1$ s), the composition path crosses the binodal, entering the unstable region. In this unstable region, demixing in a polymer-rich phase (point 2) and a polymer-lean phase (point 3) occurs. These phases respectively develop into the solid matrix and the pores of the ultimate membrane. The tie line connects the compositions of the polymer-rich and polymer-lean phase with the same chemical potential which are thus in equilibrium with each other. By instantaneous demixing which occurs when the solvent and non-solvent are

readily miscible, porous membranes (micro- and ultrafiltration) are obtained. This mutual affinity ensures a quick non-solvent diffusion into the solidifying film and solvent diffusion into the coagulation bath, hence fast demixing kinetics.

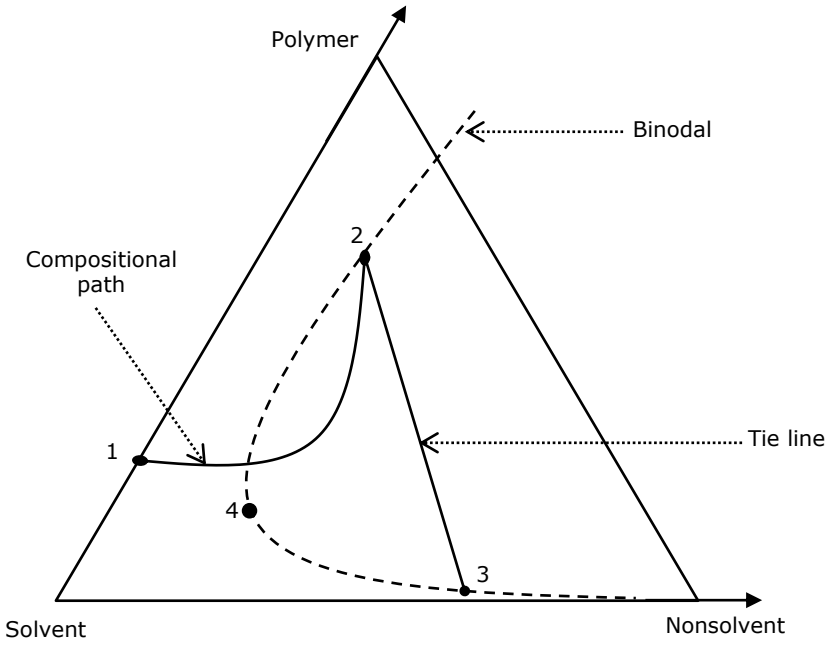

Figure 2.4: Ternary phase diagram with a liquid-liquid demixing gap. (1) starting composition of polymer solution (composition bottom of film), (2) polymer-rich phase (composition top of film), (3) polymer-lean phase, (4) critical point [7].

The membrane morphology is strongly dependent on the location and shape of the compositional path (Figure 2.4). Factors that affect the compositional path and thus the morphology are [7]:

- Polymer selection
- Composition of casting solution, i.e. concentration of polymer, solvent and possible additives (salts, non-solvents, co-solvents, etc.)
- Thickness of the cast film
- Composition and temperature of coagulation bath
- Evaporation time and conditions (humidity, temperature) of cast film prior to immersion in coagulation bath (dry-wet phase inversion)
- Gelation and crystallisation behaviour of the polymer

Both the thin-film PTMSP layers and the porous support membranes are prepared by tape-casting, using an automatic thin film applicator (Braive Instruments, Belgium) and a doctor blade with adjustable casting gap (Figure 2.5). The four primary factors affecting the film thickness in tape-casting are (1) the casting blade gap, (2) casting speed, (3) suspension viscosity and (4) reservoir height [8]. The doctor blade was placed on top of the substrate, filled with an excess of polymer(-silica) suspension, and subsequently moved along the substrate by the automatic film applicator set at a coating velocity of 3.4×10^{-2} m s^{-1}.

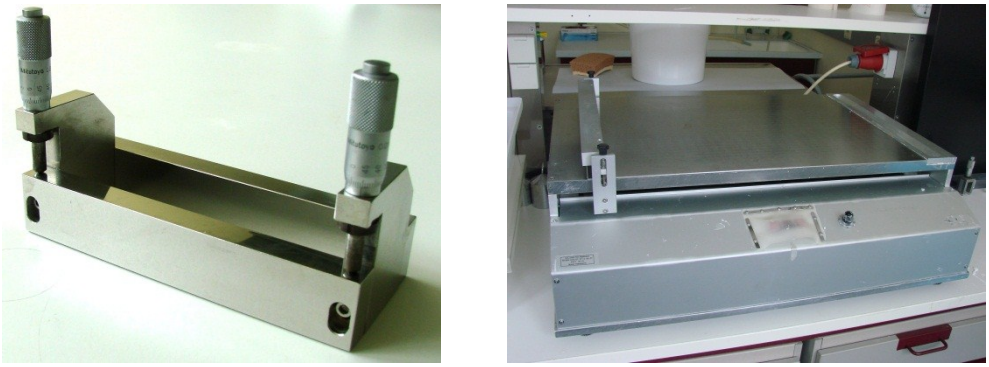

(a) (b)

Figure 2.5: (a) Doctor blade and (b) automatic film applicator used in this work.

2.4 Characterization

Throughout this thesis several characterization techniques are used, covering both fundamental and more applied aspects of polymers and membranes. In this section the most frequently used characterization techniques are described, while additional techniques are discussed in the following chapters.

2.4.1 Gel Permeation Chromatography

One of the most important polymer properties with regard to membrane synthesis is the polymer's molecular weight. It determines the rheology of the casting suspension and can affect the polymer chain orientation in the membrane and thus its permeation properties. In GPC or size exclusion

chromatography, a dilute polymer solution is injected onto a column which is packed with porous beads. The low molecular weight fraction can enter the pores more easily and therefore spend more time in these pores, increasing their retention time. The higher molecular weight polymers on the other hand, spend little if any time in the pores and will therefore elute quickly. A polymer's molecular weight distribution can thus be derived from the elution profile of all fractions [7]. If standards of a known size are run previously, a calibration curve is obtained allowing to determine the size of the polymer molecules.
From each PTMSP batch, a sample was dissolved in THF and injected on a TSP GPC column with a Shodex RI-71 refractometer. The column was calibrated with polystyrene (PS) standards. From the GPC curves, the weight average molecular weight (M_w), the number average molecular weight (M_n) and polydispersity index ($P_d = M_w/M_n$) are derived.

2.4.2 X-ray Fluorescence Spectroscopy

The polymerisation of PTMSP occurs in the presence of a $TaCl_5$ catalyst, which is washed out after completion of the reaction. Unfortunately, as the purification step is complicated due to the stiffness and high M_w of the PTMSP chains, the catalyst is partially entrapped in the polymer. The tantalum (Ta) concentration, as a measure of the amount of residual catalyst in each polymer batch, was determined by XRF. The sample is irradiated with high energy X-rays or gamma rays, ionizing the atoms. Once the irradiation is stopped, the excited electrons emit characteristic secondary X-rays when falling back to their equilibrium energy state. These photons with characteristic wavelength are detected and assigned to specific chemical elements. In this work, a WDXRF type SRS 3000 from Bruker (Belgium), controlled by Spectraplus® software, was used.

2.4.3 Rheology measurements

The viscosity of the PTMSP(-silica) suspensions is of great importance for the tape-casting process since it directly influences the final layer thickness [8]. Viscosity measurements were performed on a HAAKE Modular Advanced Rheometer System (Germany) equipped with a cylindrical Z41 titanium measuring geometry and controlled by RheoWin® software. During the

isothermal measurements at 25 °C, the shear rate was linearly increased to 500 s^{-1} in 300 s, then kept constant for 30 s, and finally decreased to 0 s^{-1} in 300 s.

2.4.4 Scanning Electron Microscopy

SEM analysis was used to determine the surface porosity of the UF support membranes, the thickness of the different layers of the TFC membranes and the size of the silica aggregates in the PTMSP membranes. A JEOL cold field emission scanning electron microscope (FEGSEM) type JSM6340F (Japan) was used to observe membrane surfaces and cross-sections at an acceleration voltage of 5 keV. Cross-sections were obtained by a JEOL cross-section polisher type SM-09010 which uses an argon ion beam. To avoid charging under the electron beam during SEM observation or in the cross-section polisher, the samples were coated with a thin Pt(80)/Pd(20) (surface) or Au (cross-section) layer (~1.5 nm) using a Cressington 208 HR (UK) and a Balzers Union SCD 040 (Liechtenstein) high-resolution sputter-coater, respectively. Surface porosities were determined from the SEM images using ImageJ software, as described by Mullens *et al.* [9].

2.4.5 Positron Annihilation Lifetime Spectroscopy

2.4.5.1 Theory

PALS is a non-destructive technique which can be used to probe the free volume cavity sizes in a polymer sample. While this technique was initially used to determine defects in metals, semi-conductors and zeolites, during the last 20 years it has also been applied in polymer science [10-12]. The positrons are used to acquire information about the electrons and their properties in condensed matter. Figure 2.6 shows a schematic presentation of the principle of PALS.

A positron is the anti-particle of the electron with the same mass but an opposite charge. It is emitted during the radioactive decay of instable isotopes like ^{22}Na. Together with the formation of such a positron, a γ-ray with an energy of 1.28 MeV is emitted. When entering condensed matter, the positron will thermalize or lose kinetic energy due to elastic and inelastic collisions with molecules of the surrounding media, causing ionization of these molecules.

Along the path of thermalization, electrons, positive ions and radicals are formed [10,11]. The last part of the thermalization, just before the positron loses all its kinetic energy, is called the positron spur. The positron could annihilate with an electron as 'free' positron, thereby emitting two γ-rays of 511 keV in about 0.3 – 0.5 ns. Alternatively, a positron could form a meta-stable bond with one of the spur-electrons, i.e. a positronium (Ps). Depending on the spin of the positron and the electron, two types of Ps can be formed. In *para*-positronium (*p*-Ps), the positron and electron spins are opposite, while in *ortho*-positronium (*o*-Ps) they are parallel [12]. The *p*-Ps is instable and will annihilate after 125 ps, emitting two γ-rays of 511 keV. The *o*-Ps is more stable and will only exhibit intrinsic annihilation in vacuum after 142 ns, with the formation of three γ-rays. In condensed matter however, the *o*-Ps lifetime decreases to 1 – 6 ns before it annihilates with a surrounding electron of opposite spin and emits two γ-ray of 511 keV, a phenomenon referred to as pick-off annihilation. The *o*-Ps and positron lifetimes are thus determined by the electron density in the sample. For high free volume polymers, the large free volume cavities have a low electron density and thus a larger *o*-Ps lifetime is expected since it takes longer for the *o*-Ps to find an electron to annihilate with. The lifetime of these positrons can be measured by the detection of the emitted γ-rays. The start signal is detected as the 1.28 MeV γ-ray emitted during the formation of the positron, while the 511 keV γ-rays emitted upon annihilation represent the stop signal.

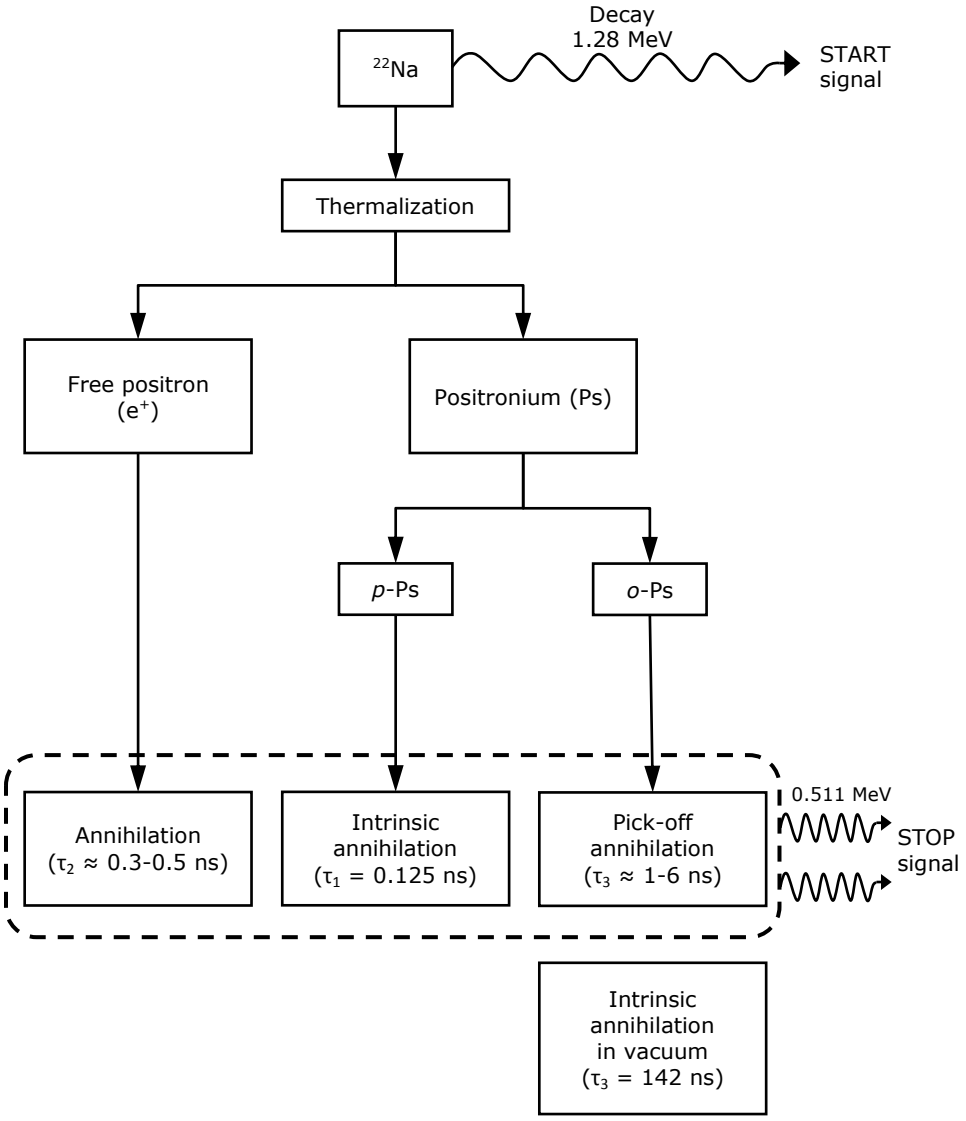

Figure 2.6: Positron annihilation process in condensed matter.

During PALS analysis a spectrum is obtained (Figure 2.7) which is built up of several decaying exponential components (Equation 2-1) [13]:

$$f(t) = R(t) \times \sum_{j=1}^{k_0} A_j e^{-t/\tau_j} + B \quad (2\text{-}1)$$

$$I_j = \frac{A_j \tau_j}{\sum_{j=1}^{k_0} A_j \tau_j} \quad (2\text{-}2)$$

with $f(t)$ the model function, $R(t)$ a time resolution function, k_0 the number of decaying exponentials, A_j the pre-exponential factor, t the time, τ the value of the mean lifetime, I_j the relative intensity (%) and B the constant background. The experimentally obtained spectra differ from the analytical description by convolution with the time resolution function $R(t)$. The latter is equipment dependent and is a sum of Gaussians obtained from reference measurements on Kapton® foils. Kapton® polyimide foil is used as a reference since it has a distinct spectrum which is well known by researchers. Any deviation from this theoretical spectrum is compensated for by the generated time resolution function, which can thus be considered as a compensation function for all artifacts of the experimental setup.

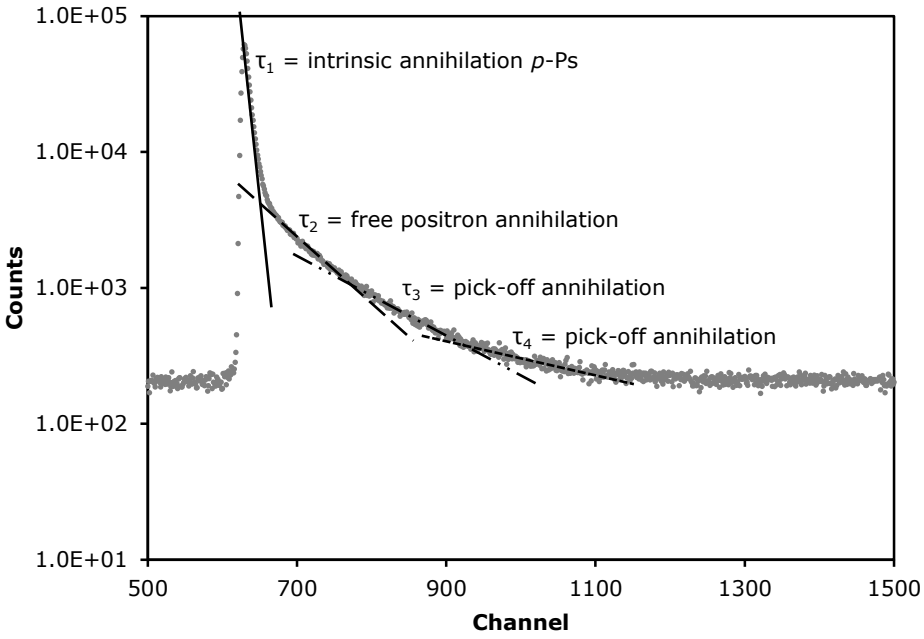

Figure 2.7: A typical positron lifetime spectrum of a PTMSP sample. The tangent lines indicate contributions from annihilation of *p*-Ps, free positrons and *o*-Ps. The tangent lines are only for illustrative purpose.

For most polymers, three lifetime components can be detected, but PTMSP exhibits four lifetime components. The third *o*-Ps lifetime component (τ_3) represents the channel like holes, interconnecting the larger cages, represented by the fourth *o*-Ps lifetime component (τ_4) [6]. The pick-off annihilation thus consists of two components, each representing a distinct free volume cavity size distribution. In mixed matrix PTMSP-silica membranes, a fifth *o*-Ps lifetime component (τ_5) is present, describing the mesopores in the silica aggregates [6]. The size of the free volume cavities can be deduced from the Tao-Eldrup equation [14,15]. This model relates the free volume cavity radius (R) and size v_{o-Ps} to the *o*-Ps lifetime (τ_{o-Ps}) according to the following semi-empirical relationships [14,15]:

$$\tau_{o-Ps} = 0.5\left(1 - \frac{R}{R_0} + \frac{1}{2\pi} sin\frac{2\pi R}{R_0}\right)^{-1} \qquad (2\text{-}3)$$

$$v_{o-Ps} = \frac{4\pi R^3}{3} \quad (2\text{-}4)$$

This Tao-Eldrup model assumes that *o*-Ps is localized in an infinite spherical potential well with a radius R_0 covered by an electron layer with a thickness $\Delta R = R_0 - R$. The model does not take into account the irregular structure of free volume cavities. This semi-empirical relationship has been validated using a number of molecular solids and zeolites and has been successfully applied to *o*-Ps lifetimes in several polymers assuming an electron layer thickness of 0.166 nm [14]. Together with each *o*-Ps lifetime (τ), the PALS measurements yield an intensity (I) which expresses the relative probability of *o*-Ps formation. The *o*-Ps lifetime intensity (I_{o-Ps}) is primarily determined by the availability of electrons with which a positron can combine to form a Ps. Therefore I_{o-Ps} is strongly dependent on the chemical nature of the sample, as well as on the irradiation dose, exposure to visible light and temperature. High electron affinity groups, like nitro and halogen groups, can reduce the electron availability and thus Ps yield [12,16,17]. Since I_{o-Ps} is influenced by the chemical nature, it does not reveal any information on the number of free volume cavities.

2.4.5.2 Experimental

A ^{22}Na salt, encapsulated between two sheets of Kapton® polyimide foil, was used as the positron source. The samples were applied in a sandwich configuration with the PTMSP films being stacked at a total thickness of 1 mm on either side of the source. During the measurements, each spectrum was built up of 2.5 million counts. The spectra were recorded on a fast-fast coincidence spectrometer system equipped with CsF crystals. All samples were measured five times and the spectra were analyzed with PALSFIT 1.54 software.

2.4.6 Pervaporation tests

PV measurements were carried out on a laboratory-developed test unit, shown in Figure 2.8. Two Amafilter test cells (The Netherlands), type TPA 025, with an effective membrane area of 3.7 cm² each, were used. The feed was circulated with a Speck centrifugal pump (UK), model PY-2071.0671. A HAAKE immersion heating circulator with microprocessor control (USA), type DC3, and a stainless

steel bath with an internal volume of 3 L (HAAKE, type B3) were used to keep the feed at the desired temperature. Heating elements were placed on top of the permeate vessels to prevent the pipelines from freezing and early condensation of the permeate vapours in the piping. Vacuum at the permeate side of both membranes was maintained with a Pfeiffer rotary vane vacuum pump (Germany), type DUO 5M, and monitored on a Leybold-Heraeus thermovac system (Germany), type TM 220.

Two circular disks with a diameter of 25 mm were cut from the same membrane sheet, placed into the test cells and sealed with Viton or Kalrez O-rings. Subsequently the feed mixture was circulated through the unit and membrane test cells at approximately 12 L h^{-1}. The feed was kept isothermally, and the vapour-side pressure was maintained at approximately 0.04 mbar. The permeates were condensed in two stainless steel vessels, each immersed in a cooling cylinder filled with liquid nitrogen. The permeates collected during the first 2-3 hours were discarded because of the initial non-equilibrium conditions. After, permeate samples were collected during at least 3-4 more hours. The onset of steady-state conditions was determined by collecting permeate samples each hour and measuring the membrane performances as a function of filtration time. For all PV tests, steady-state conditions were reached after approximately 3 h, since the standard deviation of flux and selectivity corresponding to two subsequent permeate samples did not exceed 3 and 6 %, respectively.

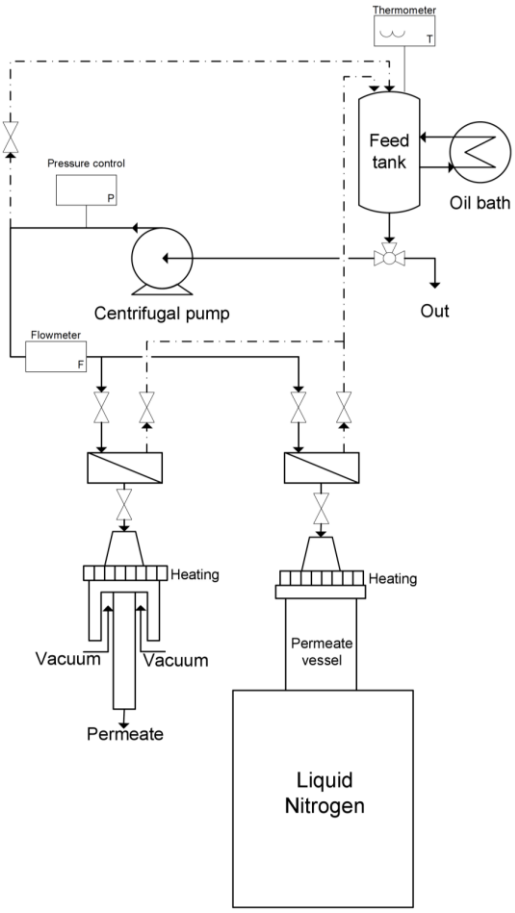

(a)

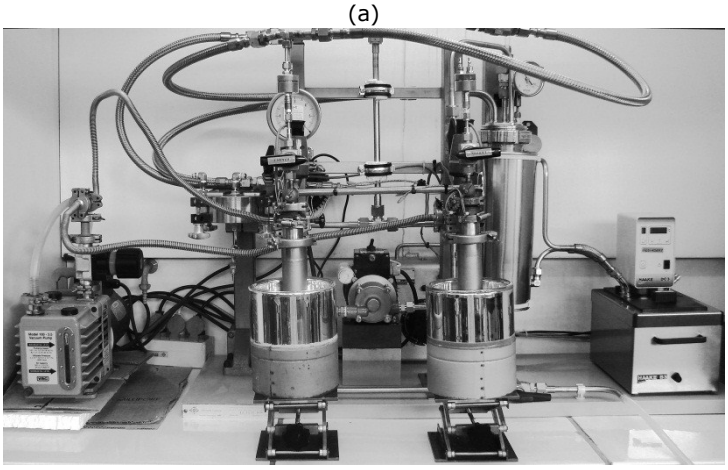

(b)

Figure 2.8: (a) Schematic presentation and (b) picture of the PV test unit.

Feed, concentrate and permeate samples were analysed for water on a semi-automatic, volumetric Metrohm Karl-Fisher (KF) titrator (Belgium), model 720 KFS, equipped with a 703 Ti stand and a platinum electrode. This titration is based on the reaction between iodine and sulphur dioxide in an aqueous medium:

$$I_2 + SO_2 + 2H_2O \leftrightarrows 2HI + H_2SO_4$$

This reaction occurs after injection of the sample in a pyridine/methanol solution. For each mole of water, one mole of iodine is consumed. Once all the water is consumed, the presence of excess iodine can be detected voltametrically by the platinum electrode; this is the end of the titration. The amount of water is then quantified by the volume of used KF reagent.
Figure 2.9 displays the KF calibration curve of an EtOH/H_2O mixture at room temperature. Each mixture is measured three times and the average and standard deviation of the measurements are plotted as a function of the H_2O concentration of the prepared model mixtures. For high H_2O concentrations (90 - 100 wt.%), the standard deviation increases, indicating a decrease in sensitiveness of the KF titration in this region. This means that for the measurement of the feed and retentate samples the accuracy is somewhat lower. Therefore, at least three KF titrations were performed on all PV samples (feed, retentate and permeate) and the average values were used in the calculation of the separation factor.

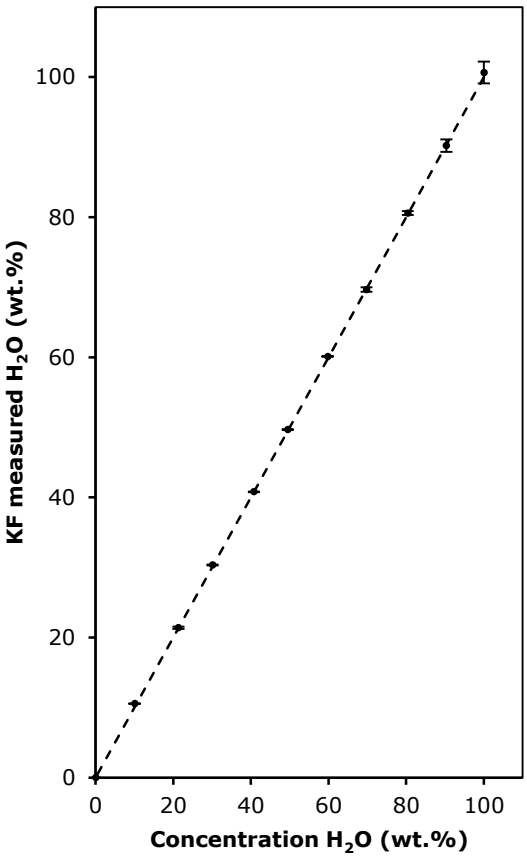

Figure 2.9: KF calibration curve for an EtOH/H_2O mixture at room temperature.

Membrane fluxes J (kg m^{-2} h^{-1}) were determined by weighing the permeates at the end of each test, and calculated according to Equation 2-5:

$$J = \frac{m}{A\,t} \tag{2-5}$$

where m denotes the weight of permeated liquid per unit membrane area A and time t.

To facilitate comparison of flux data in this work, thickness-corrected fluxes or specific permeation rates R (m kg m^{-2} h^{-1}) are reported. These are obtained by multiplying the flux J with the membrane thickness l, as expressed by Equation 2-6:

$$R = \frac{l\,m}{A\,t} \quad (2\text{-}6)$$

The membrane thickness of unsupported membranes was determined with an analogue Mitutoyo micrometre Series 102 (The Netherlands). For the supported membranes, the PTMSP top layer thickness was determined via SEM image analysis (ImageJ software).

The A/H_2O separation factor α_{A/H_2O} was calculated according to Equation 2-7:

$$\alpha_{A/H_2O} = \frac{Y_A}{Y_{H_2O}} \times \frac{X_{H_2O}}{X_A} \quad (2\text{-}7)$$

in which X and Y represent the weight fractions in the feed and permeate, respectively.

To summarize membrane flux and separation factor in one figure of merit, the PV separation index (PSI) was calculated using [18]:

$$PSI = J\,(\alpha - 1) \quad (2\text{-}8)$$

where J is expressed in kg m^{-2} h^{-1}.

REFERENCES

[1] K. Nagai, T. Masuda, T. Nakagawa, B. D. Freeman, I. Pinnau, Poly[1-(trimethylsilyl)-1-propyne] and related polymers: synthesis, properties and functions, *Prog. Polym. Sci.* **26** (2001) 721 – 798.

[2] T. Uragami, T. Doi, T. Miyata, Control of permselectivity with surface modifications of poly[1-(trimethylsilyl)-1-propyne] membranes, *Int. J. Adhes. Adhes.* **19** (1999) 405 – 409.

[3] K. De Sitter, A. Andersson, J. D'Haen, R. Leysen, S. Mullens, F. H. J. Maurer, I. F. J. Vankelecom, Silica filled poly(4-methyl-2-pentyne) nanocomposite membranes: Similarities and differences with poly(1-trimethylsilyl-1-propyne)-silica systems, *J. Membr. Sci.* **321** (2008) 284 – 292.

[4] K. De Sitter, P. Winberg, J. D'Haen, C. Dotremont, R. Leysen, J. A. Martens, S. Mullens, F. H. J. Maurer, I. F. J. Vankelecom, Silica filled poly(1-trimethylsilyl-1-propyne) nanocomposite membranes: Relation between the transport of gases and structural characteristics, *J. Membr. Sci.* **278** (2006) 83 – 91.

[5] K. De Sitter, R. Leysen, S. Mullens, I. Vankelecom, F. Maurer, Silica filled poly(1-trimethylsilyl-1-propyne) and poly(4-methyl-2-pentyne) membranes: similarities and differences in structural characteristics and membrane performance, *Desalination* **199** (2006) 293 – 295.

[6] P. Winberg, K. De Sitter, C. Dotremont, S. Mullens, I. F. J. Vankelecom, F. H. J. Maurer, Free volume and interstitial mesopores in silica filled poly(1-trimethylsilyl-1-propyne) nanocomposites, *Macromolecules* **38** (2005) 3776 – 3782.

[7] M. Mulder, Basic principles of membrane technology, Kluwer Academic Publishers, Dordrecht, The Netherlands, 1997, pp. 71 – 156.

[8] R. E. Mistler, E. R. Twiname, Tape casting: theory and practice, The American Ceramic Society, Ohio, USA, 2000, pp. 127 – 143.

[9] S. Mullens, J. Luyten, J. Zeschky, Characterization of structure and morphology, in: M. Sheffler, P. Colombo (Eds.), Cellular Ceramics, Wiley-VCH, Weinheim, 2005, pp. 227–263.

[10] Y. C. Jean, P. E. Mallon, D. M. Schrader, Principles and application of positron & positronium chemistry, World Scientific, London, 2003.

[11] D. M. Schrader, Y. C. Jean, Positron and positronium chemistry, Elsevier, New York, 1988.

[12] O. E. Mogensen, Positron annihilation in chemistry, Spinger-Verlag, Berlin, 1995.

[13] P. Kirkegaard, J. V. Olsen, M. Eldrup, N. J. Pedersen, PALSfit: A computer program for analysing positron lifetime spectra, RisØ National Laboratory for Sustainable Energy, RisØ-R-1652 (2009).

[14] M. Eldrup, D. Lightbody, J. N. Sherwood, The temperature-dependence of positron lifetimes in solid pivalic acid, *Chem. Phys.* **63** (1981) 51 – 58.

[15] S. J. Tao, Positronium annihilation in molecular substances, *J. Chem. Phys.* **56** (1972) 5499 – 5510.

[16] K. Hirata, Y. Kobayashi, Y. Ujihira, Effect of halogenated compounds on positronium formation in polycarbonate and polysulfone matrices, *J. Chem. Soc. – Faraday Trans.* **93** (1997) 139 – 142.

[17] A. E. Hamielec, M. Eldrup, O. Mogensen, P. Jansen, Positron-annihilation techniques in polymer science and engineering, *J. Macromol. Sci. – Rev. Macromol. Chem. Phys.* **C9** (1973) 305 – 337.

[18] R. Y. M. Huang, C. K. Yeom, Pervaporation separation of aqueous mixtures using crosslinked poly(vinyl alcohol) (PVA). II. Permeation of ethanol-water mixtures, *J. Membr. Sci.* **51** (1990) 273 – 292.

Chapter 3

Thin film silica filled PTMSP membranes

3.1 Introduction

For the separation of EtOH/H_2O mixtures, several commercial PDMS-based membranes are available, e.g. Pervatech PDMS, Sulzer PERVAP 4060 and Solsep 3360. The latter is sold as a nanofiltration membrane, but shows fluxes up to 1.8 kg m^{-2} h^{-1} and an EtOH/H_2O separation factor of 8 in the PV of a 5 wt.% EtOH/H_2O mixture at 44 °C [1]. Fluxes of 0.550 and 0.995 kg m^{-2} h^{-1} and separation factors of 8.4 and 5.2 have been reported for PERVAP 4060 and Pervatech PDMS membranes, respectively, in the separation of a 5 wt.% EtOH/H_2O feed mixture at 30 °C [2].

PTMSP membranes are known to exhibit much higher EtOH/H_2O separation factors and would result in high fluxes if applied as thin films. Table 1.3 provides an overview of PTMSP-based PV membranes in the separation of EtOH/H_2O mixtures. A broad range of fluxes (0.015 – 1.05 kg m^{-2} h^{-1}) and separation factors (2 – 22) is reported for aqueous feed mixtures containing up to 10 wt.% EtOH. All reported PTMSP membranes are dense and unsupported with thicknesses ranging from 14 to 175 µm. According to the solution-diffusion model, in an ideal system the membrane flux is inversely proportional to the membrane thickness as expressed by Equation 1-8. Decreasing the membrane thickness would thus result in an enhanced permeability. However it remains to be seen whether in practice, in non-ideal membrane preparation conditions, the membrane thickness and flux still correspond to this simple inverse linear relationship and which effect top layer reduction has on the separation factor.

Besides decreasing the top layer thickness, altering the free volume of a polymer could also significantly affect the membrane performance. Addition of

hydrophobic silica is known to positively affect the free volume of polyacetylene membranes [3-7]. The silica particles form aggregates in the PTMSP matrix and the interstitial cavities in between the primary particles of these silica aggregates, result in significantly increased gas fluxes [4,7].

Inspired by the beneficial effect of silica on the gas flux of PTMSP membranes [3-7] and the theoretical inverse flux-thickness proportionality, this chapter describes the synthesis of highly permeable and selective, supported PTMSP-silica membranes. The preparation of thin film composite silica filled PTMSP membranes and their application in PV has never been reported in literature. Firstly, the used porous support membranes are characterized. Subsequently, the influence of the hydrophobic silica filler and of the top layer thickness on the membrane performance is investigated. All prepared membranes are tested in the separation of a 5 wt.% EtOH/H_2O mixture at 50 °C and benchmarked with commercial hydrophobic PV membranes.

3.2 Experimental

3.2.1 Materials

Porous support membranes were prepared from polyacrylonitrile (PAN, $M_w \sim 5.10 \times 10^5$ g mol^{-1}), purchased from Faserwerke Lingen GmbH (Germany), and polyvinylidene fluoride (PVDF, $M_w \sim 5.73 \times 10^5$ g mol^{-1}, Solef 1015/1001), supplied by Solvay Solexis (France). The polyester fabric 3701 was obtained from Ahlstrom (USA). The PVDF-based UF membrane NADIR® MV020T was purchased from Microdyn Nadir GmbH (Germany).

Selective top layers were prepared from PTMSP ($M_w \sim 250 \times 10^3$ g mol^{-1}, Pd = 3.85 and 0.43 wt.% Ta) obtained from Gelest, Inc. (USA), and hydrophobic silica (Cab-O-Sil TS 530) purchased from Cabot (Germany).

The commercial hydrophobic PV membranes PERVAP 4060 and Pervatech PDMS were purchased from Sulzer ChemTech (Switzerland) and Pervatech BV (The Netherlands), respectively.

Toluene, ethanol (EtOH) and 1-butanol (BuOH), were obtained from Merck (Belgium), N-methyl-2-pyrrolidone (NMP) and formaldehyde from Acros Organics (Belgium). All solvents were of analytical grade and used as received.

Dextrans with a molecular weight of 10, 40 and 500 kDa and sodium nitrate ($NaNO_3$) were purchased from Sigma-Aldrich (Belgium).

3.2.2 Membrane preparation

3.2.2.1 Support membranes

Support membranes were prepared from NMP-based casting solutions containing 15 wt.% PAN or PVDF. After 1 day of magnetic stirring, the homogeneous dope solutions (typically 20 ml) were cast on a polyester fabric using an automatic film applicator and a doctor blade set at a casting gap of 300 µm. Immediately after casting, the nascent polymer films (typically 560 cm^2) were immersed in a distilled water bath at room temperature where demixing and solidification took place. After 30 min, the membranes were removed from the coagulation bath and gently boiled for 1 h in distilled water, and subsequently cooled down to room temperature and stored in an aqueous formaldehyde solution (1 wt.%) to inhibit pore collapse and microbial growth.

3.2.2.2 Unsupported PTMSP(-silica) membranes

To investigate the influence of the silica filler on the membrane performance, dense unsupported PTMSP(-silica) membranes were prepared. Unfilled and silica filled PTMSP films were prepared from toluene solutions containing 3 wt.% of solids (polymer and filler). Toluene-based hydrophobic silica dispersions were prepared at a silica concentration of 0.6, 0.9 and 1.5 wt.%, then PTMSP was added so as to obtain polymer concentrations of 2.4, 2.1 and 1.5 wt.%, respectively. The viscosity of these suspensions decreased with increasing filler loading. Since these membranes were synthesized by pouring the suspension in a Petri dish (Chapter 2), the viscosity was less important for controlling the membrane thickness.

3.2.2.3 Supported PTMSP(-silica) membranes

Three PTMSP(-silica) solutions, each containing 5 wt.% PTMSP and either 0, 1.7 or 5 wt.% silica, were prepared. Casting solutions containing 25 and 50 wt.% of silica on total solids basis were thus prepared, as well as a reference solution containing 5 wt.% of PTMSP and no silica.

The viscosity of the polymer suspensions is shown in Figure 3.1. The suspension containing 5 wt.% silica exhibit shear thinning behavior, while the suspension containing 1.7 wt.% silica and reference PTMSP solution behave as a Newtonian fluid. In contrast to the suspensions used for the preparation of the unsupported membranes (paragraph 3.2.2.2), the viscosity of these suspensions increases with the silica filler loading since the total solid concentration increases with increasing silica filler content.

The solutions were tape-casted as thin layers on top of the selected support membrane (Chapter 2) using a doctor blade and an automatic film applicator. After 24 h of evaporation in ambient air, the resulting composite membranes were thermally treated for 1 h at 70 °C in a vacuum oven to remove the residual toluene. The final membrane sheets (14 cm × 40 cm) were stored under dry conditions. By varying the casting gap of the doctor blade between 30 and 500 µm, supported PTMSP-silica nanohybrid membranes with varying dry membrane thickness were prepared.

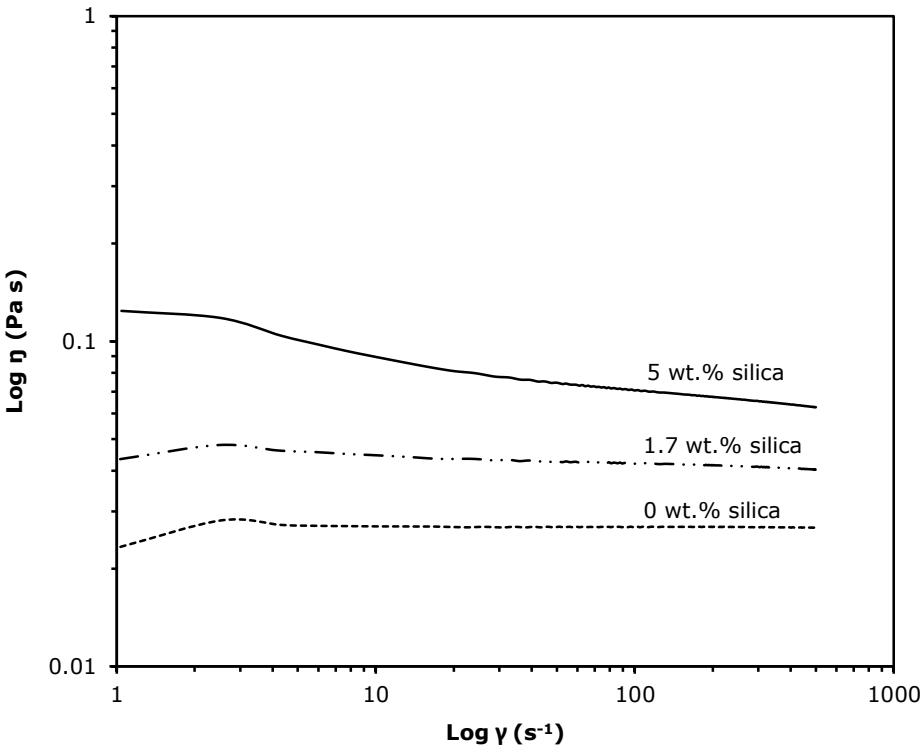

Figure 3.1: Viscosity of suspensions containing 5 wt.% PTMSP as a function of the shear rate and the silica filler load in the suspension.

3.2.3 Membrane characterization

3.2.3.1 Clean water flux

A Minitan™ test cell (Millipore, USA) was used for the filtration experiments on the porous support membranes. Distilled water was circulated over the membrane by a CRN2 centrifugal pump (Grundfos, Belgium). All filtration parameters were monitored and controlled through in-house developed Mefias® software. For each membrane, the clean water flux (l m^{-2} h^{-1}) was gravimetrically measured at three different pressures. By plotting fluxes against pressure, the mass transfer coefficient *k* (l m^{-2} h^{-1} bar^{-1}) could be derived as the slope of the curve. The *k* value was used as an indicator for the affinity of water for the membrane and its degree of porosity.

3.2.3.2 *Molecular weight cut-off (MWCO)*

MWCO experiments on the porous support membranes were performed on the same filtration cell as used for the clean water flux measurements (see Section 3.2.3.1), according to a European standard procedure, developed in the framework of the CHARMME network [8,9]. An aqueous mixture of three dextrans with different molecular weights (10, 40 and 500 kDa) present at a concentration of 0.1 wt.% each and containing 0.1 wt.% $NaNO_3$, was circulated over the membrane at a constant cross-flow velocity of 2 m s^{-1} and a permeate flux around 40 l m^{-2} h^{-1}. Once a stable flux was reached, concentrate and permeate samples were collected and analysed on a Waters gel permeation chromatograph. The chromatographic system consisted of a HPLC pump type 510, an auto sampler type 717 plus, and a refractive index detector type 2414. The samples were injected on an ultrahydrogel 500 column coupled to an ultrahydrogel 120 column (7.8 × 300 mm), and Millenium 32 software was used to control the system. For each molecular weight of dextran, the individual retention was calculated as 1 - C_p C_r^{-1}, where C_p and C_r denote the solute concentrations of the permeate and retentate, respectively. By plotting the retentions against the molecular weights of the dextrans, cut-off curves were obtained, from which the MWCO value was deduced as the solute size that is retained for 90%.

3.2.3.3 Contact angle

Contact angle measurements are indicative for the surface chemistry of the porous support membranes, and thus for the adhesion of the selective PTMSP layers that are applied on top. A good adhesion is crucial for the integrity of the final composite membrane. The contact angle, which is a quantitative measure of the wettability of a solid, is geometrically defined as the angle formed by a liquid at the three phase boundary where liquid, gas and solid intersect. Measurements were performed on a Data Physics type OCA 15+ system (Germany) according to the static sessile drop method. A droplet of water was placed on a dry membrane sample and the angle formed between the liquid/solid interface and the liquid/vapour interface was determined by a high-resolution camera and SCA 20 software.

3.2.3.4 Surface roughness

A smooth support is expected to enhance the overall quality, i.e. homogeneity and defect-freeness, of PTMSP(-silica) top layers. On the other hand, a certain roughness might enhance the adhesion between top layer and support. A Veeco optical 3D profiling system, type Wyko NT3300 (Germany), was used to determine the surface roughness. Air-dried support samples were placed in the centre of the sample table and stabilized under vacuum. The samples were focused by carefully lowering the objective without contacting the surface. Average roughness values were calculated according to:

$$R_a = \frac{1}{n}\sum_{i=1}^{n}|y_i| \qquad (3\text{-}1)$$

where R_a is the average roughness, n the number of measurements and y the measured height.

3.2.3.5 PALS

PALS was used to demonstrate the difference in free volume among the unsupported dense PTMSP(-silica) membranes. Unfortunately, the available setup is not designed to perform measurements on thin film supported membranes.

The count rate during the PALS analyses was 590 s^{-1} and each spectrum was built up of 2.5 million counts. The unfilled PTMSP sample was analysed with a four-component analysis, while the filled samples were analysed with a five-component analysis. The third *o*-Ps lifetime (τ_3) represents the channel-like holes interconnecting the larger cages which are in turn represented by the fourth *o*-Ps lifetime (τ_4). The extra fifth *o*-Ps lifetime (τ_5) represents the interstitial cavities created by the silica aggregates [3-6]. The variance of fit was close to unity (0.98–1.1) for all performed analyses.

3.3 Characterization and selection of porous support

In general, a support should offer mechanical stability to the top layer and be highly porous to ensure high fluxes in PV. On the other hand, the surface should be sufficiently smooth to allow the application of a thin, defect-free PTMSP-silica layer on top. Table 3.1 reveals no significant difference in surface roughness between the two supports synthesized in this work. The commercially available PVDF membrane on the other hand, has a slightly rougher surface. Both PVDF membranes show a larger water contact angle than the PAN membrane, suggesting a more hydrophobic membrane surface. The difference in contact angle between the laboratory-prepared and commercial PVDF membrane could be partially explained by the variation in surface roughness, which influences the contact angle measurements.

Table 3.1: Overview of support membrane properties.

Characteristic	Membrane		
	PAN[†]	PVDF[†]	MV020T[‡]
k (l m^{-2} h^{-1} bar^{-1})[a]	397	576	1954
MWCO (kDa)[b]	633 ± 123	876 ± 69	/
Surface roughness (µm)[b]	1.4 ± 0.4	1.4 ± 0.1	1.7 ± 0.1
Water contact angle (°)[b]	44 ± 1	79 ± 0	93 ± 4
Surface pore diameter (nm)[c]	9 ± 4	26 ± 16	144 ± 60

[†] Membrane made at VITO, [‡] Commercial membrane (Microdyn Nadir), [a] Average of two measurements, [b] Average of three measurements, [c] Pore size distribution based on SEM image

Furthermore, a tighter and more regular surface structure with considerably smaller pores is observed by SEM for the PAN support as compared to both PVDF membranes (Figure 3.2). The irregular sponge-like surface morphology of the commercial PVDF membrane makes the determination of the surface pore size difficult. The surface pore diameter of the MV020T membrane in Table 3.1 is therefore indicative and the pore size distribution, as presented in Figure 3.3, was impossible to measure. The histogram of the surface pores of the laboratory prepared membranes is presented in Figure 3.3. The PVDF membrane clearly

shows a broader pore size distribution than the PAN membranes, as can be observed from the SEM images (Figure 3.2 a/b).

The MWCO curves of both laboratory-prepared membranes, obtained after filtration with an aqueous solution of dextrans, are similar (Figure 3.4). However, the PAN membrane exhibits a sharper MWCO curve, resulting in a considerably lower MWCO value (Table 3.1). The relatively diffuse MWCO curve of the PVDF membrane reflects its broad surface pore size distribution (Figure 3.2b). The higher average equivalent pore diameter, mass transfer coefficient *k* and MWCO of the PVDF support all confirm this more open surface structure, and suggest that surface hydrophobicity is less important for the water transport through these membranes.

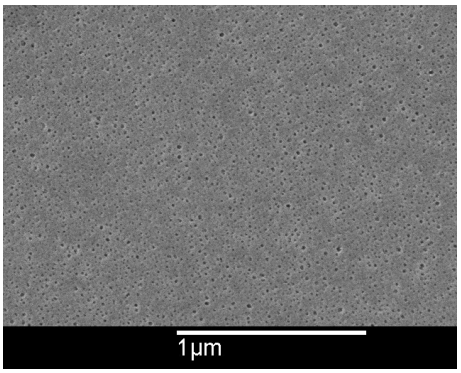

(a)

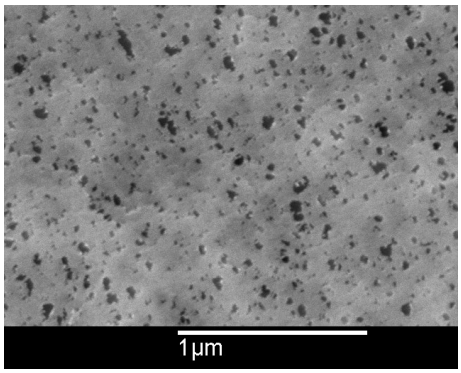

(b)

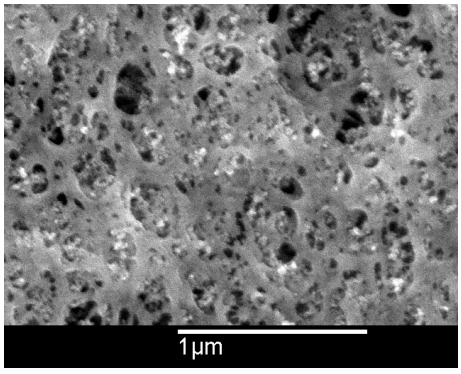

(c)

Figure 3.2: Surface SEM image of the support membranes (25 000 ×, 5keV): (a) PAN membrane, (b) laboratory-prepared PVDF membrane and (c) commercial PVDF MV020T membrane.

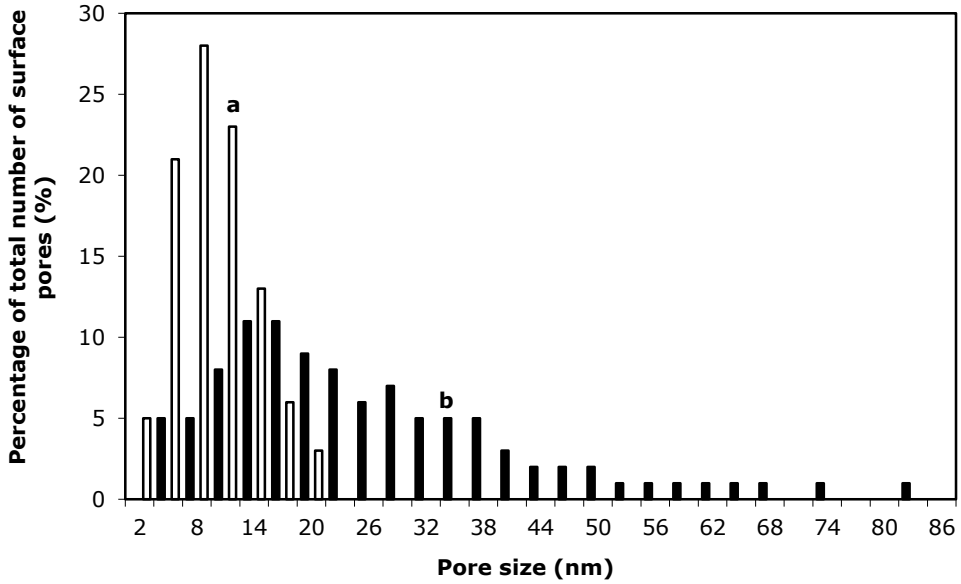

Figure 3.3: Histogram of the surface pores of the self-prepared support membranes: (a) PAN membrane and (b) PVDF membrane.

Judging from its superior water flux, open structure and hydrophobic nature, the PVDF membrane is the preferred support for subsequent application of thin PTMSP(-silica) top layers. The mass transfer coefficient *k* indicates that the commercial PVDF membrane is clearly more permeable to water than the laboratory-prepared PVDF membrane. This high *k* value, a slightly higher hydrophobicity and more open surface structure, favour the use of the MV020T membrane. The slightly higher surface roughness of the commercial membrane compared to the self-prepared PVDF support could enhance the adhesion of the top layer. Moreover, as the commercial membrane is manufactured on a large scale coating line, it is more homogeneous and uniform than the support membranes cast in this work due to the limitations of the used lab-scale casting set-up. Therefore, the commercial PVDF support membrane was used throughout the thesis.

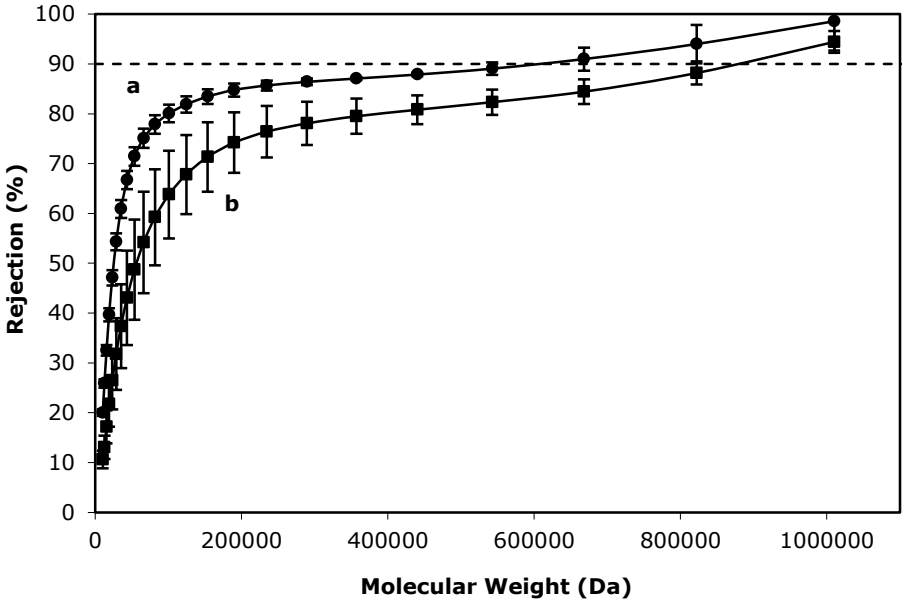

Figure 3.4: MWCO curves of the self-prepared support membranes: (a) PAN membrane and (b) PVDF membrane.

3.4 Influence of hydrophobic silica on membrane structure, free volume and PV performance

The influence of the silica filler loading on the membrane structure, free volume and PV performance is reported for unsupported PTMSP membranes containing 0, 20, 30 and 50 wt.% silica. Large silica aggregates can clearly be observed on the SEM cross-section image of a PTMSP-silica (10 wt.%) membrane (Figure 3.5). The histogram in Figure 3.6 shows the fractions of silica aggregates as a function of their diameter, obtained from Figure 3.5 by ImageJ software according to De Sitter *et al.* [3].

Figure 3.5: SEM cross-section image of a dense PTMSP-silica (10 wt.%) membrane.

The silica aggregate distribution presented in Figure 3.6 is in good accordance with the distribution reported by De Sitter *et al.* [3] for PTMSP-silica (10 wt.%) membranes. While most of the aggregates have a diameter between 50 and 300 nm, more than 30 % of the aggregates are larger than 300 nm. Of this 30 %, 81 % of the aggregates have a diameter in between 300 nm to 1 µm and 19 % of 1 - 3 µm. These large aggregates could cause defects when PTMSP-silica suspensions would be coated as a thin film on top of a porous support, as will be discussed later in this chapter.

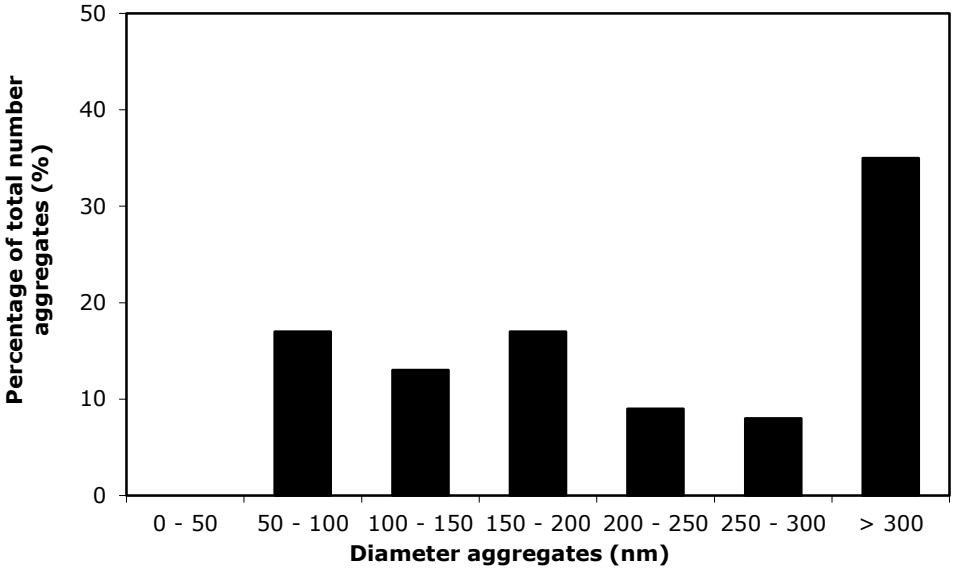

Figure 3.6: Percentage of the total number of silica aggregates as a function of the diameter of the aggregates.

PALS measurements on these membranes revealed a lifetime τ_3 of about 2.4 ns, which remains fairly constant with increasing silica loadings (Figure 3.7). This lifetime corresponds to the channel-like holes in the membrane [4,6] with mean free volume radii ranging between 0.30 and 0.32 nm (Table 3.2). With increasing concentration of silica filler in the membrane, the component τ_4, representative of the larger cages, slightly increases [4,6] (Figure 3.7). The mean radius of these larger cages expanded from 0.53 to 0.58 nm as more silica is incorporated (Table 3.2). This slight increase can be attributed to the PTMSP polymer chain interruption due to the presence of silica aggregates. For the silica filled membranes, a fifth component τ_5 was found, corresponding to the interstitial cavities in the silica aggregates [4,6]. These mesopores inside the silica aggregates correspond to a mean radius of approximately 1.2 nm. The fifth lifetime is fairly constant for all silica-filled membranes, while its intensity clearly increases with increasing filler content (Table 3.2). The trend of τ_5 with increasing silica loading does not correspond to the PALS data reported by Winberg *et al.* [6] who reported a clear increase of τ_5 (from 29 to 40 ns) with increasing silica filler loading. Firstly, this could tentatively be explained by

possible differences between the PTMSP batches. Unfortunately, Winberg *et al.* did not supply any information on the M_w of the polymer they used nor on the viscosity of the PTMSP-silica suspensions [6]. Varying viscosities could understandably result in differences in the silica aggregate formation. A second explanation can be found in the slightly different preparation method of the membranes, compared to the procedure used in this work (section 2.3.1). After the ultrasonic treatment of the toluene/silica suspensions, Winberg and co-workers added an extra magnetic stirring step prior to addition of PTMSP [6]. This extra step could possibly alter the formation of the silica aggregates. A third explanation could be the differences in drying time and conditions of the cast films. While Winberg and coauthors exposed their membranes to ambient conditions for 4 days, in this thesis a delayed evaporation of 10 days was applied.

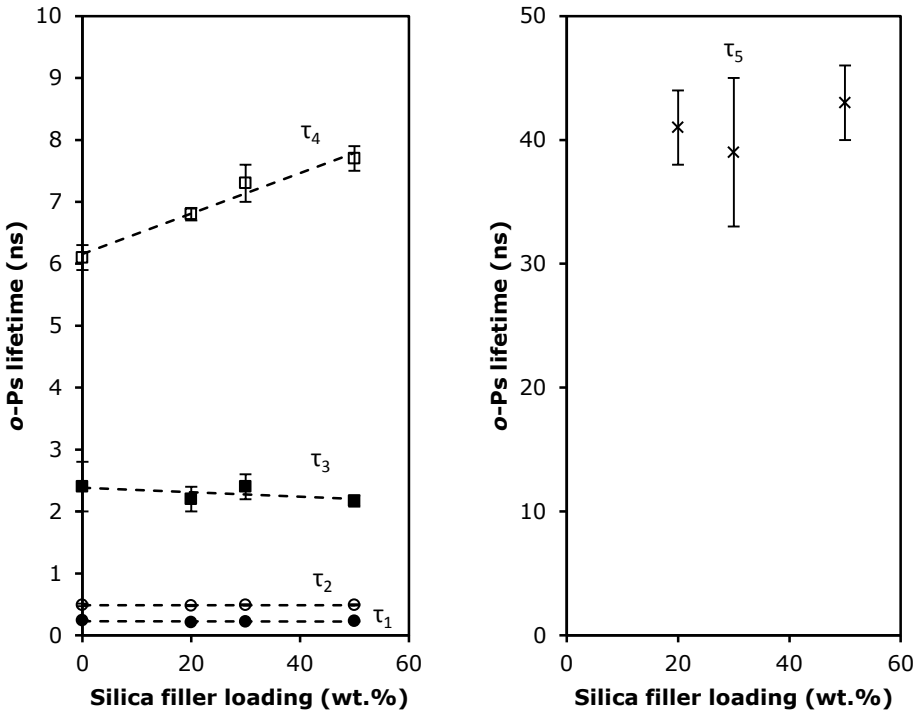

Figure 3.7: *o*-Ps lifetimes of unsupported PTMSP films as a function of the silica filler loading. The symbols (●) represent τ_1, (○) τ_2, (■) τ_3, (□) τ_4 and (×) τ_5. The dotted lines are just guides for the eye.

Table 3.2: *o*-Ps lifetime intensities and mean free volume radii of unsupported PTMSP membranes with varying silica filler loadings.

Membrane	I_1	I_2	I_3	I_4	I_5
PTMSP	21 ± 3	39 ± 3	9 ± 2	31 ± 2	-
PTMSP-silica (20 wt.%)[a]	18 ± 2	40 ± 2	7 ± 1	33 ± 1	2.5 ± 0.3
PTMSP-silica (30 wt.%)[a]	18 ± 2	43 ± 2	8 ± 1	24 ± 1	6.3 ± 0.1
PTMSP-silica (50 wt.%)[a]	18 ± 1	46 ± 1	7 ± 0	17 ± 0	11.8 ± 0.2
Membrane			R_3 (nm)[b]	R_4 (nm)[b]	R_5 (nm)[b]
PTMSP			0.32	0.53	-
PTMSP-silica (20 wt.%)[a]			0.31	0.55	1.18
PTMSP-silica (30 wt.%)[a]			0.32	0.57	1.14
PTMSP-silica (50 wt.%)[a]			0.30	0.58	1.20

[a] Silica content in membrane (wt.%) between parentheses.
[b] Calculated from average τ values.

The unsupported PTMSP(-silica) films with thicknesses ranging from 70 to 140 µm were then tested in PV. A 10 wt.% aqueous ethanol feed at 50 °C was circulated across the membrane surface and a 0.04 mbar pressure was applied at the permeate side of the membranes. Figure 3.8 shows that the thickness-corrected flux or specific permeation rate *R* of the dense membranes increases with increasing filler content, up to 50 x 10^{-3} m kg m^{-2} h^{-1} for the membranes containing 50 wt.% silica. The EtOH/H_2O separation factors amount to 15.0 ± 0.4 with negligible influence of the filler content.

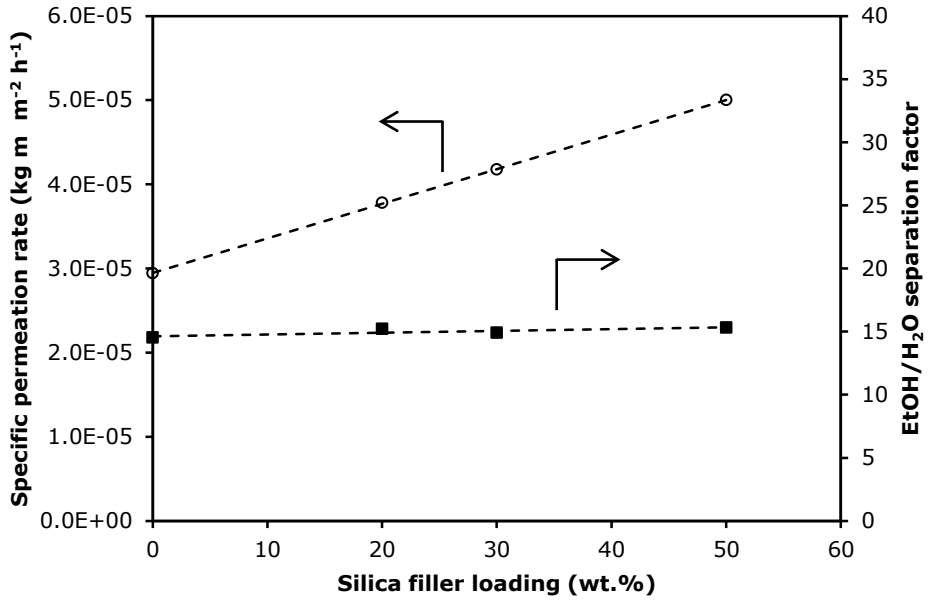

Figure 3.8: PV performance of dense PTMSP membranes as a function of the silica filler loading. (○) represents the specific permeation rate and (■) the EtOH/H_2O separation factor. The dotted lines are just guides for the eye.

Despite their high EtOH/H_2O separation factor and the clear flux-enhancing effect of silica filler addition, the permeate fluxes of the prepared unsupported PTMSP membranes are still relatively low (0.21 – 0.58 kg m^{-2} h^{-1}). These fluxes would be greatly enhanced if thin, defect-free PTMSP-silica top layers could be applied on porous supports.

3.5 Influence of membrane thickness on PV performance

Unfilled PTMSP membranes have been applied as thin films on top of a porous support. To form a complete picture of the influence of the membrane thickness on the PV performance, membranes with thicknesses ranging from 1.5 to 85 μm were prepared. The membranes of 30 - 85 μm thickness are unsupported and act as reference samples for the supported thin films with thicknesses between 1.5 and 30 μm. This broad range of membranes allows discovering trends in PV performance upon decreasing the membrane thickness. Figure 3.9 shows the PV performance of unfilled PTMSP membranes as a function of the membrane thickness in the separation of a 5 wt.% EtOH/H_2O mixture at 50 °C. A decrease in membrane thickness clearly has a positive effect on the flux. The EtOH/H_2O separation factor on the other hand, decreases slightly upon decreasing the membrane thickness down to approximately 8 μm, followed by a sharp decrease to an EtOH/H_2O separation factor of 14 for a PTMSP top layer with thickness of 2 μm. The decrease in separation factor could be explained by (1) the occurrence of more defects upon decreasing the membrane thickness and/or (2) the changes in polymer chain packing and conformation due to different evaporation rates. In thinner films, the chains have less time to be rearranged to their equilibrium conformation than in thicker films because of a shorter evaporation time. Changes in polymer chain configuration could understandably influence both the polymer/liquid interaction and the free volume, thus affecting the PV performance. This phenomenon was previously described by Huang *et al.* [10] and González-Marcos *et al.* [11].

The highest flux of 6.9 kg m^{-2} h^{-1} is found for a membrane with a PTMSP top layer of 1.5 μm thickness, showing a separation factor of 16. This membrane has a 4-fold higher flux and a 2-fold higher EtOH/H_2O separation factor than the reported commercially available PDMS-based membranes [1,2]. In a next step the combined effect of hydrophobic silica incorporation and top layer reduction on the PV performance of PTMSP membranes was investigated.

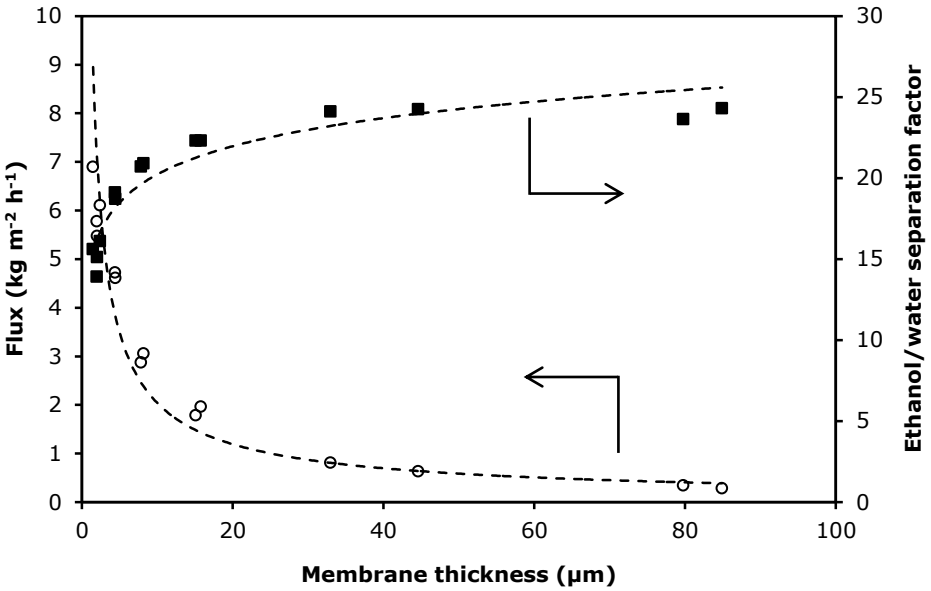

Figure 3.9: PV performance of unfilled, supported PTMSP membranes as a function of the membrane thickness. (○) represents the flux, (■) the EtOH/H_2O separation factor. The dotted lines are just guides for the eye.

3.6 Optimization of thin film silica filled PTMSP membranes

Since both the addition of hydrophobic silica (paragraph 3.4) and the reduction of the top layer thickness (paragraph 3.5) had a positive effect on the permeation properties of PTMSP membranes, this section aims at finding the optimal silica filler loading and top layer thickness. The criteria of the optimal membrane are obviously dependent on the separation target and the specified process yield. While in some processes the main focus is on the throughput and thus on the total flux, other processes require a high product purity and therefore membranes with maximal alcohol/H_2O separation factor.

In this section the membranes are optimised for the removal of alcohols from aqueous solutions. As mentioned in Chapter 1, *in situ* removal of ethanol or butanol from fermentation media by PV has great potential. In these fermentation processes, it is important that the produced alcohol is removed at a sufficiently high rate to prevent inhibition of the producing cells. Higher alcohol removal rates can be achieved by either installing more membrane area or by

using more permeable membranes. As a larger membrane area implicates a different module design, larger vacuum pumps and a higher overall cost, the development of high flux alcohol-selective membranes remains an attractive route. Therefore in this section, the aim is to optimize PTMSP membranes in such way that they show much higher fluxes and alcohol/water separation factors than the standard PDMS-based PV membranes.

3.6.1 Membrane thickness and homogeneity

Figure 3.10 shows the cross-sections of three supported PTMSP membranes: (a) an unfilled membrane and (b,c) PTMSP-silica membranes containing 25 and 50 wt.% silica. These three membranes are cast with a casting gap of 60, 45 and 30 μm, respectively. The top layer thickness increases from 1.96 μm for the unfilled membranes to 2.69 and 5.19 μm for the 25 and 50 wt.% silica filled membranes. Figure 3.11 represents the final dry thickness of membranes with 0, 25 and 50 wt.% silica as a function of the corresponding casting gap. Clearly, the top layer thickness increases with increasing silica filler loading. For unfilled, 25 and 50 wt.% silica-filled membranes, the polymer suspensions contained 5, 6.7 and 10 wt.% total solids, respectively. Since the casting gap was adjusted to compensate for the difference in total solid concentration, the increase in top layer thickness could mainly be attributed to the increasing viscosity of the casting solutions, already illustrated in Figure 3.1. The viscosity of the suspensions is known to greatly affect the flow characteristics under the doctor blade and therefore the final membrane thickness [12].

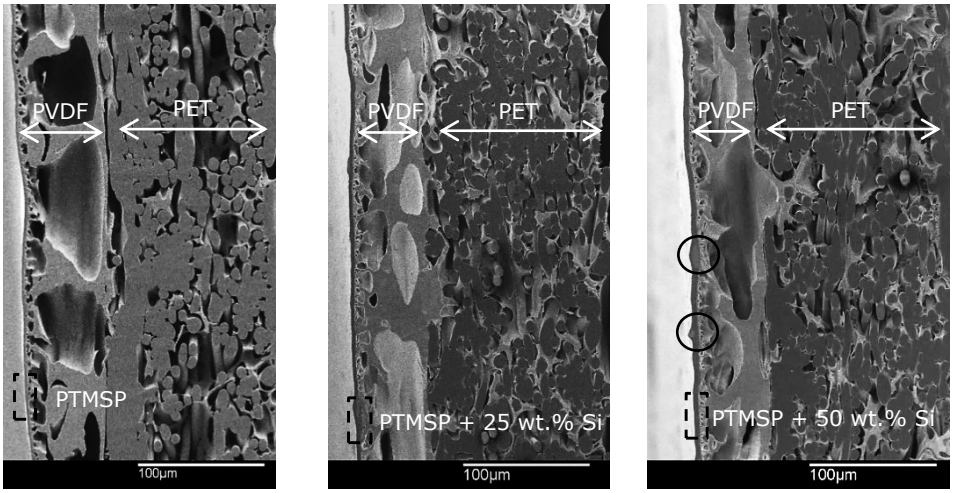

(a) (b) (c)

Figure 3.10: SEM cross-section images (250 ×, 5.0 keV) of (a) an unfilled, (b) 25 wt.% silica filled and (c) 50 wt.% silica filled supported PTMSP membrane.

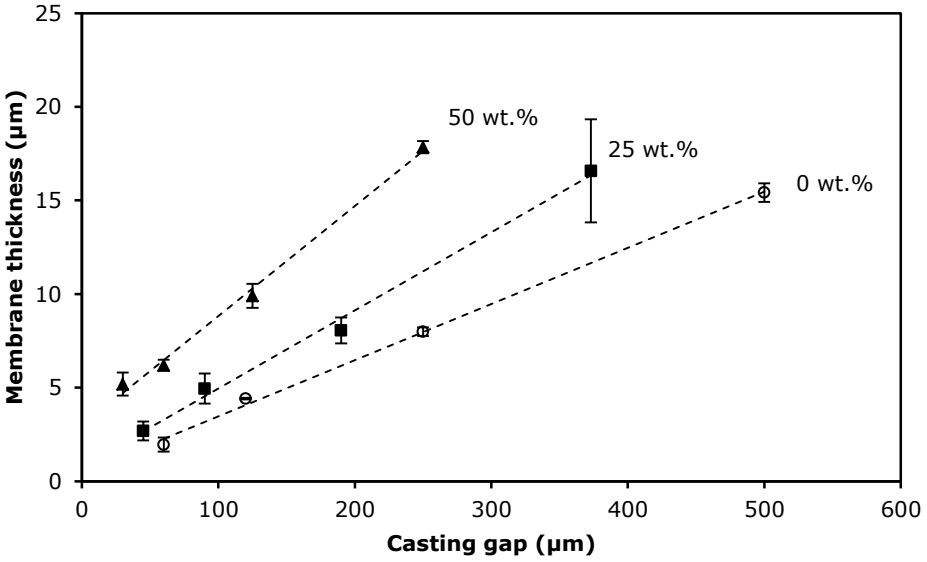

Figure 3.11: Final dry membrane thickness as a function of the casting gap distance for (○) unfilled, (■) 25 wt.% silica filled and (▲) 50 wt.% silica filled PTMSP membranes. The dotted lines are just guides for the eye.

Addition of silica resulted in the formation of aggregates (Figure 3.6) which could cause large clusters in the membrane. For relatively thick membranes (10

– 20 µm), the occurrence of these clusters is not directly problematic since they are encapsulated by selective polymer (Figure 3.12a). Once the top layer thickness is below 10 µm, the silica clusters could cause non-selective pathways through the dense PTMSP matrix. With increasing silica filler loading, the occurrence and size of these large clusters in the top layer increases. While the 25 wt.% silica filled membranes exhibit sporadic small deformations of the top layer due to the presence of relatively small silica aggregates, considerably larger silica clusters are observed in the 50 wt.% silica filled membranes (Figure 3.12b).

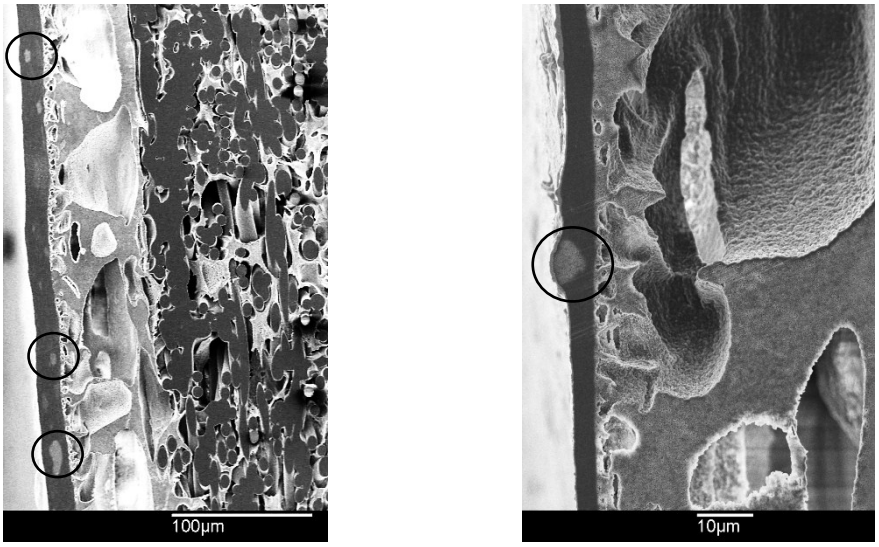

(a) (b)

Figure 3.12: SEM cross-section images (5.0 keV) of 50 wt.% silica filled supported PTMSP membranes with a top layer thickness of (a) 17 µm (250 ×) and (b) 5 µm (1000 ×).

A higher number of silica aggregates renders more inhomogeneously cast top layers and represents a higher risk for defects. On the other hand, the presence of these aggregates is desired because of their beneficial effect on the PV performance, i.e. the flux, of PTMSP membranes, as explained earlier [3-5]. Therefore an optimal top layer thickness and silica filler load must exist where the membranes perform best. An attempt to find this optimum in the separation of EtOH/H_2O mixtures is reported in the following section.

3.6.2 Performance in PV on EtOH/H_2O mixtures

The effect of the silica filler and top layer thickness on the performance of the prepared PTMSP(-silica) membranes in the separation of a 5 wt.% EtOH/H_2O mixture at 50 °C was investigated. Besides the supported thin film membranes (1.5 – 30 µm), the prepared unsupported PTMSP(-silica) membranes (30 – 180 µm) were tested as well. Figure 3.13 shows the total permeate fluxes of all membranes as a function of the membrane thickness. A steep flux increase with decreasing membrane thickness can be observed, up to 11.1 kg m^{-2} h^{-1} for a 25 wt.% silica filled PTMSP membrane with a top layer thickness of 2.8 µm. The positive influence of the silica filler on the flux is clearly demonstrated in the expanded view of Figure 3.13 and can be explained by the enlargement of the free volume discussed above. In Figure 3.7, it was shown that besides the appearance of an extra fifth ortho-positronium lifetime (τ_5) representing the 'non-selective' mesopores in the silica aggregates, the fourth lifetime component (τ_4) also increases with increasing filler concentration. Since τ_4 represents the larger cages in the polymer matrix, also the selective transport is improved by the incorporation of silica particles [4-7].

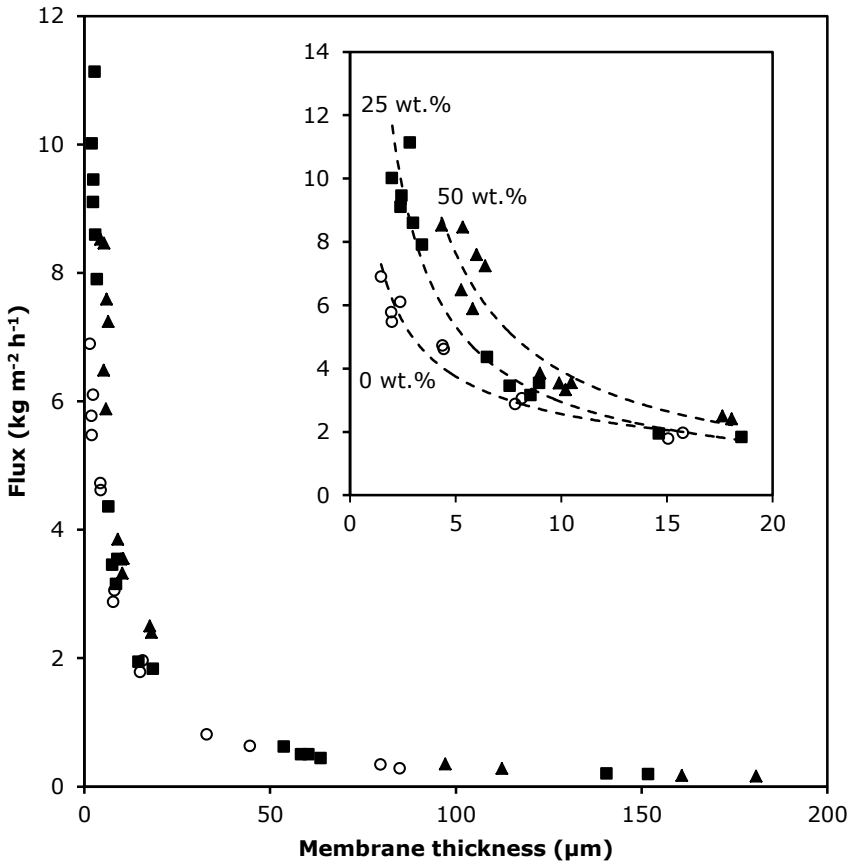

Figure 3.13: Total permeate flux as a function of membrane thickness of (○) unfilled, (■) 25 wt.% silica filled and (▲) 50 wt.% silica filled PTMSP membranes. The dotted lines are just guides for the eye.

As mentioned previously, the solution-diffusion model predicts that the total flux is inversely proportional to the membrane thickness in an ideal system (Equation 1-8). A plot of the total flux of all prepared membranes as a function of the inverse membrane thickness is displayed in Figure 3.14. The positive influence of the silica filler on the flux is again clearly demonstrated as the slope of the curve increases with incorporation of higher silica loadings. While the experimental flux data of the 50 wt.% silica filled PTMSP membranes can be fitted with a linear plot, the unfilled and 25 wt.% silica filled membranes deviate from linearity for top layer thicknesses below 4.4 and 3 µm, respectively. González-Marcos *et al.* already reported a deviation from Fick's law below 40 µm

for unfilled dense PTMSP membranes [11]. The deviation from linearity observed in this work for much thinner membranes could be attributed to different interactions (diffusion) between the membrane polymer and the permeating component. The conformation of the polymer chains strongly depends on the rate of evaporation, which increases with decreasing membrane thickness [10].
The outlier appearing in the 25 wt.% silica series could be explained by the occurrence of defects in the membrane. This PTMSP-silica(25 wt.%) membrane with top layer of 2.8 µm thickness exhibited the highest flux (11.1 kg m^{-2} h^{-1}) of all prepared membranes. Remarkably, a thinner PTMSP-silica(25 wt.%) membrane with a top layer of 2 µm thickness exhibited a lower flux of 10.01 kg m^{-2} h^{-1}, suggesting the presence of defects in the PTMSP-silica(25 wt.%) membrane with top layer of 2.8 µm thickness. The occurrence of defects is confirmed by Figure 3.15 where an EtOH/H_2O separation factor of about 12 can be observed for this PTMSP-silica(25 wt.%) membrane of 2.8 µm thickness, being the lowest observed separation factor. The thinner membrane of 2 µm thickness, on the other hand, exhibits a considerably higher EtOH/H_2O separation factor (17.2). Although the PTMSP-silica(25 wt.%) membrane with top layer thickness of 2.8 µm probably exhibits defects, its performance is still significantly better than that of the commercial PDMS-based membranes, which would imply that the defects could better be described as a few small non-selective pathways.

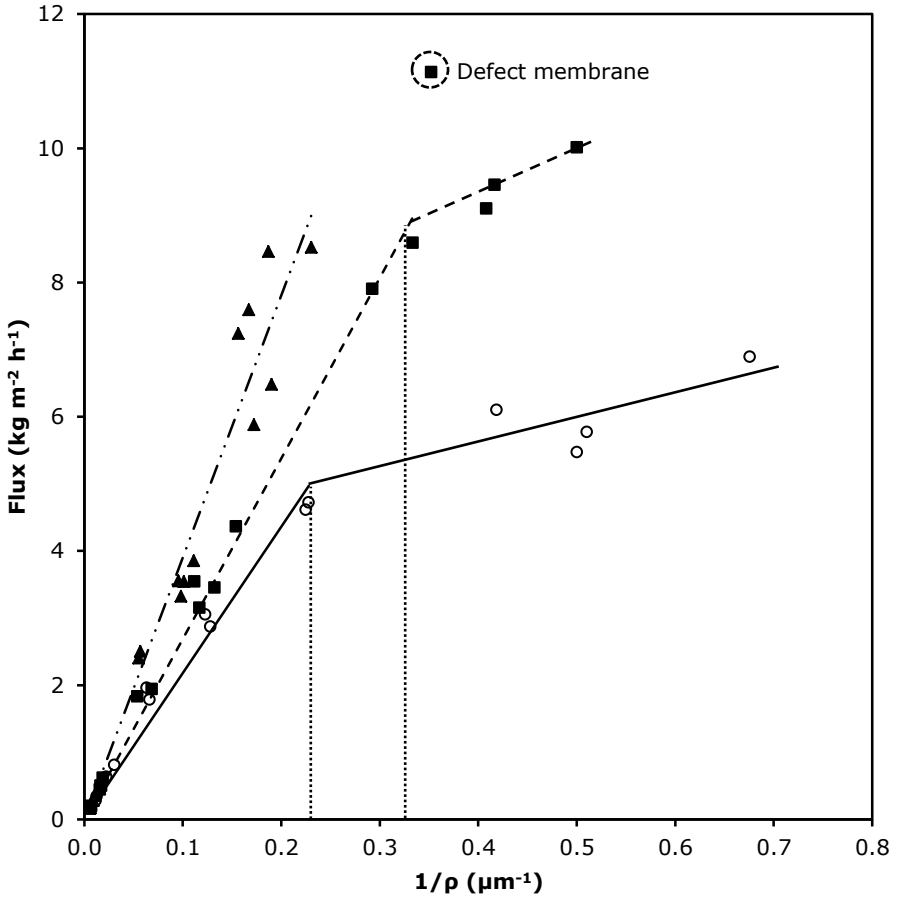

Figure 3.14: Total flux as a function of inverse membrane thickness of (○) unfilled, (■) 25 wt.% silica filled and (▲) 50 wt.% silica filled PTMSP membranes. The linear relationship is represented by (—) for unfilled, (– –) for 25 wt.% silica filled and (— - - —) 50 wt.% silica filled PTMSP membranes.

Figure 3.15 plots the EtOH/H_2O separation factors of the prepared PTMSP(-silica) membranes versus the membrane thickness. For unsupported membranes (30 - 180 μm) the separation factors are comparable, around 21-24. At lower membrane thicknesses however, the 50 wt.% silica filled membranes exhibit a lower EtOH/H_2O separation factor than the unfilled and 25 wt.% silica filled membranes (Figure 3.15). Overall, the 50 wt.% silica filled PTMSP membranes exhibit a slightly lower separation factor over the complete membrane thickness

range, demonstrating the negative effect of this high silica filler loading on the EtOH/H_2O separation factor.

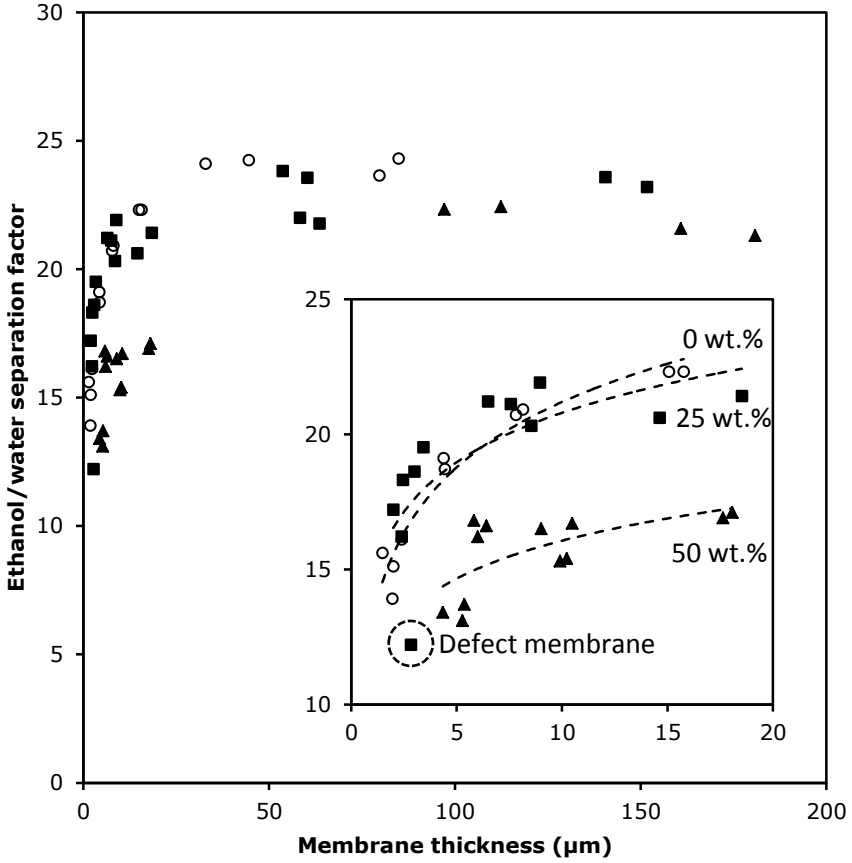

Figure 3.15: EtOH/H_2O separation factor as a function of membrane thickness of (○) unfilled, (■) 25 wt.% silica filled and (▲) 50 wt.% silica filled PTMSP membranes. The dotted lines are just guides for the eye.

The PV separation index (PSI), combining the flux and separation factor in one measure, enables comparison of the overall PV performance of all prepared membranes (Figure 3.16). The highest PSI (164) was found for a 25 wt.% silica filled PTMSP membrane with a top layer thickness of 2.4 µm, exhibiting a flux of 9.5 kg m^{-2} h^{-1} in combination with an EtOH/H_2O separation factor of 18.3. Although some membranes exhibit higher fluxes or higher separation factors, this membrane shows the most favourable overall performance based on PSI.

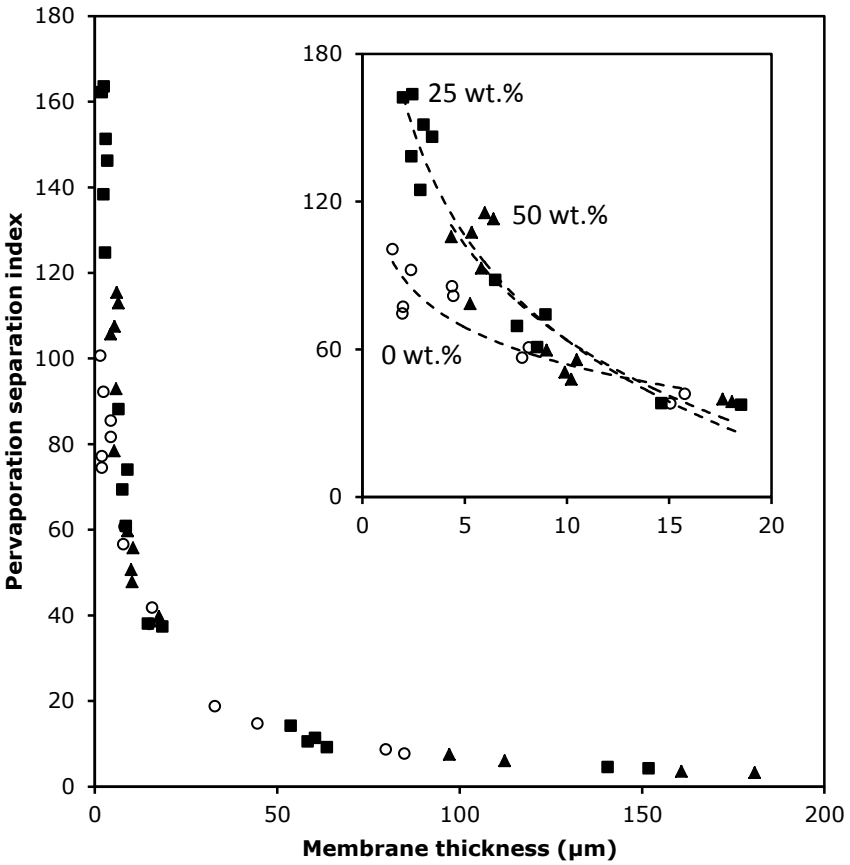

Figure 3.16: PV separation index as a function of membrane thickness of (○) unfilled, (■) 25 wt.% silica filled and (▲) 50 wt.% silica filled PTMSP membranes. The dotted lines are just guides for the eye.

3.7 Benchmark study of PV performance

Subsequently, the thin film membrane with the highest PSI, the 25 wt.% silica filled PTMSP membrane with a separating layer of 2.4 µm thickness (hereinafter referred to as VITO 1), was benchmarked against two commercially available hydrophobic PV membranes. Two PDMS-based thin film membranes were selected, i.e. PERVAP 4060 and Pervatech PDMS. Table 3.3 shows the superior performance of the VITO 1 membrane compared to both PDMS-based membranes in the purification of a 5 wt.% EtOH/H_2O mixture at 50 °C. The

calculated PSI values for Pervatech PDMS and PERVAP 4060 are 15 and 8, respectively. With a PSI of 164, the VITO 1 performs considerably better than the tested commercial PV membranes.

The potential of the prepared PTMSP-silica membranes was further investigated by testing the VITO 1 membrane and the PERVAP 4060 reference membrane in the separation of a 5 wt.% BuOH/H_2O mixture at 50 °C. Again the VITO 1 membrane clearly performs better than the commercial membrane in terms of both flux and BuOH/H_2O separation factor (Table 3.3), further indicating the potential of the VITO 1 membranes in the PV of aqueous alcohol mixtures (Table 3.3) and thus *in situ* product recovery of bio-alcohols.

Table 3.3: PV performance of VITO 1 and two commercial hydrophobic PV membranes in the separation of a 5 wt.% R-OH/H_2O mixture at 50 °C.

Membrane	Feed	Flux (kg m^{-2} h^{-1})	R-OH/H_2O separation factor	PSI
VITO 1	5 wt.% EtOH/H_2O	9.5 ± 0.2	18.3 ± 0.9	164
PERVAP 4060		1.3 ± 0.3	7.1 ± 1.3	8
Pervatech PDMS		2.6 ± 0.4	6.7 ± 1.0	15
VITO 1	5 wt.% BuOH/H_2O	9.5 ± 0.7	104 ± 1	978
PERVAP 4060		3.4 ± 0.2	39 ± 2	129

The VITO 1 membrane also shows an improved performance compared to previously reported non-commercial, laboratory-developed membranes in relation with EtOH or BuOH removal from water. PAN supported POMS membranes reported by García *et al.* exhibited fluxes up to approximately 0.6 kg m^{-2} h^{-1} and an EtOH/H_2O separation factor of approximately 9 (5wt.% EtOH at 53 °C) [13]. For a hydrophobic ZSM-5 zeolite membrane, an EtOH/H_2O separation factor of approximately 76, combined with a total flux of about 1 kg m^{-2} h^{-1} (40 °C, 6 mbar) [14] was reported by Weyd and co-workers. While this zeolite membrane is considerably more ethanol selective than the supported

PTMSP-silica membrane prepared in this study, their flux is almost one order of magnitude lower than the flux of the VITO 1 membrane [14].
BuOH/H_2O separation factors between 40 and 70, and fluxes around 0.15 kg m^{-2} h^{-1} have been reported by Fadeev *et al.* for dense unsupported PTMSP membranes tested on binary BuOH/H_2O mixtures (0.1 - 0.35 wt.%) at 25 °C [15]. To our knowledge, PSI values up to 164 for EtOH and 978 for BuOH have never been reported before, making the prepared PTMSP-silica membranes attractive candidates for application in real industrial processes.

3.8 Conclusion

High flux, silica filled PTMSP membranes were prepared and optimised in terms of the silica filler loading and top layer thickness. A broad range of thin film composite PTMSP(-silica) membranes with attractive flux/selectivity combinations in the separation of a 5 wt.% EtOH/H_2O feed were prepared, ranging from a highly selective membrane with an EtOH/H_2O separation factor of about 24 combined with a total flux of about 0.28 kg m^{-2} h^{-1}, to a highly permeable membrane exhibiting a flux of 10.1 kg m^{-2} h^{-1} with an EtOH/H_2O separation factor of approximately 17. The optimal flux/selectivity combination was found for a 25 wt.% silica filled PTMSP membrane with separating layer thickness of 2.4 µm, demonstrating a flux of 9.5 kg m^{-2} h^{-1} and EtOH/H_2O separation factor of 18.3. The supported PTMSP-silica membranes performed much better than two commercial PDMS-based PV membranes, both in terms of flux and R-OH/H_2O separation factor. Testing the optimal membrane on a 5 wt.% binary BuOH/H_2O mixture (J ~ 9.5 kg m^{-2} h^{-1}, $\alpha_{BuOH/H2O}$ ~ 104), demonstrated the potential of the prepared membranes for *in situ* alcohol recovery in future bio-refinery plants.

REFERENCES

[1] A. Verhoef, A. Figoli, B. Leen, B. Bettens, E. Drioli, B. Van der Bruggen, Performance of nanofiltration membrane for removal of ethanol from aqueous solutions by pervaporation, *Sep. Purif. Technol.* **60** (2008) 51 – 63.

[2] S. Chovau, S. Gaykawad, A. J. J. Straathof, B. Van der Bruggen, Influence of fermentation by-products on the purification of ethanol from water using pervaporation, *Bioresour. Technol.* **102** (2011) 1669 – 1674.

[3] K. De Sitter, A. Andersson, J. D'Haen, R. Leysen, S. Mullens, F. H. J. Maurer, I. F. J. Vankelecom, Silica filled poly(4-methyl-2-pentyne) nanocomposite membranes: Similarities and differences with poly(1-trimethylsilyl-1-propyne)-silica systems, *J. Membr. Sci.* **321** (2008) 284 – 292.

[4] K. De Sitter, P. Winberg, J. D'Haen, C. Dotremont, R. Leysen, J. A. Martens, S. Mullens, F. H. J. Maurer, I. F. J. Vankelecom, Silica filled poly(1-trimethylsilyl-1-propyne) nanocomposite membranes: Relation between the transport of gases and structural characteristics, *J. Membr. Sci.* **278** (2006) 83 – 91.

[5] K. De Sitter, R. Leysen, S. Mullens, I. Vankelecom, F. Maurer, Silica filled poly(1-trimethylsilyl-1-propyne) and poly(4-methyl-2-pentyne) membranes: similarities and differences in structural characteristics and membrane performance, *Desalination* **199** (2006) 293 – 295.

[6] P. Winberg, K. De Sitter, C. Dotremont, S. Mullens, I. F. J. Vankelecom, F. H. J. Maurer, Free volume and interstitial mesopores in silica filled poly(1-trimethylsilyl-1-propyne) nanocomposites, *Macromolecules* **38** (2005) 3776 – 3782.

[7] D. Gomes, S. P. Nunes, K. V. Peinemann, Membranes for gas separation based on poly(1-trimethylsilyl-1-propyne)-silica nanocomposites, *J. Membr. Sci.* **246** (2005) 13 – 25.

[8] P. Aerts, I. Genné, R. Leysen, P. A. Jacobs, I. F. J. Vankelecom, The role of the nature of the casting substrate on the properties of membranes prepared by immersion precipitation, *J. Membr. Sci.* **283** (2006) 320 – 327.

[9] CHARMME Network, Harmonization of characterization methodologies for porous membranes, EC Contract SMT4-CT 98-7518, 2001.

[10] R. Y. M. Huang, Pervaporation membrane separation processes, Elsevier, Amsterdam, 1990.

[11] J. A. González-Marcos, C. López-Dehesa, J. R. González-Velasco, Effect of operation conditions in the pervaporation of ethanol-water mixtures with poly(1-trimethylsilyl-1-propyne) membranes, *J. Appl. Polym. Sci.* **94** (2004) 1395 – 1403.

[12] R. E. Mistler, E. R. Twiname, Tape casting: theory and practice, The American Ceramic Society, Ohio, USA, 2000.

[13] M. García, M. T. Sanz, S. Beltrán, Separation by pervaporation of ethanol from aqueous solutions and effect of other components present in fermentation broths, *J. Chem. Technol. Biotechnol.* **84** (2009) 1873 – 1882.

[14] M. Weyd, H. Richter, P. Puhlfürß, I. Voigt, C. Hamel, A. Seidel-Morgenstern, Transport of binary water-ethanol mixtures through a multilayer hydrophobic zeolite membrane, *J. Membr. Sci.* **307** (2008) 239 – 248.

[15] A. G. Fadeev, Y. A. Selinskaya, S. S. Kelley, M. M. Meagher, E. G. Litvinova, V. S. Khotimsky, V. V. Volkov, Extraction of butanol from aqueous solutions by pervaporation through poly[1-(trimethylsilyl)-1-propyne], *J. Membr. Sci.* **186** (2001) 205 – 217.

Chapter 4

Supercritical CO_2 as alternative to inorganic fillers

4.1 Introduction

While the incorporation of inorganic particles in a polymer matrix is known to increase the inherent high free volume and large permeability of neat PTMSP (Chapter 3), this chapter presents an alternative method. Supercritical (T_c = 31.1 °C, p_c = 7.37 MPa) or compressed CO_2 has been extensively studied as an alternative solvent to water or organic solvents due to its environmentally benign character and tunable properties [1-4]. By varying the pressure or temperature, the solubility of CO_2 can be modified. Pressurized or supercritical CO_2 ($scCO_2$) is known to swell and plasticize glassy polymers, leading to a depression of their T_g to almost the same extent as solvents or vapours [5,6]. The effect of $scCO_2$ or compressed CO_2 on the physical properties, free volume or crystal structure of several polymers has been reported [5-16], but high free volume polyacetylenes have hardly been investigated. Mohsen *et al.* studied the free volume parameters of PTMSP after sorption and desorption of CO_2 and CH_4 gases [17]. However, these authors only reported data of PTMSP samples treated at mild conditions, i.e. 1 bar and room temperature.

In this chapter, the influence of a $scCO_2$ treatment at elevated pressures and temperatures on the free volume and PV performance of PTMSP membranes is studied. Firstly, the effect of the $scCO_2$ treatment on the T_g is discussed and subsequently the influence of pressure and temperature on the free volume is demonstrated by PALS. Next, the long term and thermal stability and relaxation of the free volume are reported. Furthermore, the reproducibility of the method is investigated. Finally, the $scCO_2$-treated membranes are applied in the PV of a 5 wt.% EtOH/H_2O mixture.

4.2 Experimental

4.2.1 Materials

Poly[1-(trimethylsilyl)-1-propyne] (PTMSP, M_w ~ 4.49 x 10^5 g mol^{-1}, Pd = 4.26 and 0.98 wt.% Ta) was purchased from Gelest, Inc. (USA) and dissolved in analytical grade toluene, obtained from Merck (Belgium). Technical grade liquid carbon dioxide was purchased from Air Products (Belgium).

4.2.2 Membrane preparation

Unsupported PTMSP membranes were prepared from toluene solutions containing 3 wt.% of polymer. The polymer solutions and unsupported membranes were prepared as described in Chapter 2.

4.2.2.1 scCO2 treatment

A high-pressure reactor from Premex Reactor Ag (Switzerland) with an internal volume of 1 L was used in combination with a ProMinent Orlita MhS 30/10 diaphragm pump (Belgium). Circular disks with a thickness of approximately 100 µm and a diameter of about 9 cm were cut from the PTMSP films and placed in the reactor, which was then sealed. First, the reactor vessel, pump and piping were flushed with CO_2 until liquid CO_2 was obtained at the outlet. Subsequently, the reactor was filled with liquid CO_2 prior to heating. As the pressure increases upon heating due to phase transition and expansion of the liquid CO_2, a regulation valve was needed to prevent the pressure from crossing the set point pressure. In the present study PTMSP samples were treated at eight different conditions (Table 4.1), at pressures between 12 and 24 MPa and temperatures between 40 and 150 °C. Once the desired temperature and pressure were reached, the reactor was kept for 6 h under stable scCO_2 conditions. After, the CO_2 pressure was slowly released at 0.15 MPa s^{-1} as higher rates of depressurization can lead to foaming of the polymer. To prevent CO_2 from liquefying during depressurization, the reactor temperature was kept above 35 °C.

Table 4.1: $scCO_2$ treatment conditions used in this study.

Pressure (MPa)	Temperature (°C)			
	40	70	110	150
12	X		X	
16		X		X
20	X		X	
24		X		X

4.2.3 Membrane characterization

4.2.3.1 High-pressure differential scanning calorimetry

The influence of the pressurized CO_2 on the T_g of PTMSP was investigated by high-pressure differential scanning calorimetry (DSC). DSC curves of unsupported PTMSP membranes were recorded at three different pressures, i.e. 7.5, 24 and 35 MPa. A Sensys DSC with 3D detector from Setaram (Germany) was used. The Sensys DSC uses a fluxmeter detector that surrounds the crucible completely. This type of detection allows using specific high pressure vessels especially when it is needed to control the pressure during the test. The other advantage is that only the sample is under pressure, while the detector remains under atmospheric pressure ensuring that the calibration of the DSC is not affected. The high pressure cell was connected to the output of a high pressure pump and kept isobarically during heating. The samples were heated from 25 to 150 °C at a heating rate of 10 °C min^{-1} under constant pressure.

4.2.3.2 PALS

During the measurements, a count rate of approximately 700 s^{-1} was achieved and each spectrum was built up of about 2.5 million counts. Each sample was measured five times and the spectra were analyzed with PALSFIT 1.54 software. The spectra of the PTMSP samples were analyzed with a four-component analysis. The variance of fit was close to unity (1.0 – 1.1) for all performed analyses.

To determine the thermal stability of the $scCO_2$-treated PTMSP films, PALS measurements at increasing temperatures in the range 30 - 170 °C (increments

of 20 °C) were performed on selected $scCO_2$-treated samples as well as on a reference untreated sample. At each measuring temperature, the samples were kept isothermally for 240 min and four PALS spectra, each built up of about 2.5 million counts were recorded. During cooling, the samples were measured at the same temperatures as in the heating sequence. In all cases, the first of the four spectra was discarded to correct for temperature stabilization of the polymer sample at the start of each new measurement.

4.2.3.3 Gel Permeation Chromatography

The thermal effect of the $scCO_2$ treatment on the molecular mass (M_w) of the polymer was investigated by GPC. The samples were annealed in an oven at 160 °C for 1.5 and 8 h in a nitrogen atmosphere. The cured and reference samples were dissolved in THF and injected on a TSP GPC column with a Shodex RI-71 refractometer.

4.2.3.4 Pervaporation

The influence of the $scCO_2$ treatment on the PV performance was investigated for a 5 wt.% aqueous ethanol feed mixture, which was circulated through the membrane test cells at approximately 12 L h^{-1}. The feed was kept at 50 °C, and the vapour-side pressure was maintained at approximately 0.04 mbar.

4.3 Influence of $scCO_2$ on the glass transition temperature

$scCO_2$ is thought to act as a solvent for the membrane and therefore decrease the T_g [5,6]. The influence of the $scCO_2$ treatment on PTMSP's T_g is investigated by high-pressure DSC measurements under pressurized CO_2 atmosphere. The T_g is a second order endothermic transition, which appears as a step transition in the DSC curve rather than a peak (melting). The transition from glassy to rubbery state is a reversible process and should result in a step transition in both heating and cooling curve. Unfortunately, the pressure was not controlled during cooling, making it impossible to identify the T_g in the cooling curve. Figure 4.1 shows three successively recorded high-pressure DSC curves of the same PTMSP sample at 24 MPa.

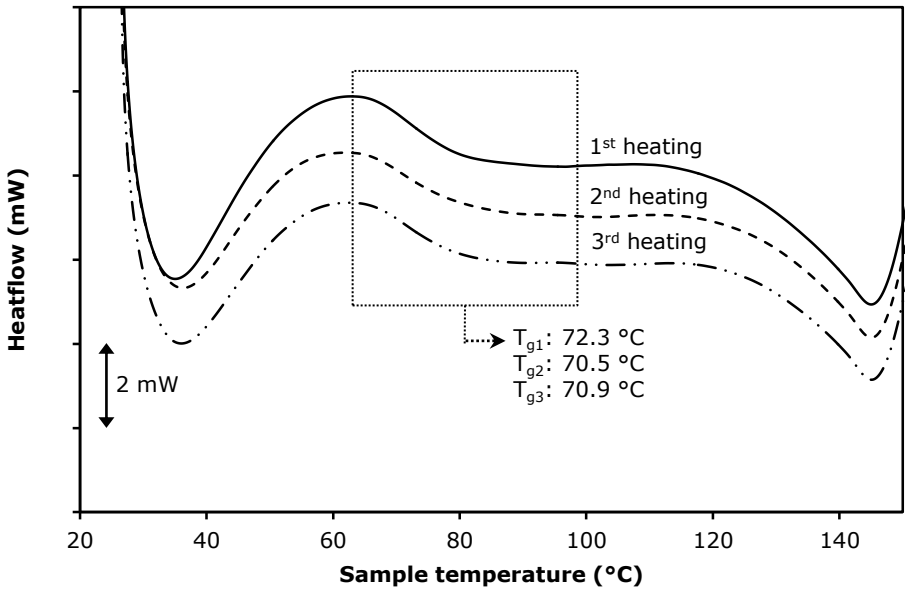

Figure 4.1: Repeated high-pressure DSC heating curves of the same PTMSP sample at 24 MPa CO_2 pressure.

The T_g is calculated at the inflexion point on the heat flow curve between two set limits. For the first heating cycle, a depression in T_g to approximately 72.3 °C is measured. Reheating the same sample resulted in a T_g of 70.5 and 70.9 °C for the second and third run, respectively, indicating the reversibility of the T_g. These values are significantly lower than the T_g of neat PTMSP reported in Chapter 1 (T_g > 300 °C). The influence of the pressure on the T_g on the other hand, is less clear. While no T_g could be derived from the DSC spectra recorded at 7.5 MPa due to the presence of a large exothermic peak around 90 °C, the DSC spectra recorded at 35 MPa revealed a T_g of approximately 74.8 °C. A saturation pressure is expected to exist, above which increasing the pressure does not further depress the T_g. Although further research is needed to interpret the effect of the CO_2 pressure on the T_g, the observed depression of PTMSP's T_g clearly demonstrates the plasticizing effect of the $scCO_2$ treatment.

4.4 Influence of $scCO_2$ on the free volume

The effect of the $scCO_2$ treatment of the PTMSP films on the *o*-Ps lifetimes τ_3 and τ_4 is shown in Figure 4.2a. Treating the films with pressurized CO_2 clearly induces an increase of the initial free volume, as reported for other polymers [8-10,17]. For the present PTMSP system, both lifetimes τ_3 and τ_4 significantly increase compared to the untreated reference sample. In the temperature range 40 – 110 °C, the treatment pressure has no significant effect on τ_3 and τ_4. At higher temperatures (150 °C), however, the effect of the pressure is more pronounced. The effect of the $scCO_2$ treatment on τ_3 is clearly larger than the effect on τ_4. Increases of 21% – 79% for τ_3 and 13% – 48% for τ_4 are observed. These values are much larger than those reported in the literature for a similar PTMSP system treated in a CO_2 atmosphere at mild conditions. Mohsen *et al.* observed a 7.4% increase of both lifetimes τ_3 and τ_4 for PTMSP after desorption of CO_2 at 1 bar and room temperature [17]. This demonstrates the large effect of pressure and temperature on the free volume expansion of $scCO_2$-treated PTMSP. For other polymers like poly(ethylene naphthalate) (PEN) [8] and syndiotactic polystyrene [10], *o*-Ps lifetime increases up to ~ 10% were reported after $scCO_2$ treatments of 6 h at 20 MPa and 100 °C and 3 – 10 h at 16 MPa and 40 °C, respectively. PALS does unfortunately not reveal any information about the number of free volume cavities.

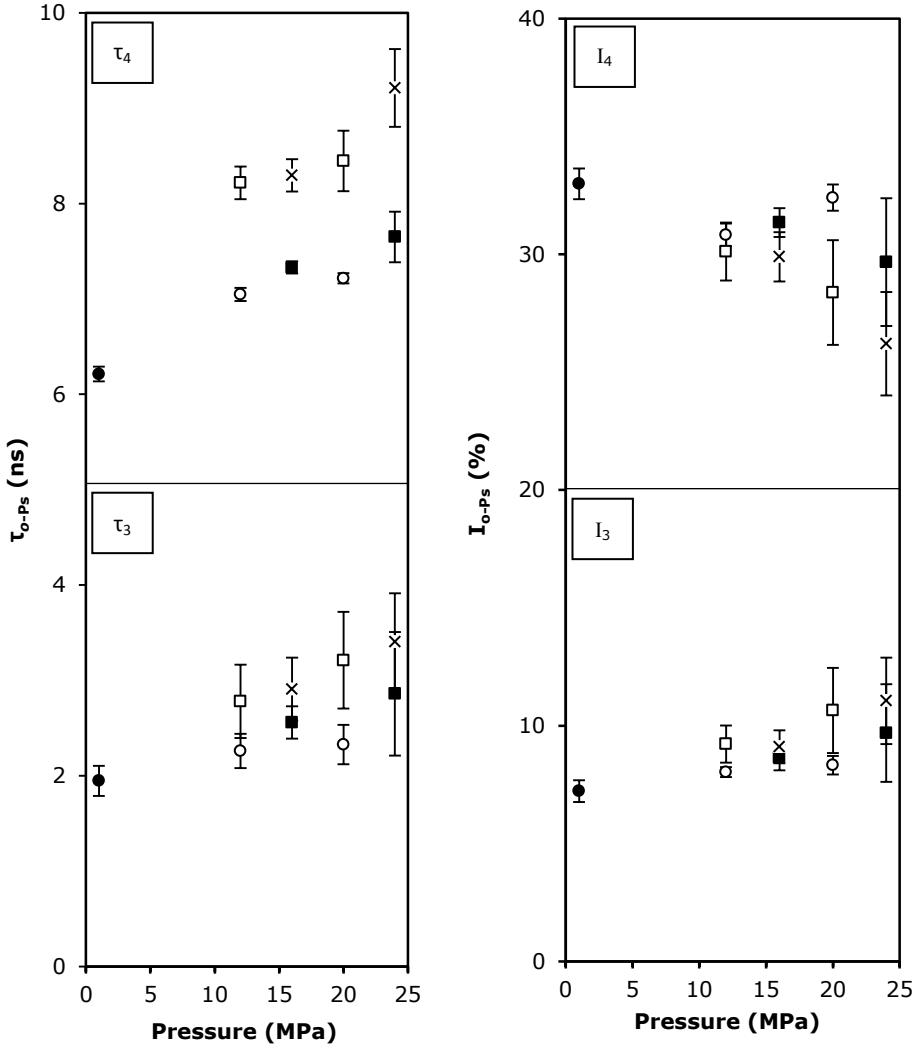

(a) (b)

Figure 4.2: (a) *o*-Ps lifetimes ($\tau_{o\text{-}Ps}$) and (b) *o*-Ps lifetime intensities ($I_{o\text{-}Ps}$) as a function of pressure and temperature of the $scCO_2$ treatment. Different treatment temperatures are represented by the following symbols: (●) room temperature, (○) 40 °C, (■) 70 °C, (□) 110 °C and (×) 150 °C.

However, information on the homogeneity or distribution of the distinct lifetime components τ_3 and τ_4 can be deduced from the standard deviation on the five spectra obtained for each of the samples. As not all standard deviations are clearly visible in Figure 4.2a, Table 4.2 gives an overview of the errors on the different τ values. It can be seen that the deviation on the τ_3 lifetimes is large

compared to those on the τ_4 values. The larger deviation on τ_3 suggests a broader distribution of the free volume cavities corresponding to the channel-like holes. In general, Figure 4.2a and Table 4.2 show a clear increase of the error on the lifetimes of the treated samples compared to the reference, indicating the broadening effect of the scCO2 treatment on the free volume distribution. At more intense pressure/temperature conditions, the standard deviations are even higher.

Each *o*-Ps lifetime results in a corresponding intensity (I), which provides information about the relative probability of *o*-Ps formation and indirectly about the chemical structure of the material. Figure 4.2b shows the intensities of $scCO_2$-treated and untreated PTMSP samples. I_3 increases with increasing treatment pressure and increasing temperature, while I_4 clearly decreases. The sum of both I_3 and I_4 is approximately constant (39-40), demonstrating that the total probability of *o*-Ps formation is unaffected. This mirroring-effect of I_3 and I_4 is caused by small variations in the analysis.

For the sample treated at 150 °C and 24 MPa, the sum of the intensities decreases to 37. This small decrease in total *o*-Ps intensity may be attributed to the chemical decomposition or degradation of the polymer under these treatment conditions.

The thermal effect of the $scCO_2$ treatment on the M_w distribution was investigated by GPC. A drop of 75% in M_w and a concomitant decrease in polydispersity of 35% were observed for a PTMSP sample that was not subjected to the $scCO_2$ treatment but was instead treated for 1.5 h at 160 °C in a nitrogen atmosphere. The onset of thermal degradation of PTMSP, investigated by thermogravimetrical analysis at a heating rate of 5 °C min^{-1}, is reported to occur around 155 °C [18]. For $scCO_2$-treated samples that have been subjected for 6 h to a temperature in the range of this degradation temperature (150 °C, isothermally), chemical modification of the polymer can be anticipated, thus explaining the observed change of the lifetime intensity. Similar to the lifetimes, the standard deviations of the I values clearly increase with the intensity of the $scCO_2$ treatment (Figure 4.2b, Table 4.2).

Table 4.2: *o*-Ps lifetimes (τ) and intensities (*I*), and calculated free volume cavities (R), of the $scCO_2$-treated samples, and standard deviations (between parentheses) on the measurements (five spectra).

	τ_3 (ns)	I_3 (%)	R_3 (nm)*	τ_4 (ns)	I_4 (%)	R_4 (nm)*
Reference	1.95 (0.16)	7.2 (0.5)	0.28	6.21 (0.08)	33.0 (0.7)	0.53
40 °C – 12 MPa	2.26 (0.18)	8.0 (0.2)	0.31	7.05 (0.07)	30.8 (0.5)	0.56
40 °C – 20 MPa	2.33 (0.21)	8.3 (0.4)	0.31	7.22 (0.05)	32.4 (0.6)	0.57
70 °C – 16 MPa	2.56 (0.17)	8.6 (0.5)	0.33	7.33 (0.06)	31.3 (0.6)	0.57
70 °C – 24 MPa	2.86 (0.65)	9.7 (2.1)	0.35	7.65 (0.27)	29.7 (2.7)	0.58
110 °C – 12 MPa	2.78 (0.38)	9.2 (0.8)	0.35	8.22 (0.17)	30.1 (1.2)	0.60
110 °C – 20 MPa	3.21 (0.51)	10.6 (1.8)	0.38	8.45 (0.32)	28.4 (2.2)	0.61
150 °C – 16 MPa	2.91 (0.33)	9.1 (0.7)	0.36	8.29 (0.17)	29.9 (1.0)	0.60
150 °C – 24 MPa	3.4 (0.5)	11.1 (1.8)	0.39	9.21 (0.41)	26.2 (2.2)	0.63

* Calculated from average τ values.

4.5 Long-term stability of the $scCO_2$ enlarged free volume

Oka *et al.* reported the relaxation of the enlarged free volume of $scCO_2$-treated polystyrene as a function of time [9]. The *o*-Ps lifetime decreased from 2.40 to 2.20 ns approximately 250 h after the treatment. Thus a decrease in lifetime of approximately 8% was noticed in this relatively short time frame, even though the lifetime remained higher than the initial 2.06 ns of the untreated polystyrene. Figure 4.3a shows the free volume relaxation of a PTMSP sample subjected to a $scCO_2$ treatment at 16 MPa and 150 °C, and of a reference untreated PTMSP sample. It can be observed that the enlarged free volume is still present after more than 800 days. The relaxation of the free volume of amorphous polymers can be fairly described according to Equation 4-1 [19,20]:

$$v - v_\infty = (v_0 - v_\infty) \times e^{-\left(\frac{t}{t_v}\right)^m} \quad (4\text{-}1)$$

with v the free volume at time t, v_0 the initial free volume, v_∞ the free volume at infinitely long times, t_v the characteristic volume relaxation time and m a constant equal to 0.4 [19,20]. Figure 4.3a shows the plotted Equation 4-1, using the minimum and maximum characteristic volume relaxation time t_v estimated from the experimental data. Since the relaxation curve is just at the onset of its decay, fitting the exact model through these data is too ambitious. However, the order of magnitude of t_v for both lifetimes can be deduced from the curves. The relaxation (t_v) of the excess free volume is expected to occur after 10^7 to 10^8 seconds (0.3 – 3 year) for the characteristic channel-like holes (v_3) and 10^8 to 10^9 seconds (3 – 30 year) for the larger cages (v_4).

The pronounced stability of the enlarged free volume at room temperature may be explained by the extremely high T_g of PTMSP, above 300 °C. Since PTMSP is at room temperature far below its T_g, the polymer chain segments of the $scCO_2$-treated samples exhibit low mobility and consequently, the excess free volume will relax extremely slow. For polymers with a much lower T_g, such as polystyrene (T_g ~ 100 °C), on the other hand, the mobility of the polymer chain segments at room temperature permits relaxation of the enlarged free volume [9]. It can be observed in Figure 4.3b that the intensities of the treated and untreated samples again exhibit the mirroring-effect, indicating that the probability for *o*-Ps formation is constant during the first 800 days.

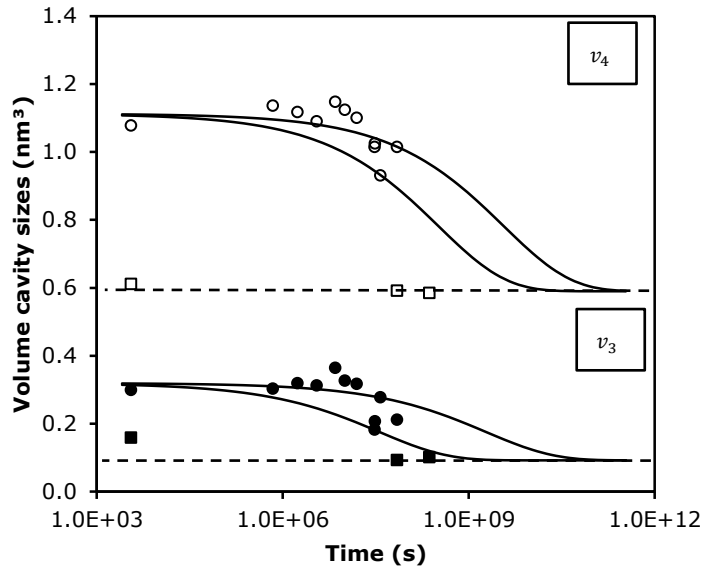

(a)

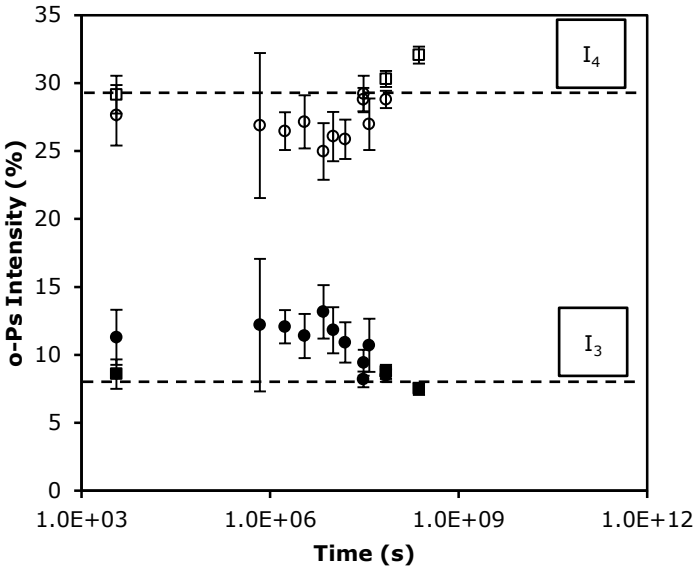

(b)

Figure 4.3: Long term measurements of untreated (■,□) and $scCO_2$-treated (●,○) PTMSP at 16 MPa and 150 °C for 6 h: (a) free volume v_3 (filled symbols) and v_4 (unfilled symbols) and (b) *o*-Ps lifetime intensity I_3 (filled symbols) and I_4 (unfilled symbols). The dotted line represents the free volume and o-Ps lifetime intensity of the untreated samples, whereas the solid line represents the relaxation curve estimated from the minimum and maximum t_v.

4.6 Reproducibility of the $scCO_2$-induced free volume enlargement

To investigate the reproducibility of the $scCO_2$ treatment, a new sample starting from a fresh PTMSP solution, was prepared and treated under equal conditions as before (16 MPa, 70 °C). Figure 4.4 shows all four *o*-Ps lifetimes of the two independently prepared and $scCO_2$-treated PTMSP samples. As can be seen in this figure, almost equal lifetimes were obtained. This almost perfect reproducibility demonstrates the robustness of the $scCO_2$ treatment and of the entire preparation method.

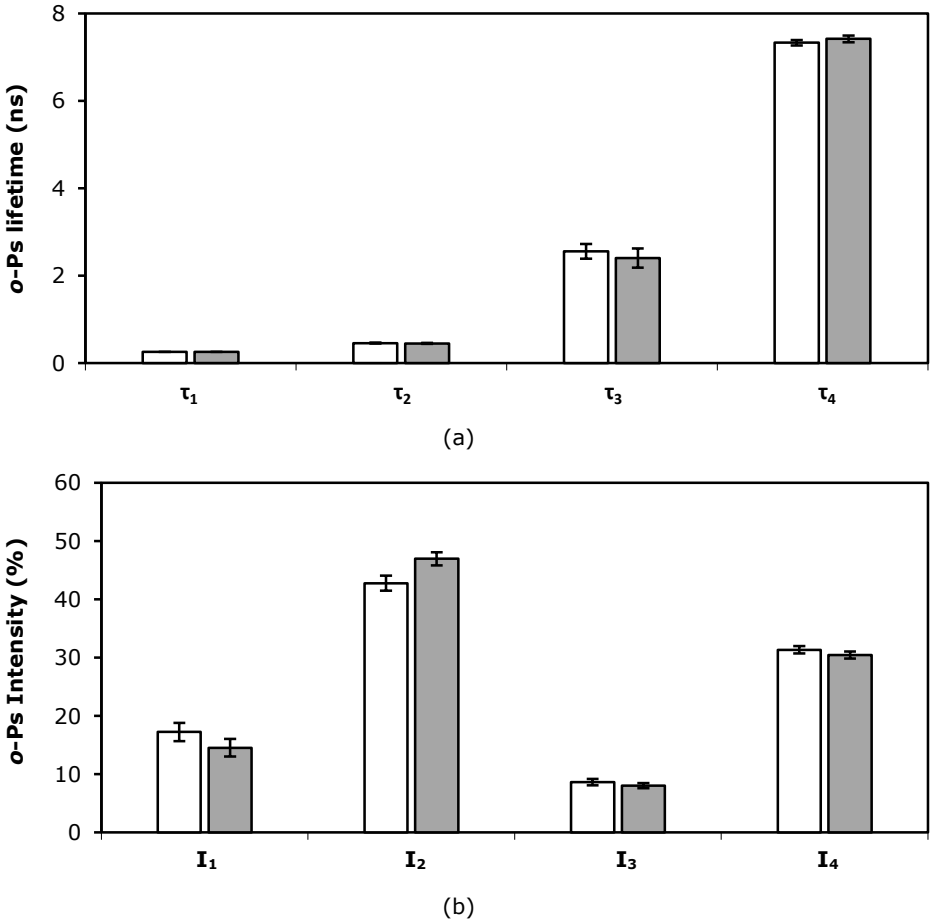

Figure 4.4: (a) *o*-Ps lifetimes and (b) corresponding intensities of $scCO_2$-treated PTMSP at 16 MPa and 70 °C. The open bars represent the sample made in the first run and the filled bars the newly prepared sample.

4.7 Thermal stability of PTMSP's free volume enlarged by $scCO_2$

The long term stability at room temperature of the free volume change achieved by subjecting PTMSP to $scCO_2$ was demonstrated in Figure 4.3. In real (membrane) applications, however, the materials are likely to be operated at higher temperatures, which could induce a decrease of the enlarged free volume if the operation temperature is close to or above the T_g. Therefore, stability measurements were carried out at higher temperatures on two selected $scCO_2$-treated samples and on the untreated reference sample. PALS measurements were performed during thermal treatment of the samples at a series of gradually increasing temperatures in the interval 30 – 170 °C. The samples were kept isothermally for 240 min (4 spectra) at each temperature in this range with increments of 20 °C. After heating up to 170 °C, the temperature cycle was completed by cooling down the samples and isothermally keeping them (4 spectra) at the same temperatures as during the heating sequence.

Since the T_g of PTMSP (> 300 °C) is well above its degradation temperature (onset around 155 °C) [18], crossing the T_g during heating was impossible. Figure 4.5a shows the changes of τ_3 and τ_4 of an untreated PTMSP sample as a function of temperature. It can be seen that after finishing the temperature cycle, both lifetimes remain unaffected, indicating that no change of the free volume cavity sizes has occurred. In general a clear expansion of the free volume due to an increase of a polymer's chain mobility could be anticipated upon heating a sample close to its T_g [8]. However, since the temperature profile is far from PTMSP's T_g, only a slight increase in τ_4 was observed, while τ_3 remained almost constant throughout the entire temperature range (Figure 4.5a). Since the onset temperature of PTMSP degradation is crossed during the temperature profile, chemical changes can be expected. A clear decrease of *o*-Ps intensity I_4 during the cooling sequence of the PALS measurement can indeed be noticed, indicating chemical changes in the polymer (Figure 4.6a).

In contrast to the untreated reference sample, the enlarged free volume of two selected $scCO_2$-treated samples was observed to partially relax when the temperature cycle was completed (Figure 4.5b/c). While a partial relaxation (±60%) of τ_4 was observed for both samples, τ_3 dropped to the initial values of the untreated reference sample (Figure 4.5a).

Andersson *et al.* reported a complete relaxation of the free volume of PEN treated for 6 h at 8 and 20 MPa CO_2 pressure and 100 °C, and subsequently subjected to an identical temperature cycle as used here [8]. In contrast to our study, the T_g of PEN (120 °C) was crossed during the temperature cycle.

In Figure 4.6b, I_4 starts far below the initial intensity of the untreated PTMSP sample (Figure 4.6a). During heating a maximum is observed at 130 °C, after which the degradation initiates and the intensity decreases. In the cooling curve a further decrease of intensity is noticed, especially at temperatures > 100 °C. For a sample treated at an even higher pressure and temperature (24 MPa and 150 °C), I_4 starts at the same level as the untreated sample, followed by a maximum at 130 °C and a drastic decrease upon cooling (Figure 4.6c). The curve of the intensity of the sample treated at 110 °C and 20 MPa (Figure 4.6b) is shifted compared to the one treated at 150 °C and 24 MPa. The reasons for this shift are unclear at this moment.

Since degradation of PTMSP starts at 155 °C, applying the $scCO_2$-treated PTMSP films above this temperature is not recommended. On the other hand, Figure 4.5b/c show that the enhanced free volume partially withstands such harsh temperature conditions, demonstrating a proper stability. Typically these polymer films could be used as membranes and applied in membrane processes at temperatures between 25 and 100 °C, far below PTMSP's degradation temperature and T_g.

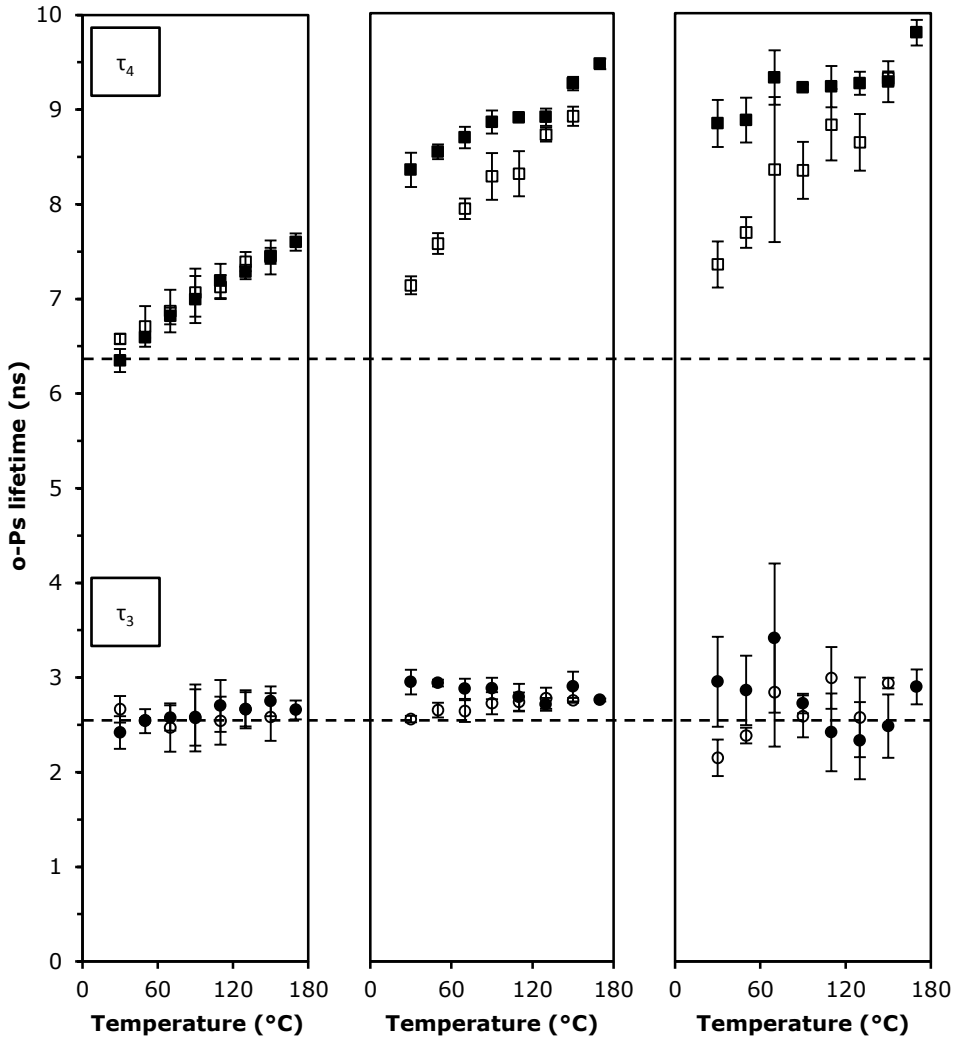

Figure 4.5: Changes of *o*-Ps lifetime τ_3 (●,○) and τ_4 (■,□) during a heating (filled symbols) and cooling (open symbols) sequence: (a) untreated PTMSP, (b) PTMSP $scCO_2$-treated at 20 MPa and 110 °C, and (c) PTMSP $scCO_2$-treated at 24 MPa and 150 °C.

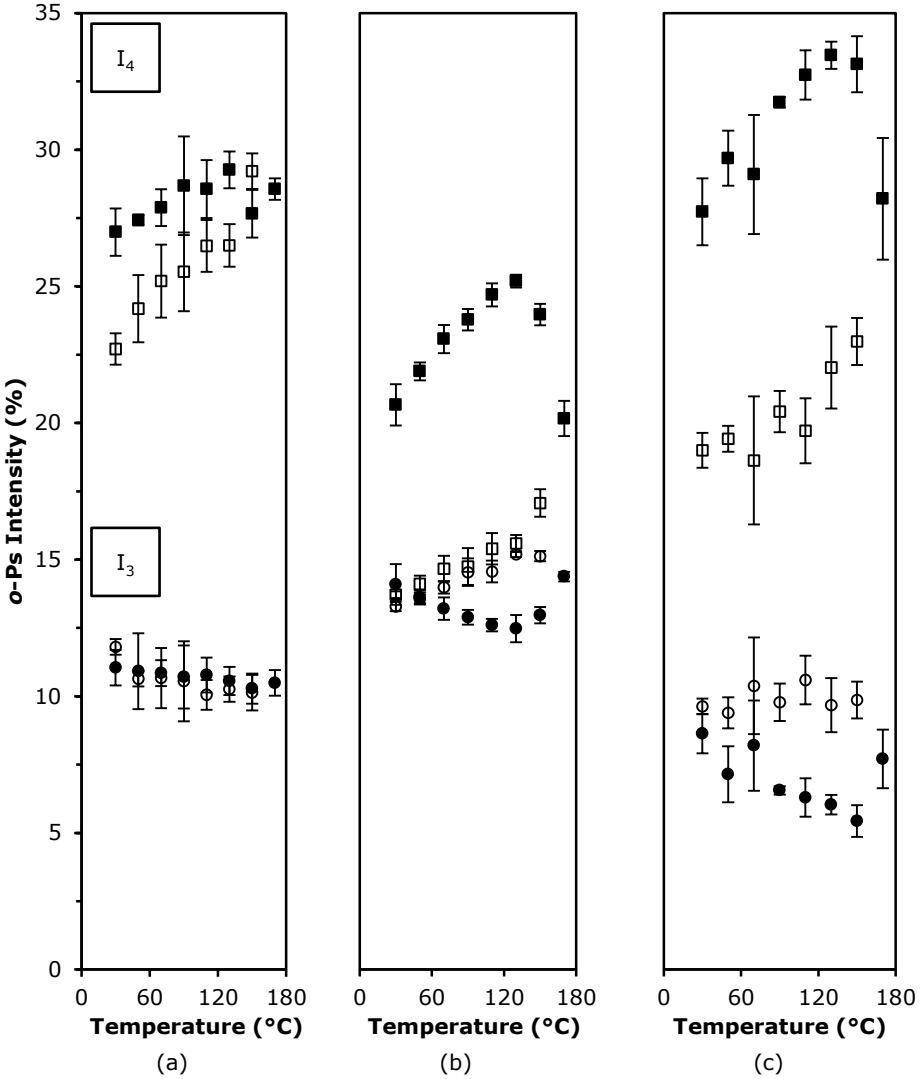

Figure 4.6: Changes of *o*-Ps intensities I_3 (●,○) and I_4 (■,□) during a heating (filled symbols) and cooling (open symbols) sequence: (a) untreated PTMSP, (b) PTMSP $scCO_2$-treated at 20 MPa and 110 °C, and (c) PTMSP $scCO_2$-treated at 24 MPa and 150 °C.

4.8 Influence of $scCO_2$ treatment on the PV performance

By applying a $scCO_2$ treatment to increase PTMSP's free volume, the presence of large non-selective holes as in silica filled membranes could be excluded. This may understandably have a positive effect on the performance of the films in membrane separations. To verify this hypothesis, all $scCO_2$-treated PTMSP membranes were screened in PV using a 5 wt.% aqueous ethanol mixture at 50 °C as a feed.

Since the $scCO_2$ treatment induces an increase in membrane thickness of 10 – 25 %, thickness corrected fluxes or specific permeation rates were calculated and presented in Figure 4.7a. A clear increase in specific permeation rate is noticed for all $scCO_2$-treated membranes compared to the untreated reference membrane, reaching a maximum of 76% for the samples treated at 70 °C and 24 MPa. This is comparable to unsupported 50 wt.% silica filled PTMSP membranes, where specific permeation rate increases up to 72% compared to unfilled reference membranes were found (Chapter 3) [21]. For samples treated at 150 °C at the same pressure, the specific permeation rate is significantly lower (Figure 4.7a). GPC data (section 4.4), *o*-Ps intensities (section 4.7) and thermogravimetrical analysis [18] revealed the partial degradation of PTMSP after treatment at high temperatures (150 °C) for 6 hours. Therefore the lower specific permeation rate at 150 °C could be tentatively explained by sample degradation or changes in chemical structure.

Figure 4.7b displays the ethanol permeate concentration of the reference and $scCO_2$-treated membranes as a function of treatment pressure and temperature. A general increase in ethanol permeate concentration is noticed for all $scCO_2$-treated samples, compared to the reference. Samples treated at 40 °C and 12 MPa, and 70 °C and 24 MPa, are markedly more ethanol-selective. The highest ethanol permeate concentrations, around 65 wt.%, are thus found at the lowest treatment temperatures, possibly due to the absence of thermal degradation during the $scCO_2$ treatment. Moreover, the polymer chain orientation in the polymer matrix is possibly altered after swelling in $scCO_2$, thereby slightly changing the affinity between the membrane and the feed mixture. Further research is needed to properly address the increased selectivity. A newly prepared sample treated at 70 °C and 16 MPa showed similar specific

permeation rates and ethanol concentrations in the permeate, demonstrating the reproducibility of the $scCO_2$ treatment as already demonstrated with PALS data in section 4.6.

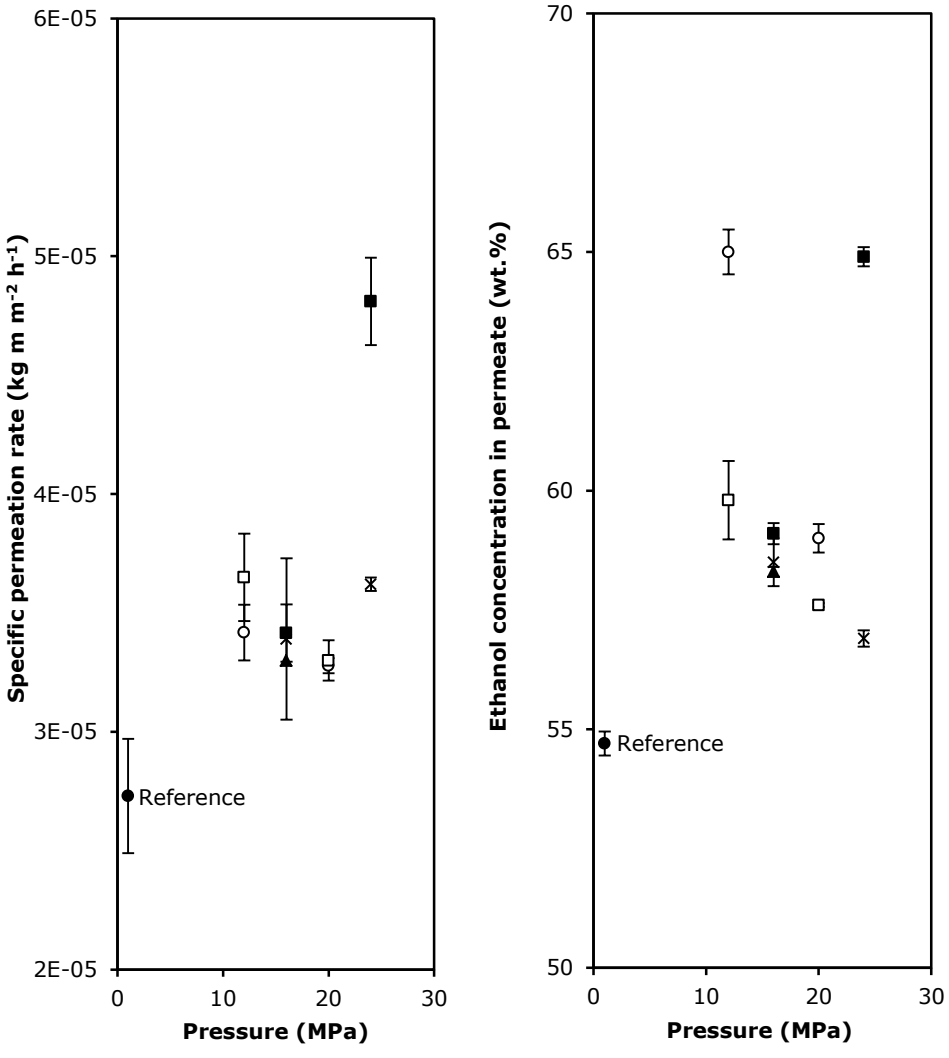

Figure 4.7: (a) Specific permeation rate and (b) ethanol permeate concentration of untreated and $scCO_2$-treated, unfilled PTMSP membranes in the separation of a 5 wt.% $EtOH/H_2O$ mixture at 50°C. Different treatment temperatures are represented by the following symbols: (●) reference sample at room temperature, (○) 40 °C, (■) 70 °C, (□) 110 °C, (×) 150 °C. A freshly prepared sample, $scCO_2$-treated at 70 °C and 16 MPa (▲) was added to evaluate the reproducibility of the treatment.

4.9 Correlation of free volume properties and permeation characteristics

Figure 4.8 shows the correlation between the free volume cavity sizes, calculated according to Equation 2-4, and the specific permeation rate of the $scCO_2$-treated PTMSP membranes in the pervaporative separation of a 5 wt.% EtOH/H_2O mixture. A clear increase in specific permeation rate with increasing free volume cavity size is observed. Although the free volume is proven to be correlated with the permeation properties [18,22], changes in the chemical structure have also a significant effect. The superior performance of the sample treated at 70 °C and 24 MPa could tentatively be explained by chemical changes due to degradation of samples treated at more elevated temperatures in combination with a possibly altered polymer chain orientation in the matrix. Both v_3 and v_4 display a similar correlation, indicating the importance of both free volume parameters for the permeation characteristics.

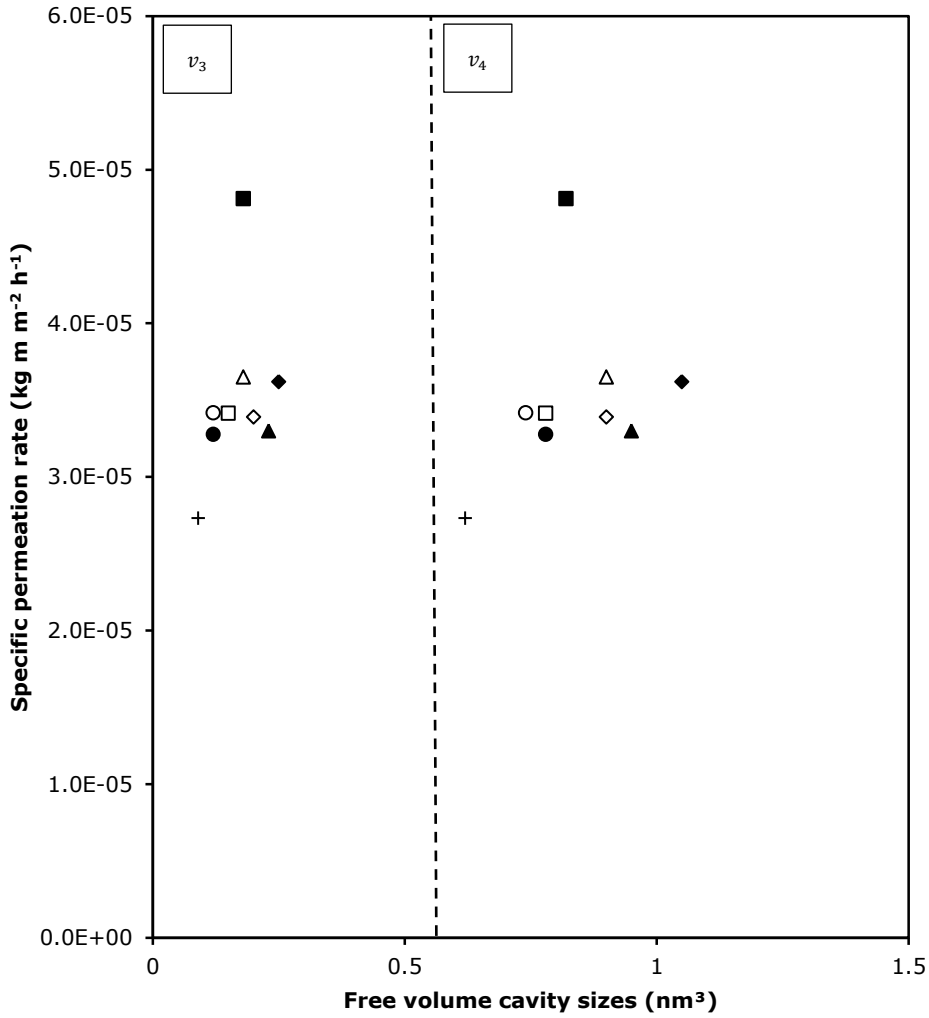

Figure 4.8: Specific permeation rate as a function of the free volume cavity sizes v_3 (left) and v_4 (right) of unfilled $scCO_2$-treated PTMSP membranes. Different treatment temperatures and pressures are represented by the following symbols: (+) reference sample at room temperature, (○,●) 40 °C, (□,■) 70 °C, (Δ,▲) 110 °C, (◇,◆) 150 °C in which the open symbols represent the lower (12 and 16 MPa) and the filled symbols the higher (20 and 24 MPa) treatment pressure.

4.10 $scCO_2$ as alternative to mixed matrix membranes

Increasing the free volume of a polymer network, either by the incorporation of hydrophobic silica or a $scCO_2$ treatment, results in increased permeabilities in PV. Figure 4.9 compares the relative increases in specific permeation rate of untreated PTMSP-silica membranes and unfilled $scCO_2$-treated PTMSP membranes, as function of the silica filler load and treatment pressure, respectively. The graph shows that by subjecting an unfilled PTMSP membrane to a $scCO_2$ treatment at 70 °C and 24 MPa, a comparable increase in specific permeation rate (76%) as produced by incorporation of 50 wt.% silica in a PTMSP membrane (72%) can be accomplished. A $scCO_2$ treatment could thus be used as a valuable alternative to the mixed matrix membranes in which hydrophobic silica aggregates are dispersed in the polymer matrix.

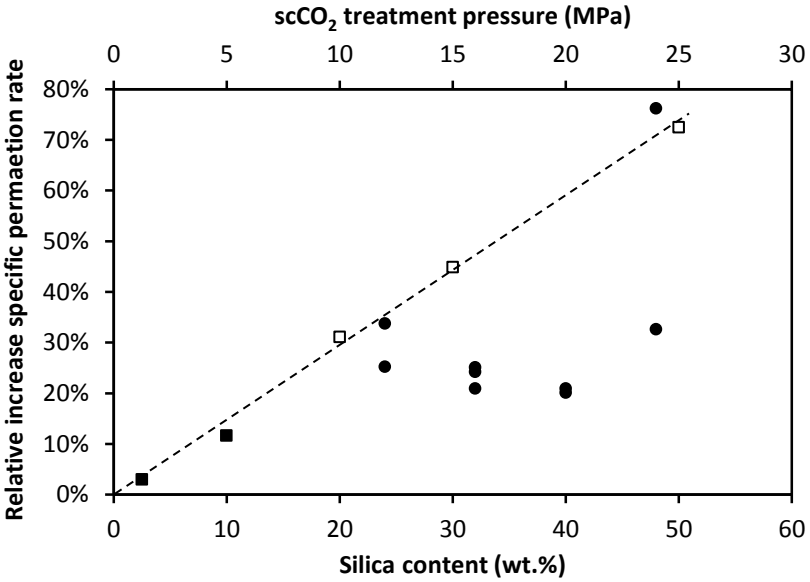

Figure 4.9: Comparison of relative increases in specific permeation rate of untreated PTMSP-silica membranes as a function of silica content (■,□), and of unfilled $scCO_2$-treated membranes as a function of treatment pressure (●). The PTMSP-silica data are taken from Chapter 5 (■) and from Chapter 3 (□). The dotted line represents the increase upon filling the membrane with silica.

Since no fifth lifetime was found in the unfilled $scCO_2$-treated samples, the increase in specific permeation rates with increasing treatment intensity can be solely attributed to increasing τ_3 and τ_4 values.

4.11 Conclusion

PTMSP films treated with $scCO_2$ at different pressures and temperatures resulted in *o*-Ps lifetime increments up to 74% for τ_3 and 48% for τ_4, as revealed by PALS. It was demonstrated that the free volume enlargement of the $scCO_2$-treated PTMSP films had a relaxation time of approximately 30 years, and that the films can be produced with good reproducibility. At high temperatures (110 – 150 °C), *o*-Ps intensities and GPC data revealed chemical changes in the polymer sample due to thermal degradation of the PTMSP film. However, at lower temperatures (40 – 70 °C), equally significant lifetime increases up to 47% for τ_3 and 23% for τ_4 could be achieved.

In PV, these $scCO_2$-treated membranes performed clearly better in terms of specific permeation rate and $EtOH/H_2O$ separation factor. For the PTMSP membranes treated at 70 °C and 24 MPa, the specific permeation rate could be increased up to 76%, which is comparable to the 72% increase observed for untreated PTMSP membranes upon addition of 50 wt.% silica filler. Additionally, the ethanol concentration in the permeate increased significantly upon treating the membranes with $scCO_2$.

This study focused on PTMSP membranes and their use in $EtOH/H_2O$ separations, but it is clear that the presented $scCO_2$ treatment method offers a novel, generic and versatile preparation route for high performance membranes, preferably based on high free volume polymers, with much wider potential applicability in gas and vapour separation.

REFERENCES

[1] B. Subramanian, Gas-expanded liquids for sustainable catalysis and novel materials: Recent advances, *Coord. Chem. Rev.* **254** (2010) 1843 – 1853.

[2] T. Deligeorgiev, N. Gadjev, A. Vasilev, S. Koloyanova, J. J. Vaquero, J. Alvarez-Builla, Green chemistry in organic synthesis, *Mini-Rev. Org. Chem.* **7** (2010) 44 – 53.

[3] F. Montanes, A. Olano, G. Reglero, E. Ibanez, T. Fornari, Supercritical technology as an alternative to fractionate prebiotic galactooligosaccharides, *Sep. Purif. Technol.* **66** (2009) 383 – 389.

[4] L. J. Wang, C. L. Weller, Recent advances in extraction of nutraceuticals from plants, *Trends Food Sci. Technol.* **17** (2006) 300 – 312.

[5] X. Li, B. D. Vogt, Impact of thickness on CO_2 concentration profiles within polymer films swollen near the critical pressure, *Polymer* **50** (2009) 4182 – 4188.

[6] Y. P. Handa, S. Capowski, M. O'Neill, Compressed gas induced plasticization of polymers, *Thermochim. Acta.* **226** (1993) 177 – 185.

[7] H. Tai, C. E. Upton, L. J. White, R. Pini, G. Storti, M. Mazotti, K. M. Schakesheff, S. M. Howdle, Studies on the interactions of CO_2 with biodegradable poly(DL-lactic acid) and poly(lactic acid-co-glycolic acid) copolymers using high pressure ATR-IR and high pressure rheology, *Polymer* **251** (2010) 1425 – 1431.

[8] A. Andersson, W. Zhai, J. Yu, J. He, F. H. J. Maurer, Free volume and crystallinity of poly(ethylene naphthalate) treated in pressurized carbon dioxide, *Polymer* **51** (2010) 146 – 152.

[9] T. Oka, K. Ito, C. He, C. Dutriez, H. Yokoyama, Y. Kobayashi, Free volume expansion and nanofoaming of supercritical carbon dioxide treated polystyrene, *J. Phys. Chem. B* **112** (2008) 12191 – 12194.

[10] W. Ma, A. Andersson, J. He, F. H. J. Maurer, Free volume changes, crystallization and crystal transition behavior of syndiotactic polystyrene in supercritical CO_2 revealed by positron annihilation lifetime spectroscopy, *Macromolecules* **41** (2008) 5307 – 5312.

[11] R. Liao, W. Yu, C. Zhou, F. Yu, J. Tian, The formation of γ-crystal in long-chain branched polypropylene under supercritical carbon dioxide, *J. Polym. Sci. Part B: Polym. Phys.* **46** (2008) 441 – 451.

[12] W. Zhai, J. Yu, W. Ma, J. He, Influence of long-chain branching on the crystallization and melting behavior of polycarbonates in supercritical CO_2, *Macromolecules* **40** (2007) 73 – 80.

[13] S. P. Nalawade, F. Picchioni, J. H. Marsman, L. P. B. M. Janssen, The FT-IR studies of the interactions of CO_2 and polymers having different chain groups, *J. Supercrit. Fluids* **36** (2006) 236 – 244.

[14] X. Chen, J. J. Feng, C. A. Bertelo, Plasticization effects on bubble growth during polymer foaming, *Polym. Eng. Sci.* **46** (2006) 97 – 107.

[15] Z. Zhang, Y. P. Handa, An in situ study of plasticization of polymers by high-pressure gases, *J. Polym. Sci.: Part B: Polym. Phys.* **36** (1998) 977 – 982.

[16] G. Dlubek, J. Pionteck, M. Q. Shaikh, L. Häußler, S. Thränert, E. M. Hassan, R. Krause-Rehberg, The free volume in two untreated, pressure-densified, and CO_2 gas exposed polymers from positron lifetime and pressure-volume-temperature experiments, *e-Polymers* **108** (2007).

[17] M. Mohsen, E. A. H. Gomaa, H. Schut, E. Van Veen, Positron annihilation lifetime studies of gas sorption and desorption in polyethylene and poly[1-(trimethylsilyl)-1-propyne], *J. Appl. Polym. Sci.* **80** (2001) 970 – 974.

[18] K. De Sitter, P. Winberg, J. D'Haen, C. Dotremont, R. Leysen, J. A. Martens, S. Mullens, F. H. J. Maurer, I. F. J. Vankelecom, Silica filled poly(1-trimethylsilyl-1-propyne) nanocomposite membranes: relation between the transport of gases and structural characteristics, *J. Membr. Sci.* **278** (2006) 83 – 91.

[19] H. C. Booij, J. H. M. Palmen, Viscoelasticity of ABS samples differing in thermal history, *Polym. Eng. Sci.* **18** (1977) 781 – 787.

[20] C. T. Moynihan, P. B. Macedo, C. J. Montrose, P. K. Gupta, M. A. DeBolt, J .F. Dill, B. E. Dom, P. W. Drake, A. J. Easteal, P. B. Elterman, R. P. Moeller, H. Sasabe, J. A. Wilder, Structural relaxation in vitreous materials, *Ann. N. Y. Acad. Sci.* **279** (1976) 15 – 35.

[21] S. Claes, P. Vandezande, S. Mullens, R. Leysen, K. De Sitter, A. Andersson, F. H. J. Maurer, H. Van den Rul, R. Peeters, M. K. van Bael, High flux composite PTMSP-silica nanohybrid membranes for the pervaporation of ethanol/water mixtures, *J. Membr. Sci.* **351** (2010) 160 – 167.

[22] S. Chovau, A. Dobrak, A. Figoli, F. Galiano, S. Simone, E. Drioli, S.K. Sikdar, B. Van der Bruggen, Pervaporation performance of unfilled and filled PDMS membranes and novel SBS membranes for the removal of toluene from diluted aqueous solutions, *Chem. Eng. J.* **159** (2010) 37 – 46.

Chapter 5

Supercritical CO_2 in combination with inorganic fillers

5.1 Introduction

The potential of the $scCO_2$ treatment to increase the free volume and enhance the PV properties of neat, unfilled PTMSP membranes has been discussed in Chapter 4. Inspired by the beneficial effect of silica filler incorporation reported in Chapter 3, PTMSP-silica membranes were prepared and subsequently subjected to an identical $scCO_2$ treatment, anticipating on the combined, potentially synergetic effect on the free volume and PV performance of the membranes. Both the free volume changes (PALS) and PV performance of the silica filled $scCO_2$-treated PTMSP membranes were investigated. The first section describes the free volume changes of PTMSP-silica membranes before and after $scCO_2$ treatment (Section 5.3). Subsequently, the temperature stability of the free volume in these systems is studied (Section 5.4), and finally the performance of the membranes in PV is presented (Section 5.5).

5.2 Experimental

The used materials, PALS analysis and PV experiments have been extensively reported in Chapter 4. In contrast to the unfilled membranes, only one $scCO_2$ treatment condition (20 MPa and 110 °C) was applied here for PTMSP membranes with varying silica filler concentrations.

Unsupported silica filled PTMSP membranes were prepared from toluene solutions containing 3 wt.% of total solids. Toluene-based silica dispersions with a concentration of 0.075, 0.300 and 0.600 wt.% of silica were prepared. To

these dispersions, PTMSP was added so as to obtain suspensions with polymer concentrations of 2.925, 2.700 and 2.400 wt.%, respectively. Membranes containing 2.5, 10 and 20 wt.% of silica were thus prepared. The precise suspension preparation and evaporation procedures have been reported in Chapter 2.

5.3 Influence of the combinatorial effect of $scCO_2$ treatment and hydrophobic silica incorporation on the free volume

PALS analysis of silica filled PTMSP membranes is typically performed with a five-component analysis [1,2]. The extra fifth *o*-Ps lifetime (τ_5) represents the interstitial cavities, created by the silica aggregates.

Figure 5.1 shows the three *o*-Ps lifetimes τ_3, τ_4 and τ_5 prior to and after the $scCO_2$ treatment. Remarkable is the absence of the enlarging effect, after $scCO_2$ treatment, on τ_3 upon filling the membrane with 2.5, 10 or 20 wt.% silica. An increased resistance to swelling of the polymer matrix by the presence of silica aggregates is suggested, leading to the diminishing of the free volume enlargement attributed to the channel like holes (τ_3) (Figure 5.1a). After treating the silica filled membranes, τ_4 increases significantly, but to a lesser extent as the unfilled PTMSP membranes (Figure 4.2a).

Figure 5.1b shows the fifth *o*-Ps lifetime component (τ_5), which displays a large variation for the 2.5 wt.% silica filled membranes and a decreasing variation with increasing filler content. This large uncertainty on the measurement could be explained by the low filler concentration, which is stressed out in an extremely low probability for *o*-Ps annihilation in the silica aggregates (Figure 5.2). The *o*-Ps lifetime intensity (I_5) increases with increasing filler concentration (Figure 5.2), partially accounting for the decreasing variation in τ_5 upon increasing the filler content (Figure 5.1b). Due to the high standard deviations on the τ_5 plot, conclusions from these data are hard to make.

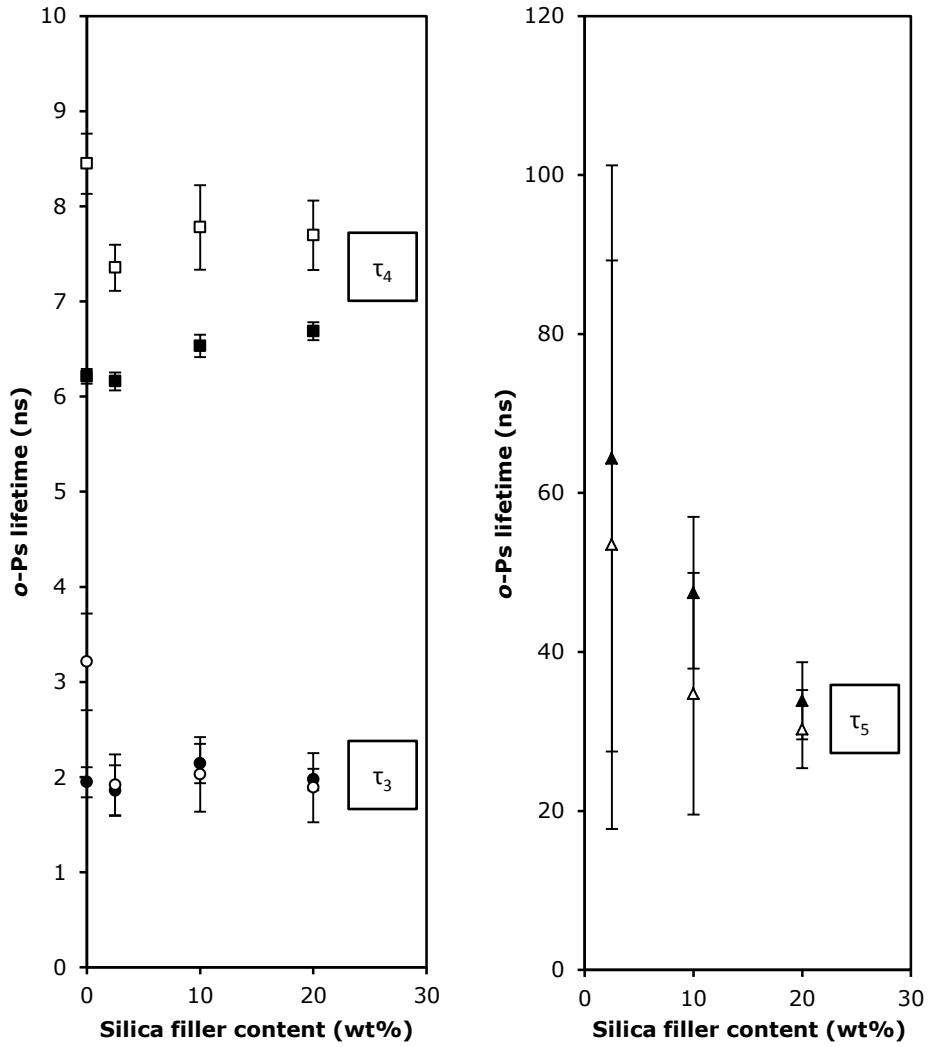

Figure 5.1: (a) *o*-Ps lifetimes τ_3 (●,○), τ_4 (■,□) and (b) τ_5 (▲,Δ) of untreated (filled symbols) and $scCO_2$-treated (open symbols) PTMSP membranes (20 MPa, 110 °C) as a function of the silica filler content.

The *o*-Ps intensities in Figure 5.2 show a decrease of I_4 with increasing filler content and thus increasing I_5 as reported earlier by Winberg *et al.* [1]. Treating the membranes with $scCO_2$ seems to affect mainly I_4 and I_5. For τ_4 a decrease in intensity is noticed after the $scCO_2$ treatment, which can be explained by the onset of degradation as reported in Chapter 4. Since $I_5 = 1 - I_1 - I_2 - I_3 - I_4$ and

I_1, I_2 and I_3 are almost not affected by the $scCO_2$ treatment, the decrease of I_4 automatically results in an increase of I_5.

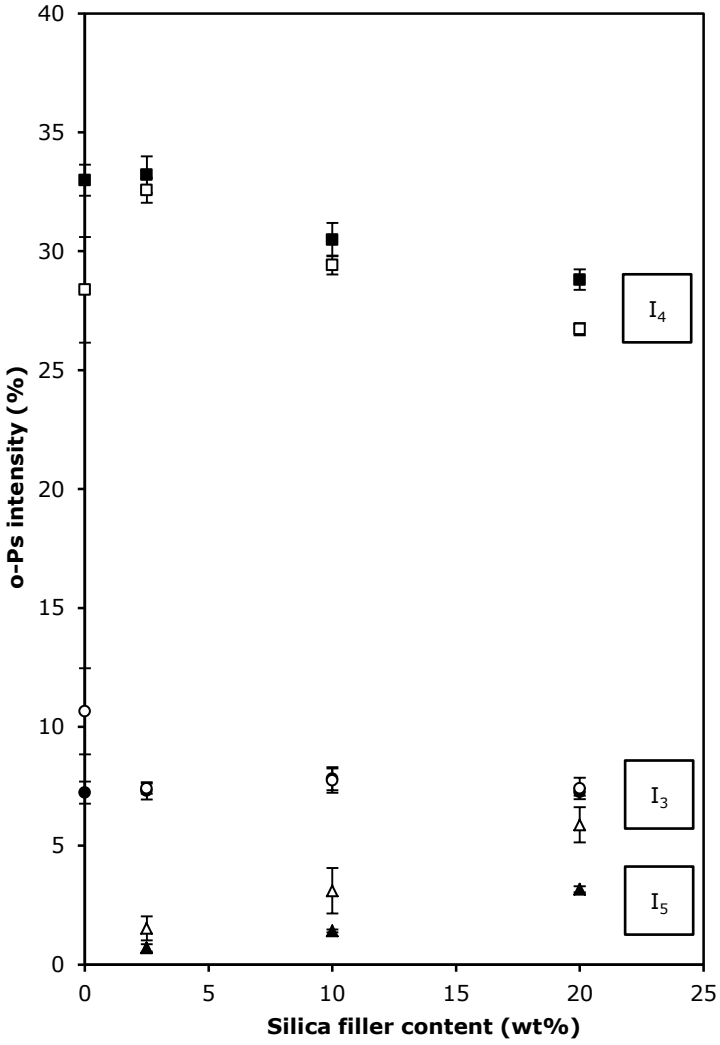

Figure 5.2: *o*-Ps intensity I_3 (●,○), I_4 (■,□) and I_5 (▲,Δ) of untreated (filled symbols) and $scCO_2$-treated (open symbols) PTMSP membranes (20 MPa, 110 °C) as a function of the silica filler content.

5.4 Thermal stability of the $scCO_2$ enlarged free volume of silica filled PTMSP membranes

The thermal stability of the enlarged free volume is evaluated with PALS measurements at elevated temperatures in a similar way as presented in Chapter 4. Figure 5.3 shows the *o*-Ps lifetime curves of untreated 20 wt.% silica filled PTMSP membranes. Heating the sample to 170 °C and cooling it down to room temperature has no significant effect on the channel – like holes (τ_3) nor on the larger cages (τ_4) (Figure 5.3a), indicating the absence of relaxation of the initial free volume after completing the thermal cycle. The interstitial cavities of the silica aggregates (τ_5), however, tend to enlarge after completion of the thermal cycle (Figure 5.3b). This could be explained by the increased mobility of the polymer upon heating, followed by a possible rearrangement of the silica aggregates.

The *o*-Ps lifetime intensities of the 20 wt.% silica filled PTMSP membrane during the thermal cycle were not included since similar curves have been reported in Chapter 4. The only significant effect is the decrease of I_4 after completion of the temperature cycle, which can be explained by the thermal degradation of PTMSP at these elevated temperatures. An almost identical decay of I_4 has been reported in Figure 4.6 for unfilled PTMSP membranes, i.e. meaning an increase of I_4 up to approximately 130 °C, followed by a decrease which is further stressed during cooling.

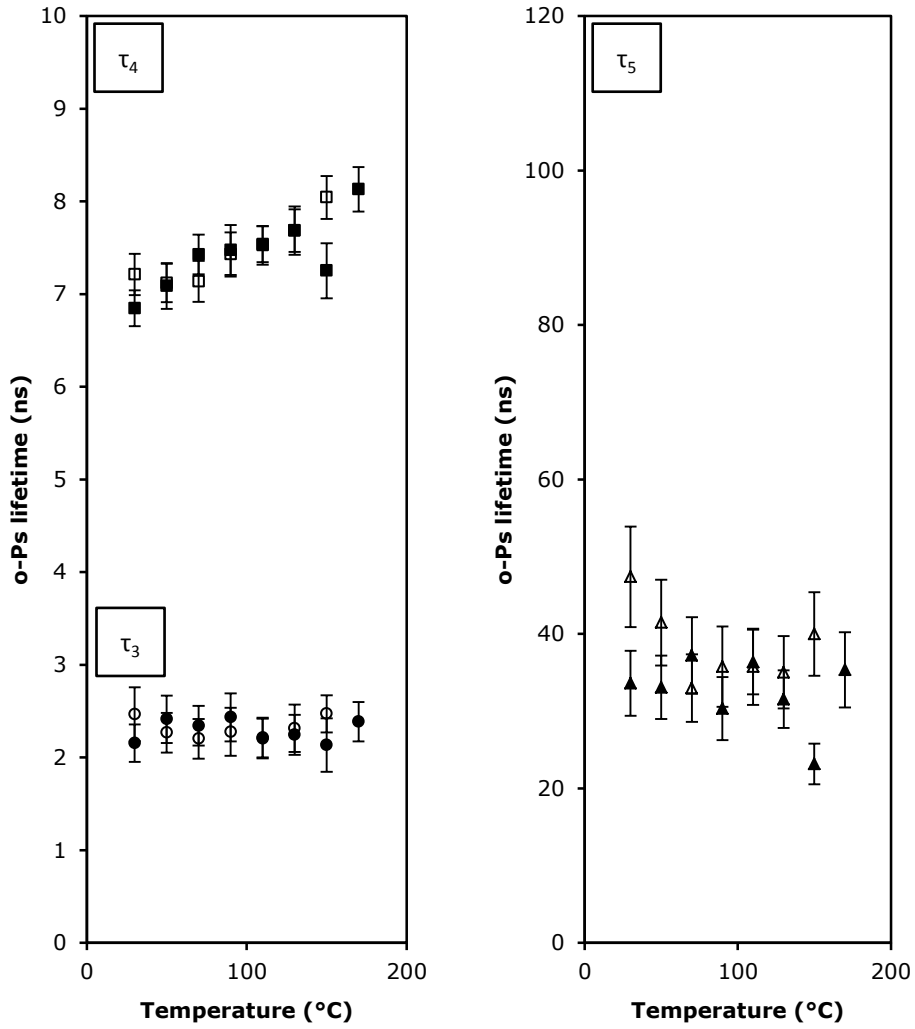

Figure 5.3: Changes of (a) *o*-Ps lifetimes τ_3 (●,○), τ_4 (■,□) and (b) τ_5 (▲,Δ) of an untreated silica filled (20 wt.%) PTMSP sample during heating (filled symbols) and cooling (open symbols).

After, a $scCO_2$-treated 20 wt.% silica filled PTMSP membrane (20 MPa, 110 °C) was subjected to the same thermal cycle and measured with PALS. It can be seen in Figure 5.4 that the excess free volume of the larger cages (τ_4) partially relaxes (44%) after completing the thermal cycle. For unfilled membranes the excess free volume relaxed up to 60% after being subjected to exactly the same

temperature cycle (Figure 4.5). No significant effect of the temperature cycle on τ_5 is noticed (Figure 5.4b). Again the corresponding *o*-Ps intensities are not shown here, since identical observations were already made in Chapter 4 for unfilled PTMSP membranes (Figure 4.6).

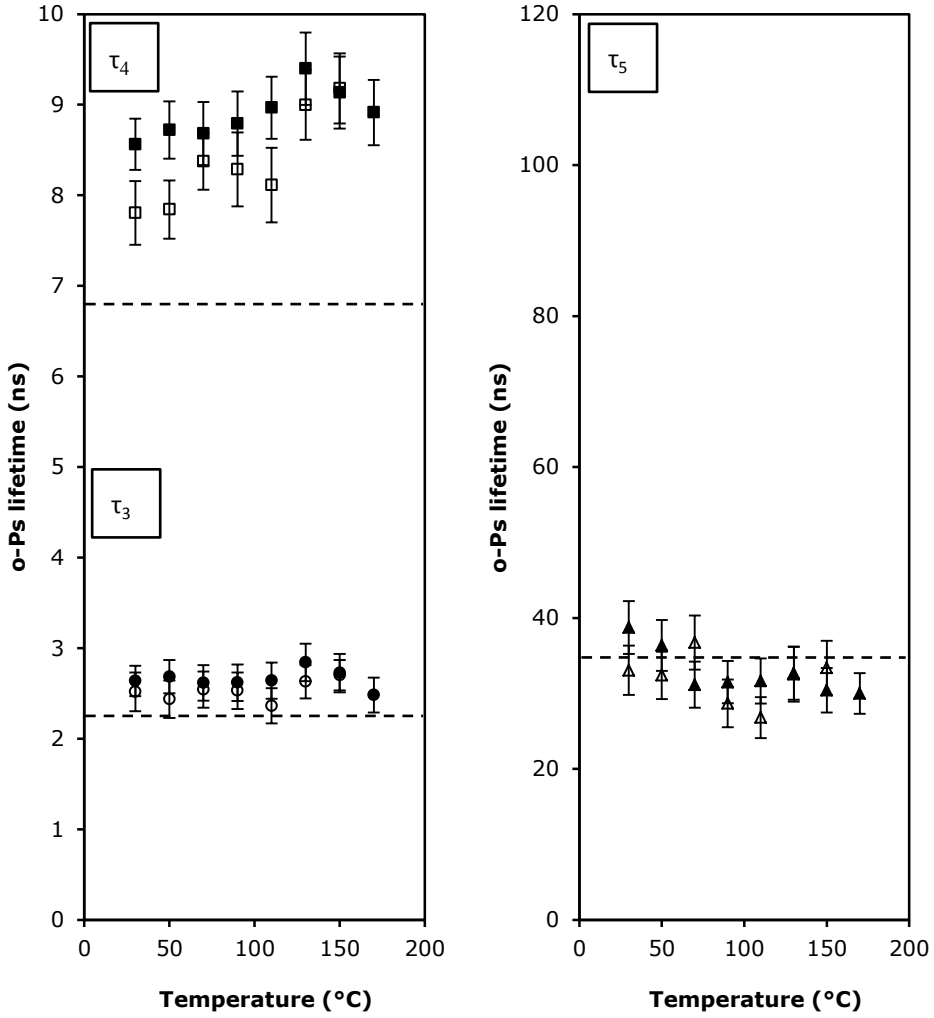

Figure 5.4: Changes of (a) *o*-Ps lifetimes τ_3 (●,○) and τ_4 (■,□), and (b) τ_5 (▲,Δ) of a $scCO_2$-treated (20 MPa, 110 °C) silica filled PTMSP (20 wt.%) sample during heating (filled symbols) and cooling (open symbols). The dotted lines represent the start points of the untreated sample (Figure 5.3).

5.5 Influence of the combinatorial effect of $scCO_2$ treatment and hydrophobic silica incorporation on the PV performance

The combined effect of silica particle addition and $scCO_2$ treatment (20 MPa, 110 °C) of PTMSP membranes on their PV performance is reported in Figure 5.5. A 5 wt.% EtOH/water mixture was used as feed. It can be seen that the $scCO_2$ treatment induces a clear increase in specific permeation rate (Figure 5.5a). Addition of silica (2.5, 10, 20 wt.%) to the PTMSP membrane increases the specific permeation rate slightly, while treating the silica filled membranes with $scCO_2$ further increases the permeation properties. It is remarkable that the specific permeation rates of all four $scCO_2$-treated samples are approximately equal, independent of the presence and concentration of the silica filler. Higher silica filler loadings may have a positive effect on the specific permeation rate, but could also increase the polymer's resistance against swelling under CO_2 and thus diminish the permeability enhancing effect of the $scCO_2$ treatment. An optimal between silica filler loading and $scCO_2$ treatment is expected.

The ethanol concentration in the permeates of all silica filled PTMSP membranes increases slightly after $scCO_2$ treatment (Figure 5.5b), compared to the untreated silica filled PTMSP samples. This effect is however less pronounced than for the unfilled $scCO_2$-treated membranes (Figure 4.7b), possibly because of the appearance of non-selective holes due to the presence of large silica aggregates.

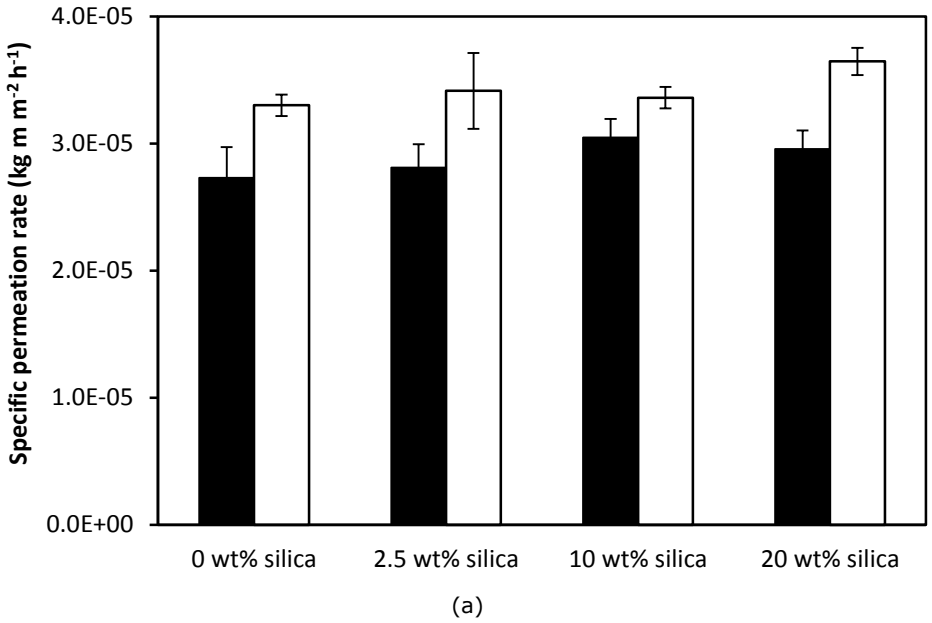

(a)

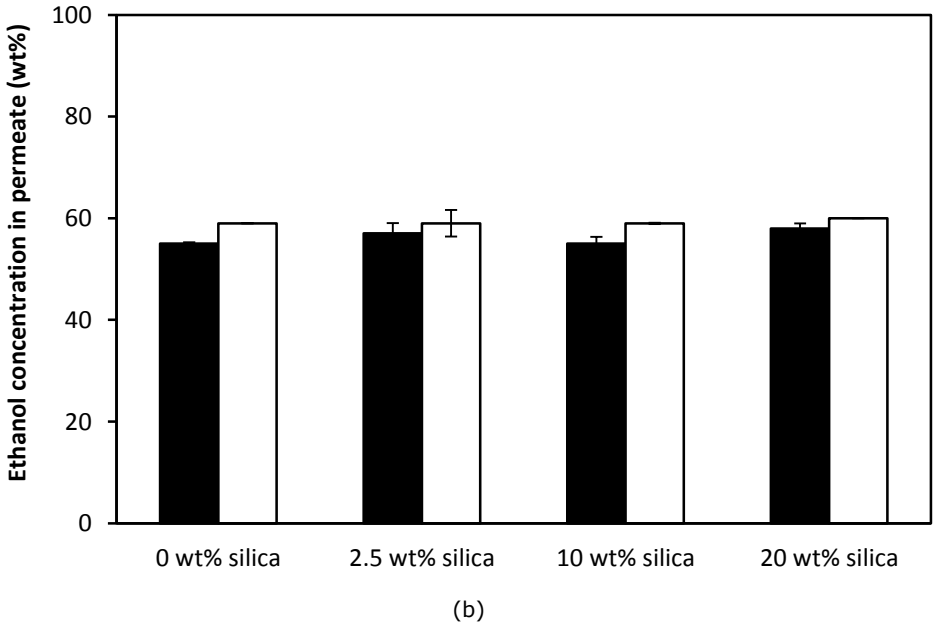

(b)

Figure 5.5: (a) Specific permeation rate and (b) ethanol concentration in the permeate of untreated (filled bars) and $scCO_2$-treated (open bars, 20 MPa / 110 °C) PTMSP membranes, as a function of the silica filler content.

5.6 Correlation of free volume properties and permeation characteristics

For the PTMSP-silica membranes, the specific permeation rate only correlates properly with the fourth lifetime component (Figure 5.6). As described already in paragraph 5.3, τ_3 is not affected by the $scCO_2$ treatment after filling the system with silica aggregates, explaining the absence of a correlation. The $scCO_2$-treated PTMSP-silica membranes with 20 wt.% silica filler resulted in the highest specific permeation rate, clearly demonstrating the synergetic effect of silica incorporation and the $scCO_2$ treatment. Due to the large variation on the fifth lifetime (Figure 5.1b), no correlation was made.

The PALS data of the $scCO_2$-treated silica filled membranes (Figure 5.1) reveal the minor effect on the interstitial cavities, compared to the larger cages present in the polymer matrix (τ_4). The interstitial cavities (τ_5) apparently compact due to the $scCO_2$ treatment (Figure 5.1b), while the channel like holes (τ_3) are not affected by the $scCO_2$ treatment. The specific permeation rate increase reported in Figure 5.5 could then be solely attributed to the increase of the free volume corresponding to the larger cages (τ_4).

Figure 4.9 showed a relative increase of approximately 72% in specific permeation rate for a 50 wt.% silica filled PTMSP membrane, compared to an unfilled membrane. The $scCO_2$-treated unfilled PTMSP membrane (Chapter 4) with a comparable effect on the specific permeation rate (i.e. increase of 76% compared to untreated membrane) exhibits a τ_4 of 7.7 ns, compared to 6.2 ns for the untreated membrane. This confirms the findings of Winberg *et al.* who reported an increase in τ_4 from 6.5 up to 7.7 ns upon filling PTMSP with 50 wt.% silica [1]. The resemblance is striking, indicating the major contribution of the fourth lifetime component in the vapour transport in PV, since the unfilled $scCO_2$ treated membranes do not exhibit a fifth lifetime component. These findings are in contradiction with the conclusions made by De Sitter *et al.* in gas separation [2]. Unfortunately, PALS data do not inform about the quantity of the free volume cavities and therefore further research is needed to elucidate the major importance of the changes in the fourth lifetime with respect to the membrane

permeability, rather than the interstitial cavities created by the silica aggregates (τ_5).

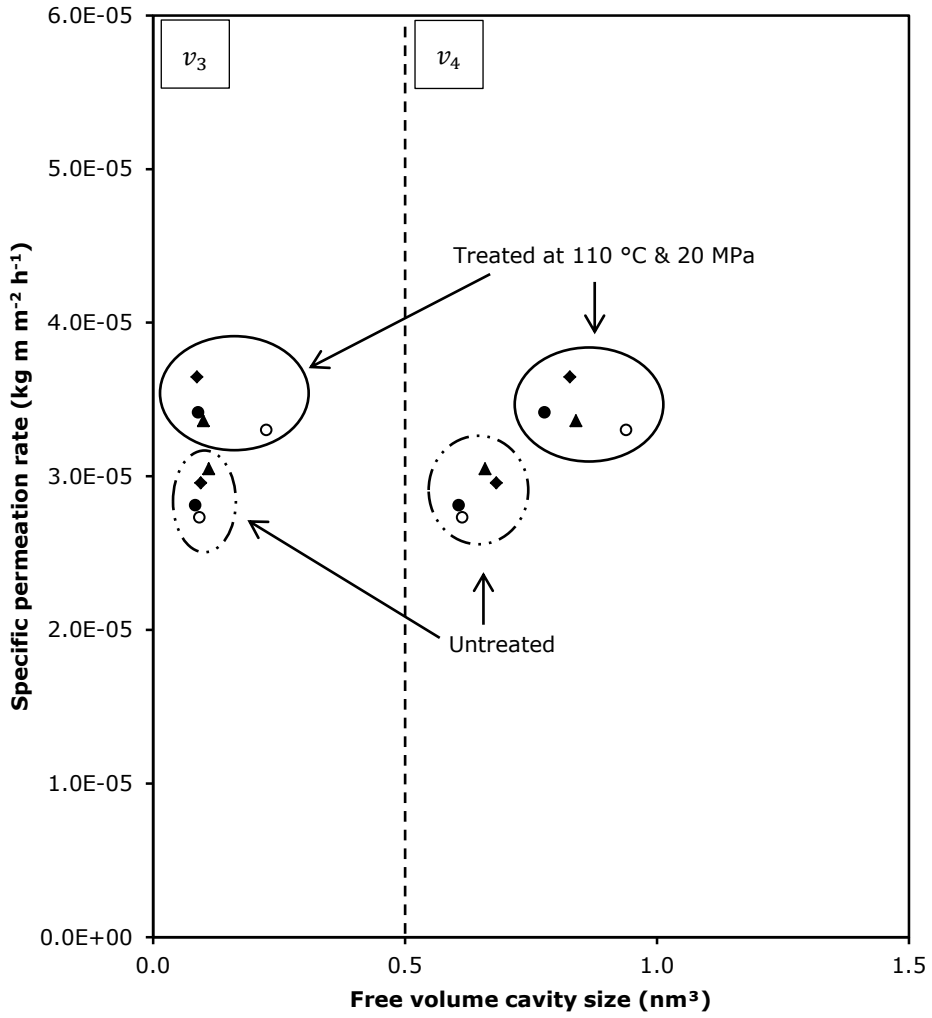

Figure 5.6: Specific permeation rate as a function of the free volume cavity sizes v_3 (left) and v_4 (right) of silica filled $scCO_2$-treated PTMSP membranes. Different silica loadings are represented by the following symbols: (○) 0 wt.%, (●) 2.5 wt.%, (▲) 10 wt.% and (◆) 20 wt.% silica.

5.7 Conclusion

PTMSP-silica membranes treated with $scCO_2$ were successfully applied in the pervaporative separation of dilute $EtOH/H_2O$ mixtures. The $scCO_2$-treated membranes performed 10 to 23 % better in terms of specific permeation rate and 7 to 10 % better in terms of $EtOH/H_2O$ separation factor. The $scCO_2$-treated 20 wt.% silica filled PTMSP membrane exhibited the highest specific permeation rate. However, the effect of the $scCO_2$ treatment on unfilled PTMSP membranes was much more pronounced.

REFERENCES

[1] P. Winberg, K. De Sitter, C. Dotremont, S. Mullens, I.F.J. Vankelecom, F.H.J. Maurer, Free volume and interstitial mesopores in sillica filled poly(1-trimethylsilyl-1-propyne) nanocomposites, *Macromolecules* **38** (2005) 3776 – 3782.

[2] K. De Sitter, P. Winberg, J. D'Haen, C. Dotremont, R. Leysen, J. A. Martens, S. Mullens, F. H. J. Maurer, I. F. J. Vankelecom, Silica filled poly(1-trimethylsilyl-1-propyne) nanocomposite membranes: Relation between the transport of gases and structural characteristics, *J. Membr. Sci.* **278** (2006) 83 – 91.

Chapter 6

Crosslinking of PTMSP membranes

6.1 Introduction

As mentioned in Chapter 1, PTMSP has great potential in PV thanks to its intrinsic nanoporosity, glassy nature (T_g > 300 °C) and pronounced hydrophobicity [1-9]. Despite these positive properties, PTMSP's relatively low solvent resistance and physical stability make crosslinking of the membrane often inevitable to achieve selective separations of more demanding feed mixtures.

Several methods have been applied, aiming to improve the chemical and physical stability of PTMSP. Blending PTMSP with rubbery polymers [10], adding nanoparticles [11,12], bromination [13] and crosslinking [14-20] are some examples. Using bis(azides) as crosslinker molecules, the solvent and physical stability of PTMSP membranes could be increased. The azide-crosslinked PTMSP films became insoluble in commonly used solvents for the manufacturing of PTMSP membranes such as toluene, cyclohexane and tetrahydrofuran (THF) [14,15].

Despite the great potential of PTMSP membranes in several separation processes like vapour [2-9], liquid [21-22] and gas separations [14-20], to our best knowledge only the latter has been reported in relation with crosslinked membranes [14-20]. Crosslinking was conducted here to circumvent an unwanted decline in gas permeability as a function of time. The application of azide-crosslinked PTMSP membranes in hydrophobic PV, in particular for the separation of more demanding feed streams, has not been reported in literature.

6.2 Principle

An amorphous polymer like PTMSP consists of a large number of randomly oriented polymer chains [23] (Figure 6.1a). These polymer chains are not chemically linked, but united by entanglements. In such an entangled structure the polymer chains are mobile. The movement of polymer chains is strongly dependent on the glass transition temperature, the polymer structure and the temperature of the environment. By crosslinking the polymer, chemical bounds will be made between two adjacent chains, rendering a rigid structure in which the movement of the polymer chains is restricted, resulting in an improved chemical and physical stability (Figure 6.1b).

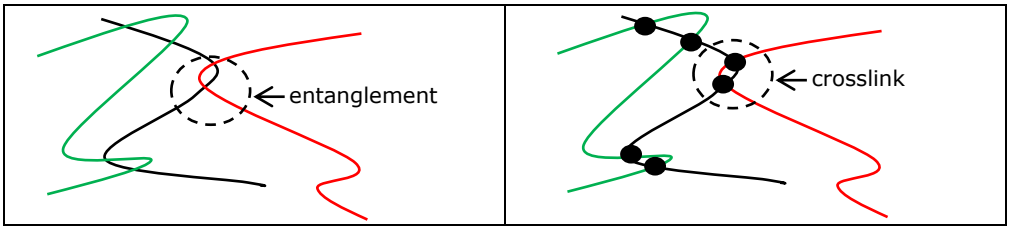

Figure 6.1: Schematic presentation of (a) an amorphous polymer and (b) a crosslinked amorphous polymer.

In the field of gas separation, successful crosslinking of PTMSP with bis(azides) has been reported [14-20]. In the following chapters the proposed crosslink mechanism is applied in the synthesis of hydrophobic PV membranes.

The crosslink mechanism is presented in Figure 6.2 and occurs by the decomposition of aryl azides (R – N_3) into reactive nitrenes (R – N:) and molecular nitrogen (N_2) at elevated temperatures or irradiation. These reactive nitrenes add easily to alkenes to form aziridines, or insert into carbon-hydrogen bonds to form substituted amines [18]. Since allylic C – H bonds are significantly weaker (~ 85 kcal mol^{-1}) than the C – H bonds in $Si(CH_3)_3$ (~ 100 kcal mol^{-1}), reaction at the allylic methyl groups (C = C – CH_3) along the PTMSP backbone is favoured. During crosslinking with bis(azides) nitrogen gas and reactive nitrenes are exclusively generated. Consequently, no high boiling and/or low molecular weight by-products that could contaminate the polymer are formed.

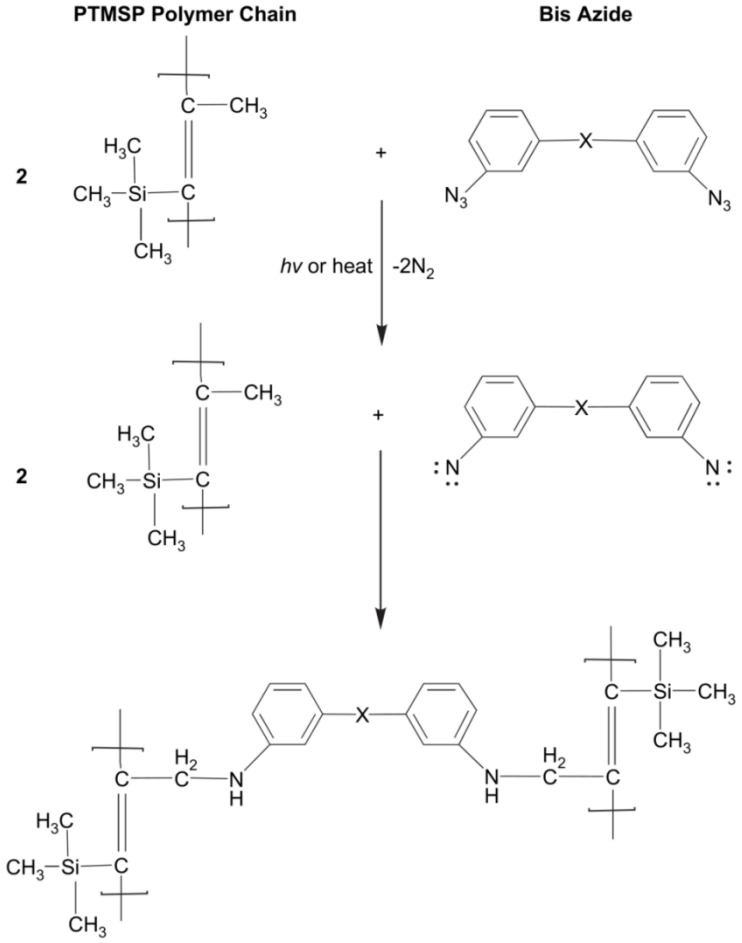

Figure 6.2: Schematic presentation of the PTMSP crosslink mechanism used in this study [18].

6.3 Experimental

6.3.1 Materials

Poly[1-(trimethylsilyl)-1-propyne] (PTMSP, M_w ~ 500 × 10³ g mol $^{-1}$, P_d = 3.7, 0.72 wt.% Ta) was purchased from Gelest, Inc. (USA). The crosslinker, 3,3'-diazido-diphenylsulfone (CL), was supplied by Chemos (Germany) (Figure 6.3). Toluene, methanol (MeOH), ethanol (EtOH), 1-butanol (BuOH), methyl ethyl ketone (MEK), methyl-*tert*-butyl ether (MTBE), n-heptane, tetrahydrofuran

(THF) and dichloromethane (DCM), all of analytical grade, were used as received from Merck (Belgium). Analytical grade ethyl acetate (EA) and N,N-dimethylformamide (DMF) were purchased from Sigma-Aldrich (Belgium) and VWR (Belgium), respectively.

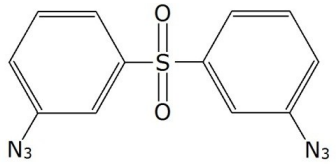

Figure 6.3: Structure of 3,3'-diazido-diphenylsulfone

6.3.2 Membrane preparation and crosslinking

6.3.2.1 Membrane preparation

Unsupported PTMSP membranes were prepared from a toluene solution containing 3 wt.% of polymer. To these solutions, 3,3'-diazido-diphenylsulfone (CL) was added so as to obtain 2.5, 5, 10 and 15 wt.% CL on total solids basis. The reported CL concentrations (w_{cl}) in the final membrane are calculated according to Equation 6-1:

$$w_{CL} = \frac{m_{CL}}{m_{CL}+m_p} \times 100 \qquad (6\text{-}1)$$

where m_{CL} is the CL mass, and m_P the polymer mass. The polymer-CL solutions were magnetically stirred and cast in a Petri dish as described in Chapter 2. Reference PTMSP and PTMSP-CL membranes containing 2.5, 5, 10 and 15 wt.% CL were treated thermally in a vacuum oven or photochemically with UV irradiation (Figure 6.4). Moreover, for each CL concentration an untreated reference sample was prepared to investigate the influence of the bis(azide) addition on the performance and characteristics of PTMSP-based membranes. The sample codes indicated in Figure 6.4 are used further on in the chapter.

6.3.2.2 Thermally induced crosslinking

Thermogravimetric analysis (TA Instruments, RT → 200 °C at 10 °C min^{-1}, 100 ml min^{-1} He) coupled with mass spectrometry (Thermolab) of the PTMSP membrane with 15 wt.% 3,3'-diazido-diphenylsulfone (CL) revealed the onset and kinetics of the decomposition of the CL, by measuring the mass loss of the sample that could be attributed to the removal of volatile N_2 during the formation of reactive nitrenes. The CL decomposition started at 160 °C and an isothermal time of approximately 8 h was required to complete it. In literature a treatment of PTMSP-CL films at 180 °C for 1.5 h has been reported [15-18]. Since both temperatures applied in this chapter, i.e. 160 and 180 °C, are above the onset of degradation of PTMSP (~ 155 °C) [24], competitive effects of degradation and crosslinking should be considered. To investigate the influence of such high temperatures on the polymer structure and PV performance, PTMSP-CL membranes were thermally treated in a vacuum oven at both 160 and 180 °C, either during 1.5 or 8 h (Figure 6.4).

6.3.2.3 Photochemically induced crosslinking

Photochemical crosslinking has been investigated as a potential alternative to the thermal treatment. The irradiating wavelength was chosen to correspond to the UV absorption band of 3,3'-diazido-diphenylsulfone, near 240 nm. Irradiation with three Philips 15 Watt UV-C TL-lamps was carried out in a sealed container, which was flushed with nitrogen gas prior to and during the photochemical treatment. Membranes were kept in the UV-C chamber during 1.5, 4 and 8 h (Figure 6.4). Throughout the entire photochemical treatment the N_2-flow was kept constant.

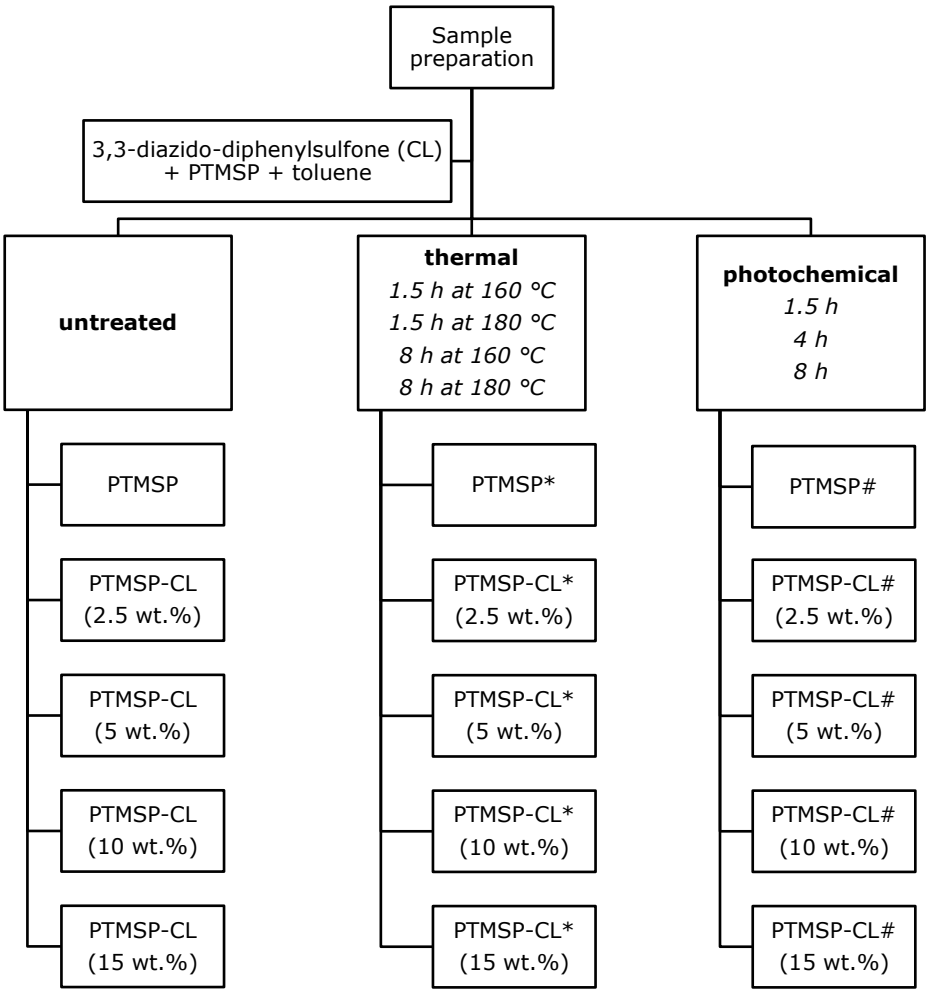

Figure 6.4: Schematic presentation of the 40 different prepared samples.

6.3.3 Characterization

All membranes were extensively characterized by means of infrared analysis, solid-state ^{1}H-wideline NMR, PALS, swelling capacity measurements and PV measurements. These techniques allowed to gain insight in the crosslink reaction mechanism, crosslink density of the crosslinked polymer network, changes in the free volume cavity sizes, solvent resistance and PV performance, respectively. Since PALS has been discussed in Chapter 2, it is not included here.

6.3.3.1 Infrared spectroscopy

Infrared analysis is a straightforward technique for monitoring the progress and effectiveness of the decomposition of bis(azides) subjected to photochemical or thermal treatment [14-20]. A clear azide absorption peak around 2120 cm^{-1} appears when CL is added to the polymer sample. After thermal treatment or UV-C irradiation, the progress of the decomposition can be semi-quantitatively evaluated by the decrease of the azide absorption peak.

Unsupported PTMSP, PTMSP-CL and thermally/photochemically treated PTMSP-CL membranes have been analysed in attenuated total reflectance (ATR) mode on a Nexus FT-IR spectrometer from Thermo Nicolet with Smart Orbit module, controlled with OMNIC™ software. Samples were analysed on both sides, to determine possible surface effects.

6.3.3.2 Solid-state ^{1}H-wideline NMR

^{1}H wideline NMR is a valuable technique which can be used to study the molecular mobility and molecular surroundings in polymers in the solid state. Since only one broad signal is recorded due to strong homonuclear ^{1}H-^{1}H dipolar couplings, no information about the chemical structure is obtained. On the other hand, the relaxation behaviour of the material as measured via this signal provides insight in the molecular dynamics. Therefore solid-state ^{1}H-wideline NMR is a useful technique to qualitatively determine the crosslink density by monitoring the relaxation decay times.

The measurements were carried out at ambient temperature on a Varian Inova 400 spectrometer in a dedicated wideline probe, equipped with a 5 mm coil,

using solid-echo methods. An in depth description of the apparatus and measuring procedure can be found elsewhere [25-28]. Samples were placed in 5 mm glass tubes and closed tightly with Teflon stoppers. On-resonance Free Induction Decays (FIDs) were acquired by applying the solid echo technique ($90°_{x'}$ – t_{se} – $90°_{y'}$ – t_{se} – acquire) to overcome the dead-time of the receiver. The 90° pulse length t_{90} was set to 1.2 µs and spectra were recorded with a spectral width of 2 MHz (0.5 µs dwell time or sampling interval) allowing an accurate determination of the echo maximum. The solid-echo is formed with a maximum at $\tau = (3t_{90}/2+2t_{se}) = 6$ µs.

The T_{1H} relaxation decay times (spin-lattice relaxation in the lab frame) were measured by placing an inversion recovery filter in front of the solid echo part ($180°_{x'}$ – t – $90°_{x'}$ – t_{se} – $90°_{y'}$ – t_{se} – acquire). The integrated proton signal intensity $I(t)$ was analysed monoexponentially as a function of the variable inversion time t according to Equation 6-2:

$$I(t) = I_0\left(1 - 2.exp\left(\frac{t}{T_{1H}}\right)\right) + c^{te} \qquad (6\text{-}2)$$

All experimental data were analysed by a non-linear least-squares fit (Levenberg-Marquardt algorithm). A preparation delay of 5 times the T_{1H} relaxation decay time was always respected between successive accumulations.

Generally spoken, molecular motions are characterized by a distribution of correlation times τ_c. This correlation time τ_c can be roughly defined as the time taken for a molecule (or part of it) to rotate over one radian. Usually it is assumed that the correlation time depends on temperature according to an Arrhenius type of function, as expressed by Equation 6-3:

$$\frac{1}{\tau_c} = v_0 exp\left(-\frac{E}{RT}\right) \qquad (6\text{-}3)$$

where E denotes the energy barrier and v_0 is the attempt frequency. Increasing the temperature thus implies an increasing mobility and therefore a decreasing correlation time τ_c. The relation between the correlation time τ_c and the relaxation time is illustrated in Figure 6.5.

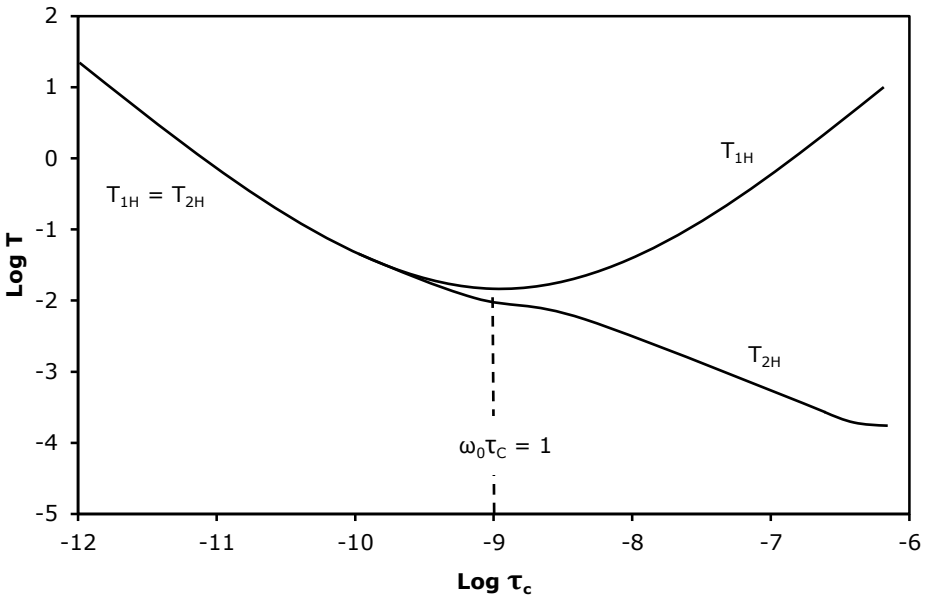

Figure 6.5: T_{1H} and T_{2H} relaxation decay times as a function of the correlation time (τ_c).

The minimum in Figure 6.5 represents the optimal spectral density of molecular motions with proton Larmor frequency ω_0. Left from this minimum, higher frequency motions of small molecules, mobile end-groups and side-chains are situated and the T_{1H} value is magnetic field independent [28]. Rigid molecules will exhibit T_{1H} relaxation times that are located at the right side of this minimum and become magnetic field dependent.

To determine on which side of the minimum the prepared PTMSP samples are located, some samples are measured at two different temperatures (25 and 40 °C).

6.3.3.3 Swelling degree experiments

The swelling capacity of a membrane determines not only its dimensional stability but also affects its permeability and selectivity. The swelling of a membrane depends on the nature of the polymer and its affinity for the used solvent, and on the crosslink density and homogeneity of the membrane. The swelling capacity was determined in a simple gravimetrical test in which a dry membrane coupon of 2 cm diameter of a certain weight was weighed again after

being immersed for 7 days in one of the following solvents: MeOH, EtOH, BuOH, MEK, MTBE, n-heptane, THF, DCM, EA or DMF. After immersion the membrane sample was removed from the solvent and the surface moisture was removed carefully by pressing the membrane for exactly 10 seconds between two dry tissue papers covered with an 8.5 kg mass. All samples were weighted on an analytical balance type AE100 from Mettler Toledo (Switzerland). The swelling capacity or degree (SD) was deduced form Equation 6-4 [29]:

$$SD\ (\%) = \frac{(w_w - w_d)}{w_d} \times 100 \qquad (6\text{-}4)$$

where w_d and w_w represent the initial weight of the dry membrane and the weight of the swollen membrane, respectively. Next, the samples were placed for 7 days in a vacuum oven at 30 °C to remove all solvent from the sample. The mass loss (ML) of the membrane due to immersion in a particular solvent was determined according to Equation 6-5:

$$ML\ (\%) = \frac{(w_d - w_a)}{w_d} \times 100 \qquad (6\text{-}5)$$

in which w_a represents the dry weight of the vacuum-dried membrane after the swelling experiment.

6.3.3.4 Gel permeation chromatography

The effect of the photochemical and thermal treatment on the molecular mass (M_w) of the polymer was investigated by GPC. Samples without CL were annealed in a vacuum oven at 160 and 180 °C, each for 1.5 or 8 h, or exposed for 1.5, 4 or 8 h to UV-C radiation in a N_2-flushed chamber. The thermally/photochemically treated samples without CL and reference samples were dissolved in THF and injected on a TSP GPC column with a Shodex RI-71 refractometer.

6.3.3.5 Pervaporation tests

All PV tests were performed as described in Chapter 2. First, all prepared samples were tested in the separation of a standard 5 wt.% EtOH/H_2O mixture at 50 °C to investigate the influence of the treatment conditions and CL concentration on the performance.

Next, the most optimal, effectively crosslinked PTMSP membrane was tested in the pervaporative separation of aqueous THF mixtures, and benchmarked with two commercially available membranes, i.e. PERVAP 4060 and Pervatech PDMS. The influence of the operating temperature (35, 50 and 70 °C) and THF feed concentration (5, 10 and 15 wt.% THF) were studied for the selected crosslinked PTMSP membrane.

6.4 Characterization of PTMSP crosslinking

As mentioned above, IR is a straightforward and widely used technique for monitoring the progress and effectiveness of the decomposition of bis(azides) subjected to photochemical or thermal treatment. Spectra demonstrating this were reported by Jia *et al.* [20], Kelman *et al.* [18] and Shao *et al.* [14,17]. In this study however, the monitoring is performed on both sides of the membrane, anticipating on the occurrence of possible surface effects. Side A represents the side facing the atmosphere during evaporation of the solvent and side B represents the side facing the bottom of the Petri dish. During the photochemical or thermal treatment, the samples were placed with side A facing the UV-C bulb and side B covering the vacuum oven shelf, respectively.

As a reference the spectra at both sides of a neat PTMSP film are displayed in Figure 6.6a. As expected both sides exhibit identical spectra, demonstrating the isotropic nature of the PTMSP membranes.

First, the effect of bis(azide) addition on the IR-spectrum is shown in Figure 6.6b for a PTMSP-CL (15 wt.%) sample. Besides the appearance of the azide absorption peak at 2120 cm^{-1}, a clear difference between both sides is observed. The azide absorption intensity is higher at side B, suggesting an inhomogeneous CL distribution. Shao *et al.* observed phase separation for a different type of bis(aryl azide) at concentrations above 4 wt.% [14,17].

Secondly, the influence of the treatment conditions on a neat PTMSP membrane without CL is demonstrated in Figure 6.6c and 6.6d. The membrane side facing the UV-C bulb (side A) clearly shows some distinct peaks (Figure 6.6c) which do not occur in the spectrum of untreated neat PTMSP (Figure 6.6a). The broad peak around 3400 cm^{-1} can be assigned to O – H stretch vibrations, the peak around 1710 cm^{-1} represents the C = O stretch, and finally the peak at 1050 cm^{-1} is typical for a C – O stretch. Moreover, the peak around 1600 cm^{-1} representing the C = C stretch is less intense when the sample directly faces the UV-C irradiation, indicating breaking of PTMSP's C = C bonds. For the opposite surface (side B), this peak is only slightly smaller compared to untreated PTMSP. These absorption peaks suggest formation of carboxylic acids at the UV-C bulb facing surface (side A), indicating the presence of oxygen during the photochemical treatment and thus an inappropriate experimental setup [30].
Figure 6.6d displays the spectra of neat PTMSP without CL after thermal treatment at 180 °C for 1.5 h. In contrast to the photochemically treated membrane, no C=O, O-H or C-O stretches are observed and both sides of the membrane are identical.

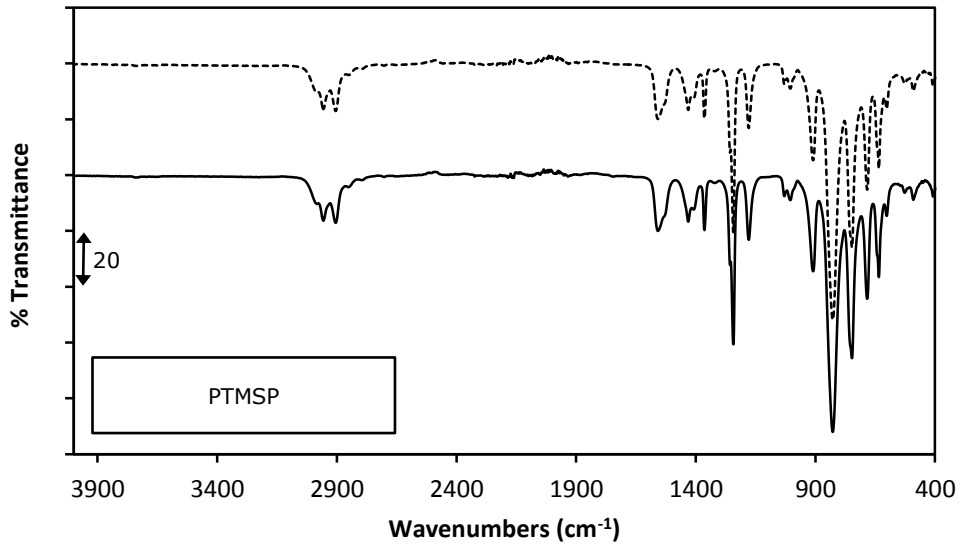

(a)

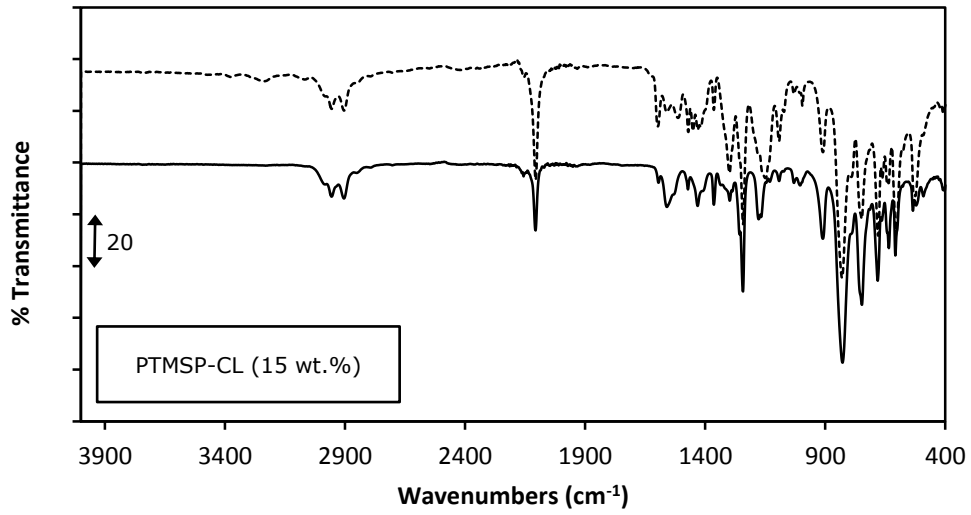
% Transmittance
20
PTMSP-CL (15 wt.%)
3900
3400
2900
2400
1900
1400
900
400
Wavenumbers (cm-1)

(b)

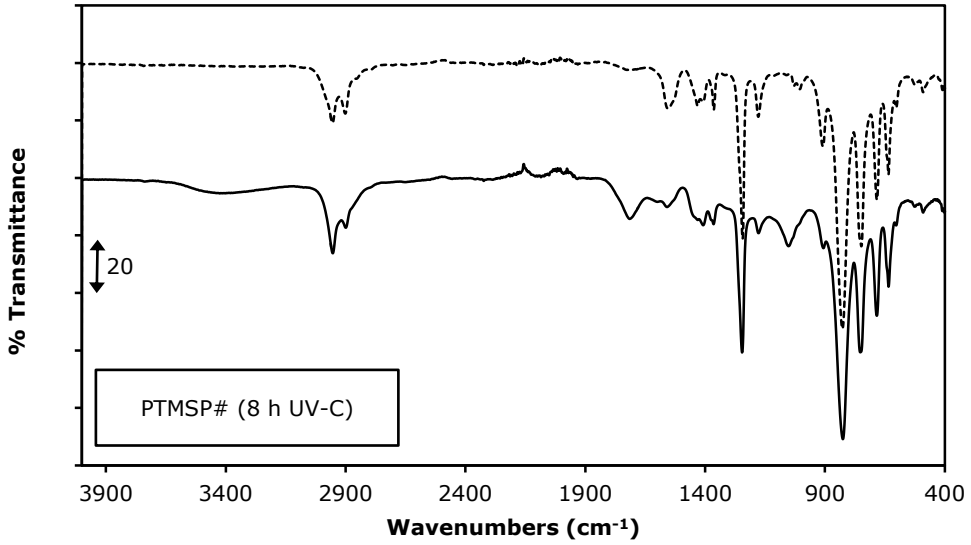
% Transmittance
20
PTMSP# (8 h UV-C)
3900
3400
2900
2400
1900
1400
900
400
Wavenumbers (cm-1)

(c)

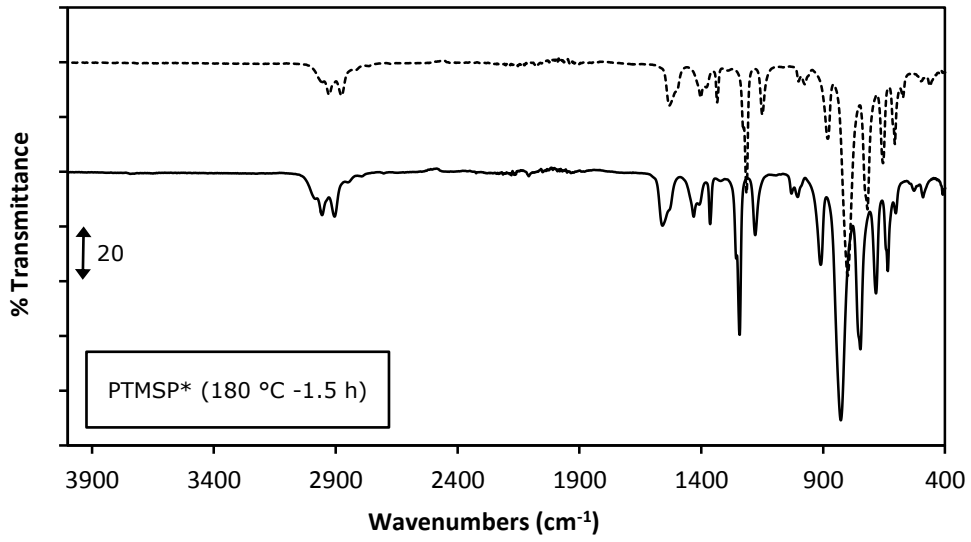

(d)

Figure 6.6: FT-IR spectra of (a) neat PTMSP, (b) PTMSP-CL (15 wt.%), (c) PTMSP# without CL irradiated with UV-C light for 8 h and (d) PTMSP* without CL annealed at 180 °C for 1.5 h. The continuous line represents the spectrum recorded at side A and the dotted line the spectrum at side B.

Figure 6.7 shows the azide absorption intensity as a function of the CL concentration in an untreated PTMSP membrane. It can be seen that the azide absorption intensity increases steadily with increasing CL concentration. After annealing at high temperatures or UV-C irradiation, the progress of the decomposition can thus be semi-quantitatively evaluated by the decrease of the azide IR absorption intensity.

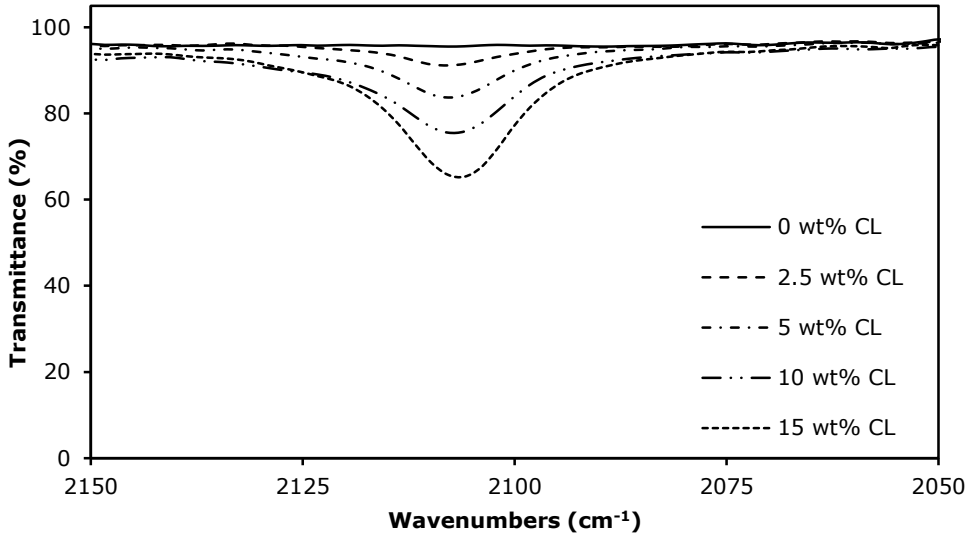

Figure 6.7: Azide absorption peak as a function of the CL concentration in untreated PTMSP membranes.

Thermal treatment of PTMSP membranes at 160 °C for 1.5 h (*) resulted in the complete decomposition of CL for concentrations up to 5 wt.%, as can be seen in Figure 6.8. For the PTMSP-CL (10 wt.%) and PTMSP-CL (15 wt.%) membranes, the residual concentrations of unreacted CL after treatment at 160 °C for 1.5 h (*) is less than 2 wt.%. For all other thermal treatment conditions, the azide absorption peak disappears completely, independent of the CL concentration, indicating the effectiveness of the thermal treatment to decompose the azide.

The photochemical treatment on the other hand, is not capable of completely decomposing the azide. Figure 6.8 shows the concentration of unreacted CL in the PTMSP membrane after UV-C irradiation for 8 h (#). Only for the sample containing 2.5 wt.% CL, the photochemical treatment resulted in the complete decomposition of the azides. PTMSP membranes with higher CL concentrations, showed 50 to 65 % CL decomposition after UV-C irradiation, demonstrating the ineffectiveness of the photochemical treatment. In fact, few authors have succeeded in the photochemical crosslinking of PTMSP with a different type of bis(aryl azide) [14,17,20], indicating the sensitiveness of the method to

variations in crosslinker, polymer properties (cis/trans configuration, M_w) and experimental setup.

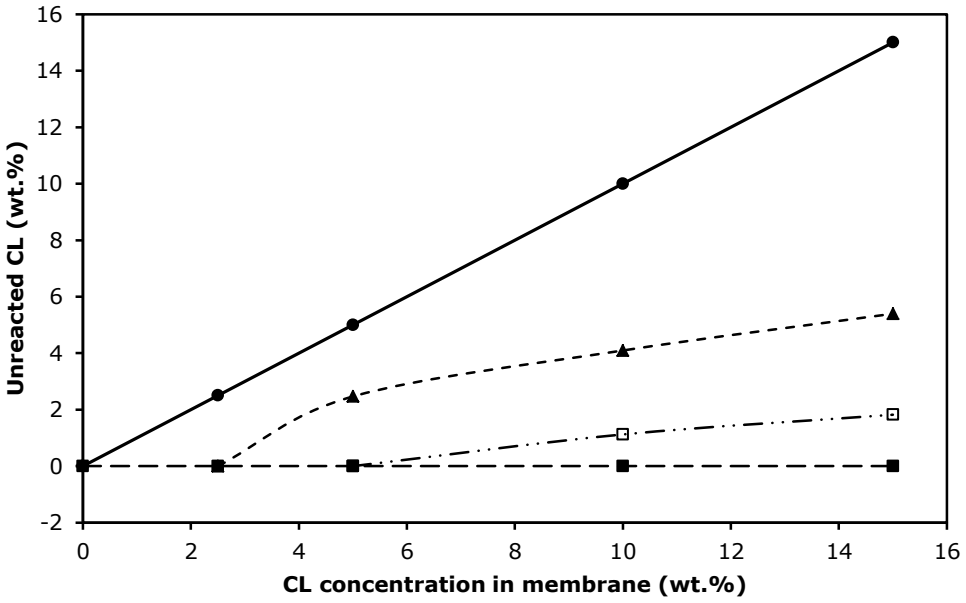

Figure 6.8: Unreacted CL concentration as a function of the initial CL concentration in (●) untreated PTMSP membranes and treated membranes subjected to (■) 160 °C for 8 h or 180 °C for 1.5/8 h (*), (□) 160 °C for 1.5 h (*) and (▲) UV-C irradiation for 8 h (#).

From the IR-spectra no conclusive evidence of successful crosslinking is obtained, since only the decomposition of the azide was monitored. To demonstrate successful crosslinking, ^{1}H-wideline NMR relaxometry is used. The T_{1H} decay times for neat PTMSP, PTMSP-CL (5 wt.%) and PTMSP-CL (15 wt.%), each thermally treated at 180 °C for 1.5 h (*) or irradiated for 8 h with UV-C (#) are reported in Table 6.1. The T_{1H} relaxation time is sensitive to the spectral density of molecular motions with frequencies around the Larmor frequency of protons, i.e. 400 MHz on a 9.4 Tesla magnet, and reveals information about the molecular mobility and/or molecular morphology of a polymer network. Since the T_{1H} relaxation behaviour of crosslinked PTMSP membranes will be discussed at temperatures well below the glass transition temperature (T_g > 300 °C), these high-frequency motions only arise from segmental chain motions of mobile end-groups and branched side-chains [28]. Since the T_{1H} decay time of neat PTMSP

increases with temperature (Table 6.1), the T_{1H} relaxation of the membranes is located on the left side (low log τ_c) of the minimum on Figure 6.5. Thus it can be concluded that a shorter T_{1H} decay time corresponds to slower chain motions. The decrease of T_{1H} decay time with increasing CL concentration for the thermally treated sample (*) therefore indicates an increase of the crosslink density (Table 6.1). For the photochemically treated sample (#), the T_{1H} decay time increases with increasing CL concentration, indicating faster molecular motions. The latter could be explained by the presence of unreacted CL which can act as plasticizer, chain breaking and/or the formation of unwanted carboxylic acids during UV-C irradiation.

Table 6.1: T_{1H} decay times of neat PTMSP, PTMSP-CL (5 wt.%) and PTMSP-CL (15 wt.%), treated at 180 °C for 1.5 h (*) and irradiated with UV-C for 8 h (#), measured at room temperature (RT) or 40 °C.

Sample	T_{1H} (ms) (untreated) *[RT → 40 °C]*	T_{1H} (ms) at RT (180 °C, 1.5h)	T_{1H} (ms) at RT (UV-C, 8h) *[RT → 40 °C]*
PTMSP	577 → 762	560	548
PTMSP-CL (5 wt.%)		535	553
PTMSP-CL (15 wt.%)		522	568 → 730

Another way to quantify successful crosslinking is by measuring the free volume changes. The density increase of polymer systems after crosslinking [20] is expected to result in a lower free volume content or smaller free volume cavity size. Several authors suggested compaction or densification of the free volume of PTMSP upon crosslinking [14-20], but only few report PALS data to demonstrate this hypothesis [15]. Kelman *et al.* reported PALS data, showing the *o*-Ps lifetimes of an uncrosslinked and thermally crosslinked (180 °C for 1.5 h) PTMSP membrane, using the same CL as in this work [15]. Upon crosslinking (5 wt.% CL), both τ_3 and τ_4 remained constant at approximately 2.0 and 9.6 ns, respectively, indicating no decrease of free volume cavity size upon crosslinking [15]. The authors assume that the *o*-Ps intensity ($I_{o\text{-}Ps}$) is representative for the amount of free volume cavities, which is not in accordance with recent understanding of the interpretation of *o*-Ps formation in polymers [31-35]. Shao *et al.* attributed the decrease in gas permeability of photochemically crosslinked

PTMSP membranes to a decrease in fractional free volume estimated according to Bondi's method [14,17]. Unfortunately, the authors didn't report experimental data of free volume cavity sizes (PALS) or free volume fractions (PVT-EOS analysis) [14,17].

In this work nine different PTMSP samples were characterized with PALS. Firstly, three untreated samples containing 0, 5 and 15 wt.% CL were measured, followed by the analysis of samples containing 0, 5 and 15 wt.% CL after UV-C irradiation for 8 h (#) or annealing at 180 °C for 1.5 h (*). Table 6.2 shows the *o*-Ps lifetimes (τ_3 and τ_4) and the corresponding *o*-Ps intensities (I_3 and I_4).

Upon addition of CL to neat untreated PTMSP membranes, the third lifetime component (τ_3), representing the channel like holes, slightly decreases while the fourth lifetime (τ_4), which represents the larger cages, increases. The decrease of τ_3 could be explained by partial blocking of the channel like holes by the CL, while its presence hinders the polymer chain packing, accounting for an increase of τ_4.

A decrease of τ_3 from 2.06 ns for neat UV-C treated PTMSP (#) to 1.79 and 1.21 ns for UV-C irradiated membranes with 5 and 15 wt.% CL, respectively, is reported in Table 6.2. τ_4 on the other hand, concomitantly increases from 6.13 ns to 6.20 and 6.54 ns. Although not all the CL is decomposed as reported previously in Figure 6.8, still a certain degree of crosslinking is expected which is demonstrated by a decrease in τ_4 of 3 % for the UV-C irradiated PTMSP-CL (15 wt.%) (#) membrane compared to an untreated PTMSP-CL (15 wt.%) membrane (Table 6.2).

A clear reduction of the free volume cavity size is observed for the thermally treated membranes (*). Thermal treatment (180 °C, 1.5 h) of PTMSP-CL* (5 wt.%) and PTMSP-CL* (15 wt.%) samples resulted in a decrease in τ_4 of 1.6 and 9 %, respectively, due to densification of the polymer matrix. Compared to neat untreated PTMSP (6.15 ns), however, τ_4 does not decrease significantly after crosslinking at 180 °C. For all crosslink concentrations and treatment conditions, τ_3 decreases steadily with increasing CL concentration (Table 6.2).

While the *o*-Ps lifetime addresses the physical properties, the *o*-Ps lifetime intensity is dependent on the chemical properties of the membrane. Addition of CL changes the chemical nature of the PTMSP membrane and thus influences the

o-Ps intensities significantly. Nitrogen-containing and halogenated compounds are known to reduce the *o*-Ps formation probability and therefore lead to a decrease of the *o*-Ps intensity [34,35]. Table 6.2 indeed shows a clear decrease of I_4 with increasing CL concentration, while for I_3 no clear trend is observed upon addition of CL.

Since no information about the number of free volume cavities is obtained by PALS analysis, the contribution of each of the two lifetime components (τ_3 and τ_4) in the total free volume of a polymer system could not be determined. Therefore, future research is needed to attribute possible permeability or flux decline to a decrease in free volume fraction, by means of PVT-EOS analysis.

Table 6.2: *o*-Ps lifetimes (τ) and intensities (I) of PTMSP membranes with different CL concentrations subjected to thermal (*) and photochemical treatments (#).

CL (wt.%)	Treatment	τ_3 (ns)	I_3	τ_4 (ns)	I_4
0	None	1.86 (0.05)	7.73 (0.23)	6.15 (0.02)	31.06 (0.18)
5		1.88 (0.07)	5.96 (0.20)	6.27 (0.03)	20.47 (0.18)
15		1.36 (0.21)	6.06 (0.80)	6.73 (0.13)	12.85 (0.32)
0	UV-C (8 h) (#)	2.06 (0.33)	7.94 (0.92)	6.13 (0.14)	30.61 (1.26)
5		1.79 (0.28)	6.09 (0.18)	6.20 (0.09)	20.77 (0.54)
15		1.21 (0.09)	7.23 (1.12)	6.54 (0.04)	13.39 (0.13)
0	180 °C (1.5 h) (*)	1.94 (0.13)	7.03 (0.13)	6.25 (0.03)	28.97 (0.33)
5		1.66 (0.14)	7.11 (0.59)	6.17 (0.05)	21.84 (0.20)
15		1.55 (0.13)	7.31 (0.29)	6.12 (0.13)	14.08 (0.38)

6.5 Influence of 3,3'-diazido-diphenylsulfone concentration and crosslink conditions on the solvent stability

Complementary to the more fundamental characterization techniques FT-IR, ^{1}H-wideline NMR relaxometry and PALS, more application oriented swelling experiments are reported here. The swelling capacity of the membranes is expected to decrease after crosslinking. A wide range of solvents was selected for these swelling tests, anticipating on the possible use of crosslinked membranes in PV for the removal of more demanding solvents from aqueous mixtures. Table 6.3 shows the relative SD (%) and ML (%) of PTMSP membranes as a function of the CL concentration and crosslink conditions. Although crosslinking of PTMSP membranes is not required for alcohol/H_2O separations, a clear decrease in SD is noticed with increasing CL concentration, independent of the crosslink conditions. Similar trends are observed for EA, MEK and DMF. For more demanding solvents like MTBE, n-heptane, THF and DCM, crosslinking of PTMSP membranes is inevitable. From the data in Table 6.3, photochemically crosslinked membranes (#) can be rejected for application in these solvents. While for the thermally crosslinked membranes (*), ML is only observed when the membranes are in contact with the more demanding solvents, photochemically crosslinked membranes (#) exhibit ML for all solvents, including those in which the neat PTMSP membrane is fully stable. For all UV-C treated membranes (#), ML increases with increasing CL concentration, demonstrating the wash-out of the unreacted CL, present in the polymer network. Anticipating on the application of crosslinked PTMSP membranes in the removal of THF from dilute aqueous solutions, the thermally induced crosslink procedure is selected.

Table 6.3: SD (%) and ML (%, between parentheses) of PTMSP membranes as a function of the CL concentration and treatment conditions. For samples which did not display any ML, '(-)' is used, while for complete dissolution of the sample the symbol '∞' is used.

CL (wt.%)	Treatment	MeOH	EtOH	BuOH	EA	MEK
0	-	64 (-)	98 (-)	148 (-)	100 (-)	98 (-)
2.5	160 °C 1.5 h (*)	59 (-)	86 (-)	136 (-)	98 (-)	92 (-)
5		51 (-)	81 (-)	127 (-)	94 (-)	87 (-)
10		51 (-)	76 (-)	113 (-)	91 (-)	71 (-)
15		48 (-)	67 (-)	114 (-)	82 (-)	78 (-)
2.5	160 °C 8 h (*)	51 (-)	87 (-)	123 (-)	88 (-)	85 (-)
5		51 (-)	75 (-)	122 (-)	85 (-)	81 (-)
10		47 (-)	73 (-)	104 (-)	81 (-)	74 (-)
15		43 (-)	63 (-)	94 (-)	77 (-)	73 (-)
2.5	180 °C 1.5 h (*)	51 (-)	81 (-)	129 (-)	91 (-)	90 (-)
5		47 (-)	81 (-)	115 (-)	85 (-)	83 (-)
10		46 (-)	67 (-)	104 (-)	82 (-)	74 (-)
15		40 (-)	67 (-)	92 (-)	72 (-)	75 (-)
2.5	180 °C 8 h (*)	50 (-)	73 (-)	158 (-)	88 (-)	80 (-)
5		46 (-)	79 (-)	138 (-)	87 (-)	77 (-)
10		45 (-)	71 (-)	108 (-)	83 (-)	72 (-)
15		39 (-)	66 (-)	113 (-)	77 (-)	64 (-)
2.5	UV 1.5 h (#)	57 (-)	95 (-)	130 (-)	98 (-)	85 (-)
5		56 (4)	82 (5)	129 (5)	92 (5)	70 (5)
10		47 (8)	78 (8)	148 (8)	90 (9)	79 (9)
15		43 (12)	67 (12)	115 (12)	77 (13)	72 (13)
2.5	UV 4 h (#)	61 (-)	89 (-)	123 (-)	93 (-)	85 (-)
5		58 (5)	77 (5)	118 (5)	91 (6)	83 (6)
10		52 (8)	82 (9)	123 (9)	85 (10)	7 (11)
15		46 (11)	68 (12)	109 (12)	81 (13)	74 (14)
2.5	UV 8 h (#)	58 (-)	88 (-)	129 (-)	92 (-)	84 (-)
5		56 (4)	85 (5)	123 (6)	93 (6)	86 (6)
10		51 (8)	82 (8)	128 (8)	90 (8)	86 (9)
15		47 (11)	76 (10)	113 (10)	82 (12)	79 (14)

CL (wt.%)	Treatment	DMF	DCM	MTBE	Heptane	THF
0	-	92 (-)	∞	∞	∞	∞
2.5	160 °C 1.5 h (*)	82 (-)	354 (32)	∞	∞	∞
5		77 (-)	316 (11)	404 (26)	317 (14)	∞
10		74 (-)	173 (-)	116 (-)	113 (-)	279 (5)
15		74 (-)	145 (-)	89 (-)	87 (-)	198 (-)
2.5	160 °C 8 h (*)	82 (-)	375 (14)	∞	∞	∞
5		77 (-)	267 (-)	246 (11)	196 (6)	484 (9)
10		75 (-)	101 (-)	95 (-)	83 (-)	210 (-)
15		75 (-)	90 (-)	73 (-)	71 (-)	136 (-)
2.5	180 °C 1.5 h (*)	93 (-)	282 (22)	∞	∞	∞
5		79 (-)	281 (5)	253 (21)	204 (9)	∞
10		71 (-)	153 (-)	109 (-)	96 (-)	213 (-)
15		67 (-)	140 (-)	81 (-)	74 (-)	157 (-)
2.5	180 °C 8 h (*)	74 (-)	263 (38)	∞	∞	∞
5		73 (-)	249 (14)	293 (24)	220 (10)	704 (31)
10		72 (-)	149 (-)	112 (-)	113 (-)	269 (11)
15		69 (-)	119 (-)	85 (-)	73 (-)	151 (-)
2.5	UV 1.5 h (#)	79 (-)	364 (19)	∞	∞	∞
5		77 (5)	322 (21)	∞	∞	∞
10		73 (8)	328 (22)	∞	∞	∞
15		68 (12)	255 (26)	∞	∞	∞
2.5	UV 4 h (#)	83 (-)	382 (12)	∞	∞	∞
5		80 (5)	465 (13)	∞	∞	∞
10		74 (9)	475 (18)	∞	∞	∞
15		74 (12)	323 (23)	∞	∞	∞
2.5	UV 8 h (#)	87 (-)	361 (20)	∞	∞	∞
5		80 (5)	387 (17)	∞	∞	∞
10		87 (8)	327 (21)	∞	∞	∞
15		71 (12)	322 (25)	∞	∞	∞

Unfortunately, the high annealing temperatures used to initiate the crosslinking are well above the degradation temperature of PTMSP, resulting in a decrease of the M_w. Table 6.4 shows the M_w of an untreated and thermally/photochemically treated PTMSP membrane without CL. Although the photochemically treated samples (#) show the highest M_w of all crosslinked membranes, the inefficient crosslinking of these samples makes them inappropriate for application in the PV of more demanding feed mixtures. For the thermally induced crosslinking (*), the least degradation is observed for PTMSP membranes annealed at 160 °C for 1.5 h (Table 6.4), while the most severe treatment conditions (180 °C, 8 h) render brittle membranes with a M_w which is 7 times lower compared to the initial M_w. The PTMSP membrane thermally crosslinked at 180 °C for 1.5 h (*) was selected for PV tests of THF/H_2O mixtures, based on the complete decomposition of CL (Figure 6.8), the slightly higher M_w compared to PTMSP membranes treated at 160 °C for 8 h (*) (Table 6.4), the comparable SD and ML data (Table 6.3), and the duration and thus energy cost of the treatment.

Table 6.4: M_w and P_d of a neat PTMSP membrane and PTMSP membranes treated at different crosslink conditions, as revealed by GPC.

Crosslink condition		M_w (Da)	Pd
-		500 000	3.7
160 °C (*)	1.5 h	185 407	2.7
	8 h	156 097	2.7
180 °C (*)	1.5 h	162 952	2.7
	8 h	68 186	2.5
UV-C (#)	1.5 h	286 846	3.8
	4 h	279 133	3.8
	8 h	111 135	2.9

6.6 Influence of 3,3'-diazido-diphenylsulfone concentration and crosslink conditions on the PV performance

Before using the thermally crosslinked membranes in PV for the separation of dilute THF/H_2O mixtures, the influence of both crosslink conditions and CL concentration on the PV performance in the separation of a standard EtOH/H_2O mixture is addressed. Although crosslinking of PTMSP membranes is not required for PV testing on dilute ethanol mixtures, possible differences in PV performance after addition of CL and/or UV-C or thermal treatment could be demonstrated. Figure 6.9 shows the specific permeation rate of uncrosslinked, and of thermally and photochemically crosslinked PTMSP membranes as function of the CL concentration. It can be seen that all crosslink conditions (UV-C and thermal) significantly decrease the specific permeation rate.

For neat PTMSP samples annealed at 180 °C for 1.5 h a decrease of 26% in specific permeation rate is noticed, while the neat PTMSP samples irradiated with UV-C light for 8 h show a 69% decrease. Most probable, this decrease can be attributed to chain scission of the polymer, as indicated by the GPC-data (Table 6.4). The M_w of neat PTMSP decreases 67 and 78 % for PTMSP treated at 180 °C for 1.5 h and irradiated with UV-C for 8 h, respectively. Since the FT-IR spectra of thermally treated PTMSP membranes did not reveal significant differences compared to untreated PTMSP (Figure 6.6), chain breaking is expected to be the main reason for the permeability decline. Additional to chain scission, the photochemical treatment leads to the formation of carboxylic acids (Figure 6.6c), contributing to the significant decrease in specific permeation rate for PTMSP membranes treated with UV-C irradiation.

Upon adding CL to untreated PTMSP membranes, the specific permeation rate decreases 34 and 67% for 5 and 15 wt.% CL, respectively (Figure 6.9). Addition of CL changes the chemical environment and free volume cavity size (Table 6.2), and thus the transport properties (solubility and diffusivity) of the membrane. Solubility measurements by Shao *et al.* and Kelman *et al.* demonstrated the major contribution of the diffusivity as no significant changes in solubility were reported [14,17,18].

Thermal crosslinking of the membrane further decreases the specific permeation rate for all CL concentrations (Figure 6.9), which can be partially explained by

the compaction of the polymer network (Table 6.2) and chain scission (Table 6.4). Photochemical crosslinking finally induces the lowest specific permeation rate for all CL concentrations, demonstrating the severe effect of the treatment. The formation of carboxylic acids (Figure 6.6c), presence of unreacted CL (Figure 6.8) and chain scission (Table 6.4) render the membranes unsuitable for PV. It is remarkable that the difference between the specific permeation rates of the untreated, photochemically and thermally crosslinked samples narrows with increasing CL concentration (Figure 6.9). For the untreated and thermally treated PTMSP membranes, the presence of reacted and unreacted CL is the major reason for the decrease in specific permeation rate. For the photochemically treated membranes on the other hand, the severity of the UV-C treatment itself explains the decline in specific permeation rate.

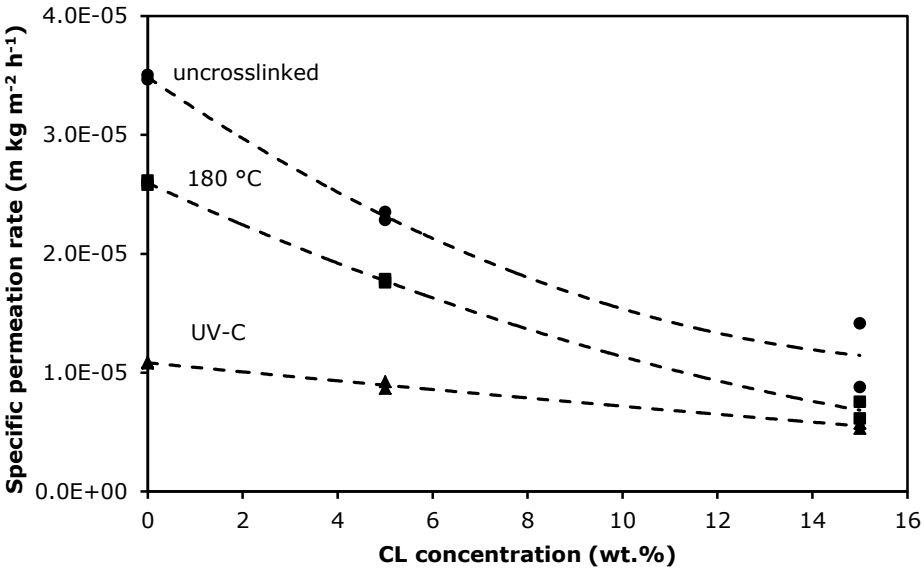

Figure 6.9: Specific permeation rate of uncrosslinked (●), thermally (180 °C, 1.5 h) crosslinked (■) and UV-C (8 h) crosslinked (▲) PTMSP membranes as a function of the CL concentration in the separation of a 5 wt.% EtOH/H_2O mixture at 50 °C. The dotted lines are just guides for the eye.

Not exclusively the specific permeation rate is influenced by the addition of CL to PTMSP membranes. The EtOH/water separation factor also significantly decreases, presumably because of the changes in chemical structure and thus

transport characteristics across the membrane (Figure 6.10). Each treatment condition itself has a significant effect on the separation factor, as shown in Figure 6.10. A photochemical (UV-C, 8 h) and thermal treatment (180 °C, 1.5 h) of the membranes result in a decrease in separation factor of respectively 95 and 17 % compared to the untreated membrane without CL addition. The severe effect of the UV-C treatment is thus confirmed as the ethanol separation factor drops to almost unity for all UV-C treated membranes, independent of the CL concentration (Figure 6.10).

Addition of CL resulted in a decrease of 16 and 53 % in separation factor for 5 and 15 wt.% CL for the untreated PTMSP membranes, respectively. For the thermally crosslinked membranes, a decrease of 21 and 72 % in separation factor for 5 and 15 wt.% CL was observed (Figure 6.10). The main reason for the general decline in separation factor is again the CL concentration for the untreated and thermally crosslinked PTMSP membranes. As for the specific permeation rate, the photochemically treated membranes suffer most from the treatment itself, much less from the addition and reaction of bis(azide).

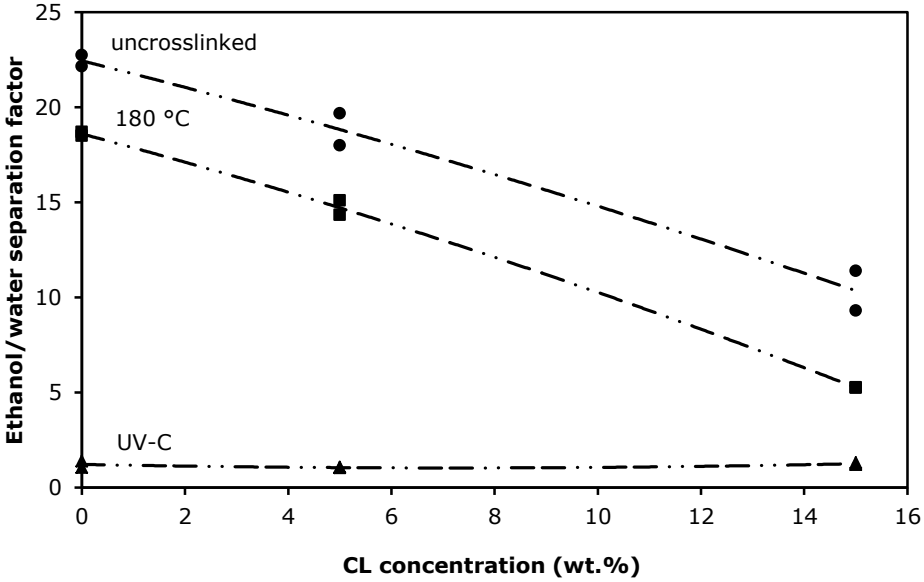

Figure 6.10: EtOH/H_2O separation factor of uncrosslinked (●), thermally (180 °C, 1.5 h) crosslinked (■) and UV-C (8 h) crosslinked (▲) PTMSP membranes as a function of the CL concentration in the separation of a 5 wt.% EtOH/H_2O mixture at 50 °C. The dotted lines are just guides for the eye.

6.7 Application test

The removal of tetrahydrofuran (THF) from water by PV is rarely studied [36], despite the frequent use of THF as solvent in the chemical industry and thus its presence in industrial waste water streams. Hydrophobic PV could be used to remove trace amounts of THF from industrial waste water streams, allowing the water to be processed via conventional waste water treatment or discharged to the sewerage. Moreover, the enriched THF stream could be reused, sold or disposed to specialised solvent recycling companies for further purification. Without PV, the disposal cost can in some cases be really high, especially when the COD is above the threshold for conventional waste water treatment. Moreover, THF removal by PV offers the additional benefit that the formation of unstable hydroperoxides due to reaction of THF with oxygen in contact with air can be avoided [36]. In other separation technologies like distillation, the peroxide concentration in the waste water could increase during processing, increasing the risk of explosion [37].

In the previous section, the poor PV performance of photochemically crosslinked PTMSP membranes in the separation of EtOH/H_2O mixtures was clearly demonstrated (Figure 6.9 and 6.10). Complementary swelling experiments revealed the complete dissolution of photochemically crosslinked membranes in THF (Table 6.3). Therefore, thermally induced crosslinked PTMSP membranes were used for the PV tests on dilute THF/water mixtures. Since the membranes treated at 180 °C for 8 h became brittle and the membranes treated at 160 °C for 1.5 h exhibited a SD of at least 200 % in THF, both membranes were excluded from the application tests. As there is no real recommendation available in literature for the maximal SD for trouble-free PV, an arbitrary limit in SD of approximately 150 % was set, estimated from the highest SD for uncrosslinked membranes in BuOH. Both membranes treated at 160 °C for 8 h and 180 °C for 1.5 h render membranes insoluble in THF at CL concentrations above 5 wt.%. Based on the set SD limit, the higher M_w (Table 6.4) and the duration of the treatment, PTMSP membranes with 15 wt.% CL treated at 180 °C for 1.5 h were selected.

6.7.1 Influence of THF feed concentration on PV performance

The performance of a thermally crosslinked PTMSP membrane in the pervaporative separation of a THF/H_2O mixture containing 5, 10 and 15 wt.% THF is shown in Figure 6.11. The total flux increases with increasing THF feed concentration, which is expected [36]. Remarkably, the separation factor equally increases with increasing THF feed concentration in the selected concentration region. Several authors reported a decrease in separation factor with increasing solvent feed concentration for a wide range of solvents [3,4,38,39] and even a THF/H_2O system [36].

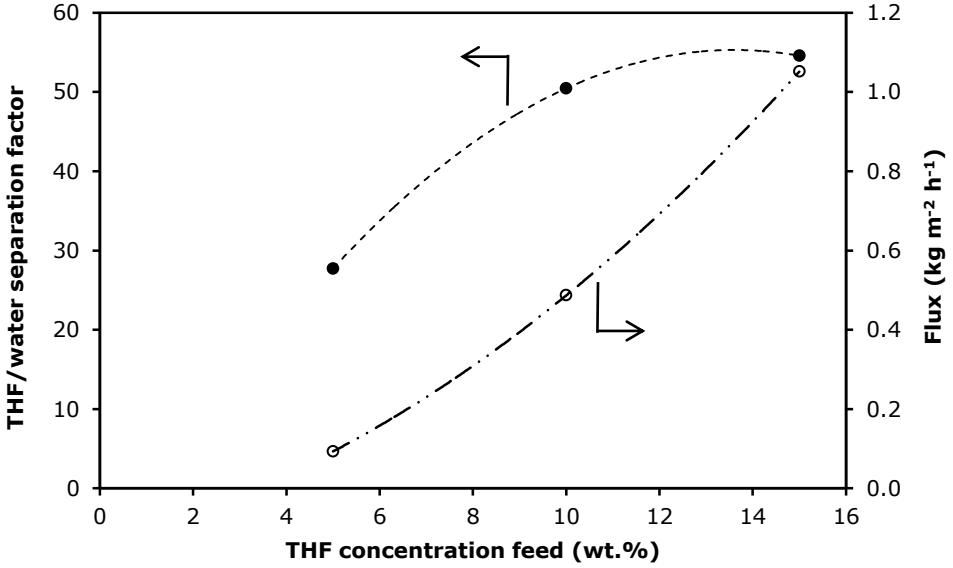

Figure 6.11: Flux (○) and THF/H_2O separation factor (●) of a thermally (180 °C, 1.5 h) crosslinked PTMSP-CL*(15 wt.%) membrane at 50 °C as a function of the THF concentration in the feed. The dotted lines are just guides for the eye.

The unusual increase in the separation factor curve can tentatively be explained by the presence of coupling phenomena between the feed mixture components [40]. For a hydrophilic PVA/PP membrane, Shahverdi and co-workers reported a clear maximum of the separation factor in the separation of an ethylene glycol (EG)/water mixture with increasing EG concentration in the feed [40]. Since the swelling of the membranes decreased with increasing EG concentration, the

maximum in separation factor could not be correlated to the swelling behaviour of the membrane, but solely to coupling effects between EG and water [40].
Further research is needed to investigate the anticipated coupling effects during PV tests with the prepared PTMSP-CL*(15 wt.%) membrane on THF/H_2O mixtures and the swelling behaviour of the membrane in these mixtures.

6.7.2 Influence of feed temperature on PV performance

The influence of the operation temperature on the membrane performance is displayed in Figure 6.12. With increasing operating temperature, the membrane flux increases significantly, without affecting the THF concentration in the permeate, as expected and reported by other authors for different systems [36,39,41].

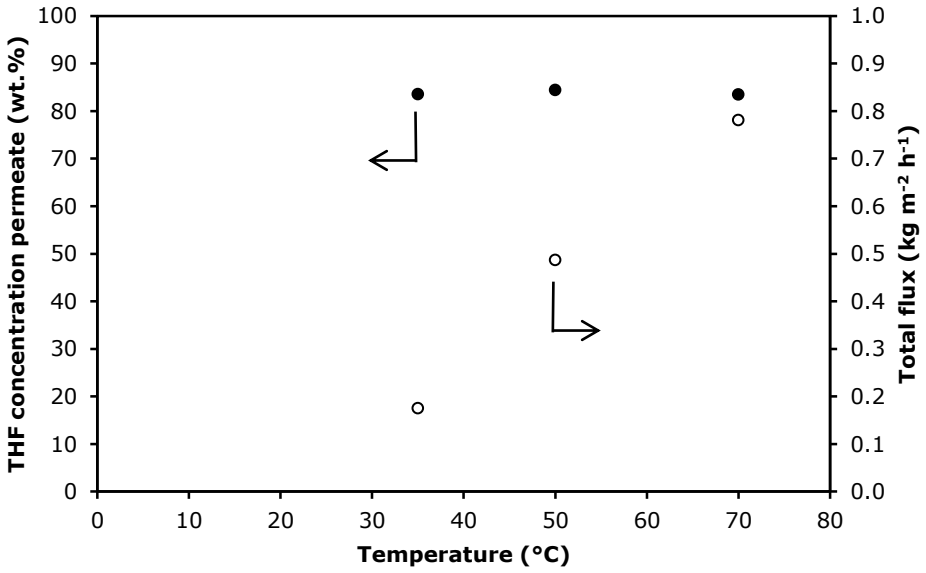

Figure 6.12: Total flux (○) and THF concentration in the permeate (●) of a thermally (180 °C, 1.5 h) crosslinked PTMSP-CL*(15 wt.%) membrane as a function of the feed temperature (10 wt.% THF/H_2O).

The temperature dependence of the component flux could be expressed by an Arrhenius-type relationship (Equation 8-1) [42]:

$$J = J_0 exp\left(-\frac{E_p}{RT}\right) \quad (8\text{-}1)$$

where J denotes the component flux (g m^{-2} h^{-1}), J_0 a constant representing the pre-exponential factor, E_p the activation energy for permeation, R the gas constant and T the temperature in kelvin units. Through the experimental data an Arrhenius relation is plotted by the least squares method (Figure 6.13). From this Arrhenius plot the THF and H_2O permeation activation energies are both estimated at 37 kJ mol^{-1}. This suggests that the effect of temperature on the permeation flux of THF and H_2O is very similar, and thus explains why the separation factor remains constant with operation temperature (Figure 6.12). Ray *et al.* reported THF activation energies (5 wt.% THF/H_2O) ranging from approximately 1 to 2.5 kJ mol^{-1} for membranes prepared from unplasticized polyvinyl chloride, polystyrene, plasticized polyvinyl chloride and blends thereof. Moreover a decrease in THF selectivity with increasing feed temperature was reported in a feed temperature range of 30 – 50 °C [36].

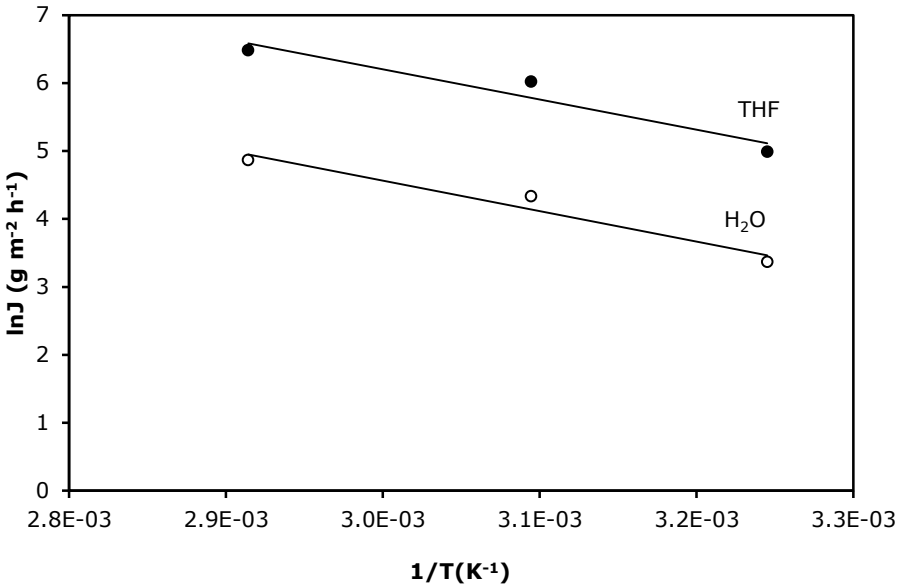

Figure 6.13: Arrhenius plot of a thermally (180 °C, 1.5 h) crosslinked PTMSP-CL*(15 wt.%) membrane, tested on a 10 wt.% THF/H_2O mixture. (●) represents the THF flux, (○) the H_2O flux and R^2_{THF} = 0.93 and R^2_{H2O} = 0.95.

6.8 Benchmark study for PV of THF/H2O

Two commercially available PDMS membranes from Sulzer and Pervatech were used to benchmark the thermally crosslinked PTMSP-CL*(15 wt%) membrane. Figure 6.14 shows the specific permeation rate and THF concentration in the permeate of these three membranes in the separation of a 10 wt.% THF/H_2O mixture at 50 °C. Since the thickness of the commercial membranes is approximately 1 µm and the crosslinked PTMSP membranes are several orders of magnitude thicker (approximately 100 µm), specific permeation rates are reported instead of membrane fluxes (Figure 6.14a). The high potential of the crosslinked PTMSP membranes can be derived from this figure, since a superior permeation rate is reported, together with a competitive selectivity (Figure 6.14b). An aqueous 10 wt.% THF mixture is enriched up to 89, 84 and 82 wt.% THF by the PERVAP 4060, PTMSP-CL*(15 wt.%) and Pervatech PDMS membranes, respectively. To be applicable in real competitive PV processes, it is clear that the PTMSP crosslinking method developed in this chapter for dense unsupported membranes should be transferred to thin film top layers.

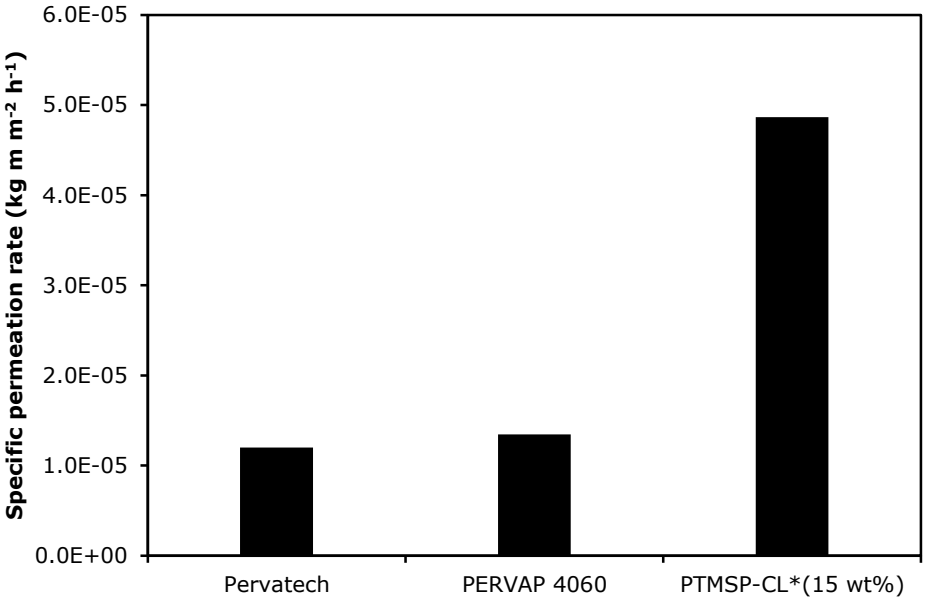

(a)

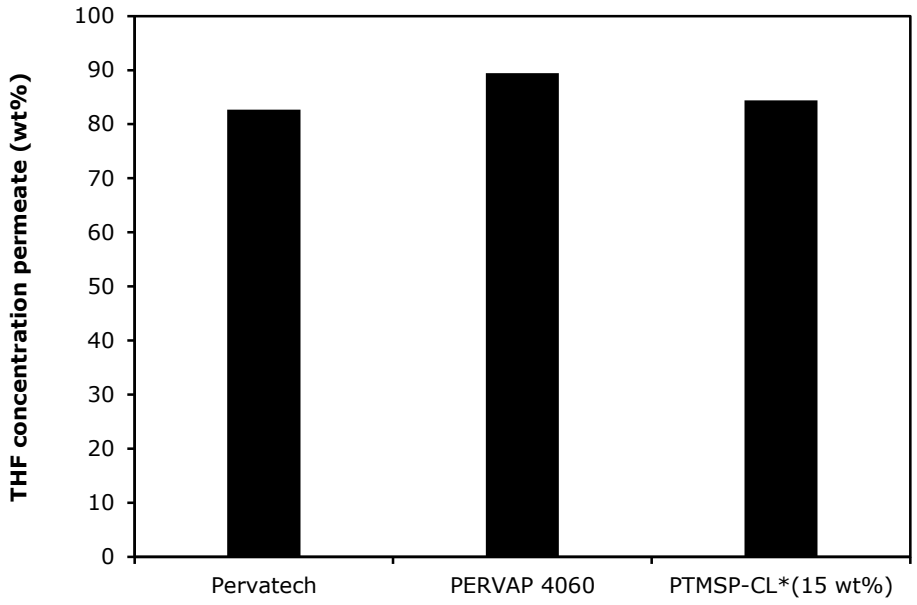

Figure 6.14: (a) Specific permeation rate and (b) THF concentration in the permeate of a thermally (180 °C, 1.5 h) crosslinked PTMSP-CL*(15 wt.%) membrane and two commercial PV membranes in the separation of a 10 wt.% THF/H_2O mixture at 50 °C.

6.9 Conclusion

3,3'-diazido-diphenylsulfone was added to a PTMSP polymer matrix and activated by photochemical or thermal treatment. The photochemical process produces insufficiently crosslinked membranes, since the crosslinker does not completely react and unwanted carboxylic acids are formed. In contrast to photochemical crosslinking, the bis(azide) decomposes completely after thermal treatment. Complete crosslinking of PTMSP is achieved by annealing the membranes at temperatures above 160 °C. At least 10 wt.% of CL and a treatment at 160 °C for 8 h or 180 °C for 1.5 h is required to make PTMSP insoluble in demanding solvents like THF, n-heptane and MTBE. The PV performance of the membranes in the separation of EtOH/H_2O mixtures is significantly affected by the crosslink conditions and CL concentrations.

Moreover the photochemically treated membranes resulted in non-selective membranes which were unsuitable for PV testing.

Thermally crosslinked PTMSP membranes demonstrate high potential in the pervaporative separation of aqueous THF mixtures, with a 4-fold increase in specific permeation rate compared to two commercially available PDMS membranes and at a competitive selectivity. The developed crosslinking method opens the application window of PTMSP membranes to PV and other liquid separation processes on more demanding feed streams.

REFERENCES

[1] K. Nagai, T. Masuda, T. Nakagawa, B. D. Freeman, I. Pinnau, Poly[1-(trimethylsilyl)-1-propyne] and related polymers: synthesis, properties and functions, *Prog. Polym. Sci.* **26** (2001) 721 – 798.

[2] C. López-Dehesa, J. A. González-Marcos, J. R. González-Valesco, Pervaporation of 50 wt.% ethanol-water mixtures with poly(1-trimethylsilyl-1-propyne) membranes at high temperatures, *J. Appl. Polym. Sci.* **103** (2007) 2843 – 2848.

[3] J. A. González-Marcos, C. López-Dehesa, J. R. González-Valesco, Effect of operation conditions in the pervaporation of ethanol-water mixtures with poly(1-trimethylsilyl-1-propyne) membranes, *J. Appl. Polym. Sci.* **94** (2004) 1395 – 1403.

[4] V. V. Volkov, A. G. Fadeev, V. S. Khotimsky, E. G. Litvinova, Y. A. Selinskaya, J. D. McMillan, S. S. Kelley, Effects of synthesis conditions on the pervaporation properties of poly[1-(trimethylsilyl)-1-propyne] useful for membrane bioreactors, *J. Appl. Polym. Sci.* **91** (2004) 2271 – 2277.

[5] A. G. Fadeev, S. S. Kelley, J. D. McMillan, Y. A. Selinskaya, V. S. Khotimsky, V. V. Volkov, Effect of yeast fermentation by-products on poly[1-(trimethylsilyl)-1-propyne] pervaporative performance, *J. Membr. Sci.* **214** (2003) 229 – 238.

[6] J. R. González-Valesco, C. López-Dehesa, J. A. González-Marcos, performance of PTMSP membranes at high temperatures, *J. Appl. Polym. Sci.* **90** (2003) 2255 – 2259.

[7] J. R. González-Valesco, J. A. González-Marcos, C. López-Dehesa, Pervaporation of ethanol-water mixtures through poly(1-trimethylsilyl-1-propyne) (PTMSP) membranes, *Desalination* **149** (2002) 64 – 65.

[8] S. Ulutan, T. Nakagawa, Separability of ethanol and water mixtures through PTMSP-silica membranes in pervaporation, *J. Membr. Sci.* **143** (1998) 275 – 284.

[9] T. Masuda, M. Takatsuka, B. Z. Tang, T. Higashimura, Pervaporation of organic liquid- water mixtures through substituted polyacetylene membranes, *J. Membr. Sci.* **49** (1990) 69 – 83.

[10] T. Nakagawa, S. Fujisaki, H. Nakano, A. Higuchi, Physical modification of poly[1-(trimethylsilyl)-1-propyne] membranes for gas separation, *J. Membr. Sci.* **94** (1994) 183 – 193.

[11] T. C. Merkel, Z. He, I. Pinnau, B. D. Freeman, P. Meakin, A. J. Hill, Effect of nanoparticles on gas sorption and transport in poly[1-(trimethylsilyl)-1-propyne], *Macromolecules* **36** (2003) 6844 – 6855.

[12] T. C. Merkel, L. G. Toy, A. L. Andrady, H. Gracz, E. O. Stejskal, Investigation of enhanced free volume in nanosilica filled poly[1-(trimethylsilyl)-1-propyne] by ^{129}Xe NMR spectroscopy, *Macromolecules* **36** (2003) 353 – 358.

[13] K. Nagai, A. Higuchi, T. Nakagawa, Gas permeation and sorption in brominated poly[1-(trimethylsilyl)-1-propyne] membrane, *J. Appl. Polym. Sci.* **54** (1994) 1353 – 1361.

[14] L. Shao, J. Samseth, M. B. Hägg, Crosslinking and stabilization of nanoparticle filled poly(1-trimethylsilyl-1-propyne) nanocomposite membranes for gas separation, *J. Appl. Polym. Sci.* **113** (2009) 3078 – 3088.

[15] S. D. Kelman, B. W. Rowe, C. W. Bielawski, S. J. Pas, A. J. Hill, D. R. Paul, B. D. Freeman, Crosslinking poly[1-(trimethylsilyl)-1-propyne] and its effect on physical stability, *J. Membr. Sci.* **320** (2008) 123 – 134.

[16] S. D. Kelman, R. D. Raharjo, C. W. Bielawski, B. D. Freeman, The influence of crosslinking and fumed silica nanoparticles on mixed gas transport properties of poly[1-(trimethylsilyl)-1-propyne], *Polymer* **49** (2008) 3029 – 3041.

[17] L. Shao, J. Samseth, M. B. Hägg, Crosslinking and stabilization of high fractional free volume polymers for gas separation, *Int. J. Greenh. Gas Control* **2** (2008) 492 – 501.

[18] S. D. Kelman, S. Matteucci, C. W. Bielawski, B. D. Freeman, Crosslinking poly(1-trimethylsilyl-1-propyne) and its effect on solvent resistance and transport properties, *Polymer* **48** (2007) 6881 – 6892.

[19] C. J. Ruud, J. Jia, G. L. Baker, Synthesis and characterization of poly[(1-trimethylsilyl-1-propyne)-co-(1-(4-azidobutyldimethylsilyl)-1-propyne)] copolymers, *Macromolecules* **33** (2000) 8184 – 8191.

[20] J. Jia, G. L. Baker, Crosslinking of poly[1-(trimethylsilyl)-1-propyne] membranes using bis(aryl azides), *J. Polym. Sci. B: Polym. Phys.* **36** (1998) 959 – 968.

[21] A. V. Volkov, V. V. Parashchuk, D. F. Stamatialis, V. S. Khotimsky, V. V. Volkov, M. Wessling, High permeable PTMSP/PAN composite membranes for solvent nanofiltration, *J. Membr. Sci.* **333** (2009) 88 – 93.

[22] A. V. Volkov, D. F. Stamatialis, V. S. Khotimsky, V. V. Volkov, M. Wessling, N. A. Plate, Poly[1-(trimethylsilyl)-1-propyne] as solvent resistance nanofiltration membrane mateiral, *J. Membr. Sci.* **281** (2006) 351 – 357.

[23] A. K. van der Vegt, L. E. Govaert, Polymeren: van keten tot kunststof, VSSD, Delft, The Netherlands, 1991.

[24] K. De Sitter, P. Winberg, J. D'Haen, C. Dotremont, R. Leysen, J. A. Martens, S. Mullens, F. H. J. Maurer, I. F. J. Vankelecom, Silica filled poly(1-trimethylsilyl-1-propyne) nanocomposite membranes: relation between the transport of gases and structural characteristics, *J. Membr. Sci.* **278** (2006) 83 – 91.

[25] R. Mens, S. Bertho, S. Chambon, J. D'Haen, L. Lutsen, J. Manca, J. Gelan, D. Vanderzande, P. Adriaensens, Solid-state NMR as a tool to describe and quantify the morphology of photoactive layers used in plastic solar cells, *J. Polym. Sci.: Part A: Polym. Chem.* **49** (2011) 1699 – 1707.

[26] R. Mens, P. Adriaensens, L. Lutsen, A. Swinnen, S. Bertho, B. Ruttens, J. D'Haen, J. Manca, T. Cleij, D. Vanderzande, J. Gelan, NMR study of the nanomorphology in thin films of polymer blends used in organic PV devices: MDMO-PPV/PCBM, *J. Polym. Sci.: Part A: Polym. Chem.* **46** (2008) 138 – 145.

[27] P. Adriaensens, R. Dams, L. Lutsen, D. Vanderzande, J. Gelan, Study of the nanomorphology of OC_1C_{10}-PPV/precursor-PPV blends by solid state NMR relaxometry, *Polymer* **45** (2004) 4499 – 4505.

[28] P. Adriaensens, R. Rego, R. Carleer, B. Ottenbourgs, J. Gelan, Solid-state NMR relaxometry study of phenolic resins, *Polym. Int.* **52** (2003) 1647 – 1652.

[29] H. Strathmann, Ion-exchange membranes, in: W.S.W. Ho, K.K. Sirkar (Eds.), Membrane handbook, Van Nostrand Reinhold, New York, United Stated of America, 1992, pp. 230 – 245.

[30] N. Yasuda, S. Yamamoto, Y. Wada, S. Yanagida, Photocrosslinking reaction of vinyl-functional polyphenylsilsesquioxane sensitized with aromatic bisazide compounds, *J. Polym. Sci. Part A: Polym. Chem.* **39** (2001) 4196 – 4205.

[31] G. Dlubek, Local Free-Volume distribution from PALS and dynamics of polymers, in: L. A. Utracki, A. M. Jamieson (Eds.), Polymer Physics: from suspensions to nanocomposites and beyond, Wiley, Hoboken, New Jersey, 2010, pp. 421 – 472.

[32] M. Schmidt, F. H. J. Maurer, Relation between free-volume quantities from PVT-EOS analysis and PALS, *Polymer* **41** (2000) 8419 – 8442.

[33] F. H. J. Maurer, M. Schmidt, Some remarks on the relation between free-volume fractions and *ortho*-positronium lifetimes in amorphous polymers, *Radiat. Phys. Chem.* **58** (2000) 509 – 512.

[34] K. Hirata, Y. Kobayashi, Y. Ujihira, Effect of halogenated compounds on positronium formation in polycarbonate and polysulfone matrices, *J. Chem. Soc. – Faraday Trans.* **93** (1997) 139 – 142.

[35] K. Hirata, Y. Kobayashi, Y. Ujihira, Diffusion coefficients of positronium in amorphous polymers, *J. Chem. Soc. – Faraday Trans.* **92** (1996) 985 – 988.

[36] S. Ray, N. R. Singha, S. K. Ray, Removal of tetrahydrofuran (THF) from water by pervaporation using homo and blend polymeric membranes, *Chem. Eng. J.* **149** (2009) 153 – 161.

[37] H. Muller, Tetrahydrofuran, in: B. Elvers, S. Hawkins, W. Russey (Eds.), Ullmann's Encyclopedia of Industrial Chemistry, vol. A26, VCH Verlagsgesellschaft mbH, Weinheim, Germany, 1995, pp. 221 – 226.

[38] P. Garg, R. P. Singh, L. K. Pandey, V. Choudhary, Pervaporative studies using polyimide-filled PDMS membrane, *J. Appl. Polym. Sci.* **115** (2010) 1967 – 1974.

[39] B. Smitha, D. Suhanya, S. Sridhar, M. Ramakrishna, Separation of organic-organic mixtures by pervaporation – a review, *J. Membr. Sci.* **241** (2004) 1 – 21.

[40] M. Shahverdi, T. Mohammadi, A. Pak, Separation of ethylene glycol-water mixtures with composite poly(vinyl alcohol)-propylene membranes, *J. Appl. Polym. Sci.* **119** (2011) 1704 – 1710.

[41] L. Li, Z. Xiao, S. Tan, L. Pu, Z. Zhang, Composite PDMS membrane with high flux for the separation of organics from water by pervaporation, *J. Membr. Sci.* **243** (2004) 177 – 187.

[42] S. Matteucci, Y. Yampolskii, B. D. Freeman, I. Pinnau, Transport of gases and vapors in glassy and rubbery polymers, in: Y. Yampolskii, I. Pinnau, B. D. Freeman (Eds.), Materials science of membranes for gas and vapor separation, John Wiley & Sons, Ltd , Chichester, England, 2006, pp. 1 – 47.

General conclusion and future work

The preconceived aim of this thesis was to develop highly permeable and selective PV membranes for the purification of aqueous feed streams.

The first part of the thesis focuses on the improvement of the flux/selectivity trade-off by decreasing the top layer thickness, adding hydrophobic silica and/or treating the membrane with $scCO_2$. The latter is seen as a valuable alternative to addition of hydrophobic silica.

Decreasing the membrane thickness is known to improve the flux of polymeric membranes. However, this work showed that it is impossible to further decrease the membrane top layer thickness without dramatically affecting the separation factor. Firstly, this would compromise the synthesis of defect free membranes. Secondly, the reduction of the thickness of the selective layer could alter the interaction of the membrane with the components of the feed mixture, thus affecting the selective transport.

Mixed matrix membranes are known to alter the PV transport properties of polymeric membranes. Adding hydrophobic silica to PTMSP increases the free volume and thus the flux of the PV membranes. However, high silica filler loadings could also compromise the formation of a defect free top layer. Therefore, 25 wt.% silica is proposed as optimal filler loading, rendering highly permeable and selective PV membranes of about 2 – 3 µm thickness. Adding silica allows to improve the flux without creating defects, thereby avoiding the need to further decrease the membrane thickness.

Thin film silica filled PTMSP membranes with superior fluxes and accompanying separation factors were prepared for the pervaporative separation of alcohol/H_2O mixtures. The synthesised membranes exhibited both a higher EtOH/H_2O flux (7×) and separation factor (5×) than the commercially available PDMS-based membranes. In the purification of BuOH/H_2O mixtures, both the flux and separation factor were 3–fold higher than the commercially available membranes. Based on the PV performance in the separation of EtOH/H_2O

mixtures, a thin film (2.4 µm) PTMSP membrane containing 25 wt.% silica was selected as optimal membrane for the selected application.
Besides the PV membrane performance reported in this thesis, the reproducibility of the polymer characteristics, the upscaling of the membrane manufacturing process, module design and long term stability should be investigated to enable the implementation of these membranes in industrial applications. Moreover, since the PV performance of the membranes is also strongly dependent on the used experimental conditions, the influence of each of the experimental parameters (temperature, pressure and feed composition) on the performance of the optimal thin film PV membrane needs to be investigated.

As an alternative to the addition of hydrophobic silica, a $scCO_2$ post-treatment was applied. By treating PTMSP membranes with $scCO_2$, their free volume cavity sizes can be increased by 74 and 48 % for the channel-like holes and larger cages, respectively. This $scCO_2$ enlarged free volume results in an increase in specific permeation rate of up to 76 % compared to untreated PTMSP membranes, which is comparable to the 72 % increase obtained by the incorporation of 50 wt.% silica. Furthermore, the $scCO_2$ enlarged free volume tends to exhibit a relaxation time of approximately 30 years. This increase in membrane performance together with the good reproducibility of the method and fair temperature stability of the treated membranes make $scCO_2$ treatment a worthy alternative to the addition of silica.
The combination of silica filler incorporation and subsequent $scCO_2$ treatment also gives rise to an increase in the free volume cavity size and thus permeability. However, the silica particles tend to resist the swelling of the polymer and therefore partially diminish the enlarging effect on the free volume cavities.
Both unfilled and silica filled PTMSP membranes demonstrated a slightly improved selectivity after the $scCO_2$ treatment, which could tentatively be explained by the altered polymer chain conformation after swelling in $scCO_2$. However, further research is needed to attribute the improved selectivity to the modification of the polymer network. Moreover, while $scCO_2$ treatment was demonstrated in this work for dense unsupported PTMSP membranes the feasibility of the method should also be investigated for thin film composite

membranes. Finally, the use of additives (co-solvents) with $scCO_2$ or different media should be investigated.

As for gas separation membranes, PTMSP-based PV membranes could be successfully crosslinked with a bis(azide), rendering solvent resistant membranes. Although both the CL concentration and crosslink conditions had a significant negative effect on the PV performance on a standard $EtOH/H_2O$ mixture, the thermally crosslinked membranes performed competitively to the commercial membranes in the pervaporative separation of THF from an aqueous mixture. A 4-fold increase in specific permeation rate was obtained for the thermally crosslinked PTMSP-CL*(15 wt.%) membranes compared to the PDMS-based commercial membranes at a similar THF/H_2O separation factor. As for the $scCO_2$ treated membranes, the crosslinking method used in this work was demonstrated for dense unsupported PTMSP membranes. Therefore further research is needed to investigate the feasibility of the crosslink method for thin film composite membranes.

At present, the development of two types of PV membranes is suggested. Firstly, an uncrosslinked membrane that could be applied in aqueous alcoholic and other less aggressive solvents streams. And secondly, a crosslinked membrane which can be used for more demanding PV feed mixtures. The first could be the supported thin film silica filled membrane synthesised in this thesis. A simple preliminary economic evaluation shows that the current material cost of the optimal supported PTMSP-silica membrane amounts to approximately 65 euro m^{-2}. For comparison, the market price of the commercially available PDMS-based membranes is 750 – 950 euro m^{-2}. Moreover the material cost is expected to further decrease upon up-scaling the production, indicating the economic potential of the developed membranes. Therefore the thin film PTMSP-silica membranes are both economic- and performance-wise an interesting alternative to the commercial PDMS-based membranes.

Scientific contributions

Publications

High flux composite PTMSP-silica nanohybrid membranes for the pervaporation of ethanol/water mixtures.
Stan Claes, Pieter Vandezande, Steven Mullens, Roger Leysen, Kristien De Sitter, Anna Andersson, Frans H. J. Maurer, Heidi Van den Rul, Roos Peeters, Marlies K. Van Bael
Journal of Membrane Science, 351 (2010), 160 – 167.

Free volume expansion of poly[1-(trimethylsilyl)-1-propyne] treated in supercritical carbon dioxide as revealed by positron annihilation lifetime spectroscopy.
Stan Claes, Pieter Vandezande, Steven Mullens, Marlies K. Van Bael, Frans H. J. Maurer
Macromolecules, 44 (2011), 2766 – 2772.

Enhanced performance in pervaporation of supercritical carbon dioxide treated poly[1-(trimethylsilyl)-1-propyne] membranes.
Stan Claes, Pieter Vandezande, Steven Mullens, Marlies K. Van Bael, Frans H. J. Maurer
Journal of Membrane Science, 382 (2011), 177 – 185.

Preparation and benchmarking of thin film supported PTMSP-silica pervaporation membranes.
Stan Claes, Pieter Vandezande, Steven Mullens, Kristien De Sitter, Roos Peeters, Marlies K. Van Bael
Journal of Membrane Science, In press: doi: 10.1016/j.memsci.2011.10.035.

Crosslinked poly[1-(trimethylsilyl)-1-propyne] membranes: Characterization and pervaporation of aqueous tetrahydrofuran mixtures.
Stan Claes, Pieter Vandezande, Steven Mullens, Peter Adriaensens, Roos Peeters, Frans H. J. Maurer, Marlies K. Van Bael
Journal of Membrane Science, In press: doi: 10.1016/j.memsci.2011.11.014.

Integrated bioprocess for long-term continuous cultivation of *Clostridium acetobutylicum* coupled to pervaporation with PDMS composite membranes.
Wouter Van Hecke, Pieter Vandezande, **Stan Claes**, Sylvia Vangeel, Herman Beckers, Heleen De Wever
Submitted to **Bioresource Technology**.

Oral presentations

Poly(1-trimethylsilyl-1-propyne) for organophilic pervaporation: how does the incorporation of silica influence the performance?
Kristien De Sitter, **Stan Claes**, Steven Mullens, Pieter Vandezande
Advanced Membrane Technology IV: Membranes for Clean and Sustainable Processes, June 7-12, 2009, Trondheim, Norway

Thin film composite PTMSP-silica nanohybrid membranes for pervaporation of alcohol/water mixtures.
Stan Claes, Pieter Vandezande, Steven Mullens, Marlies K. Van Bael
Network Young Membrains (NYM 2009), September 3-4, 2009, Mèze, France

In situ recovery of bio-alcohols with organophilic novel pervaporation membranes.
Pieter Vandezande, **Stan Claes**, Steven Mullens, Kristien De Sitter
Netherlands Process Technology Symposium (NPS-9), October 26-28, 2009, Veldhoven, The Netherlands

Optimisation of thin film silica filled organophilic pervaporation membranes.
Stan Claes, Pieter Vandezande, Steven Mullens, Marlies K. Van Bael
Innovation for Sustainable Production (i-SUP 2010), April 18-21, 2010, Bruges, Belgium

In situ recovery of bio-alcohols from aqueous solutions with novel organophilic pervaporation membranes.
Inge Genné, **Stan Claes**, Pieter Vandezande, Steven Mullens
Innovation for Sustainable Production (i-SUP 2010), April 18-21, 2010, Bruges, Belgium

Optimisation of high flux silica filled organophilic pervaporation membranes.
Stan Claes, Inge Genné, Steven Mullens, Pieter Vandezande, Marlies K. Van Bael
European Membrane Society XXVII Summer School, June 14-19, 2010, Bucharest, Romania

Optimization of thin film silica-filled PTMSP membranes for organophilic pervaporation of ethanol/water mixtures.
Pieter Vandezande, **Stan Claes**, Steven Mullens, Frans H. J. Maurer, Marlies K. Van Bael
North American Membrane Society Conference – International Conference on Inorganic Membranes (NAMS/ICIM 2010), July 17-22, 2010, Washington D.C., USA

In situ recovery of bio-alcohols from fermentation broths with organophilic pervaporation.
Pieter Vandezande, **Stan Claes**, Wouter Van Hecke, Sandra Van Roy, Heleen De Wever
CINBIOS Forum on Industrial Biotechnology, November 9, 2010, Mechelen, Belgium

In situ biobutanol recovery by organophilic pervaporation.
Wouter Van Hecke, Pieter Vandezande, **Stan Claes**, Sylvia Vangeel, Herman Beckers, Heleen De Wever
7th International Conference on Renewable Resources & Biorefineries, June 8-10, 2011, Bruges, Belgium

In situ biobutanol recovery by organophilic pervaporation.
Wouter Van Hecke, Pieter Vandezande, **Stan Claes**, Sylvia Vangeel, Herman Beckers, Heleen De Wever
International Congress on Membranes and Membrane Processes (ICOM 2011), July 24-29, 2011, Amsterdam, The Netherlands

Supercritical CO_2 treatment: an alternative way of enhancing the free volume, flux and selectivity of PTMSP membranes.
Stan Claes, Pieter Vandezande, Steven Mullens, Marlies K. Van Bael, Frans H. J. Maurer
International Conference on Pervaporation, Vapour Permeation and Membrane Distillation, September 8-11, 2011, Torun, Poland

Synthesis and optimization of high flux thin film composite PTMSP-silica membranes for pervaporation of EtOH/water mixtures.
Pieter Vandezande, **Stan Claes**, Steven Mullens, Marlies K. Van Bael
International Conference on Pervaporation, Vapour Permeation and Membrane Distillation, September 8-11, 2011, Torun, Poland

In situ biobutanol recovery by organophilic pervaporation.
Wouter Van Hecke, Pieter Vandezande, **Stan Claes**, Sylvia Vangeel, Herman Beckers, Heleen De Wever
International Conference on Pervaporation, Vapour Permeation and Membrane Distillation, September 8-11, 2011, Torun, Poland

Continuous acetone-butanol-ethanol fermentation coupled with organophilic pervaporation for solvent recovery.
Wouter Van Hecke, Pieter Vandezande, **Stan Claes**, Sylvia Vangeel, Herman Beckers, Heleen De Wever
8th European Conference of Chemical Engineering (ECCE 2011) – 1st European Congress of Applied Biotechnology (ECAB), September 25-29, 2011, Berlin, Germany

Posters

The development of modified PTMSP-membranes for pervaporation and solvent-resistant nanofiltration.
Stan Claes, Lieven Gevers, Steven Mullens, Roos Peeters, Marlies K. Van Bael
NanoMemCourse, Nanostructured materials and membranes: synthesis and characterization, November 7-16, 2007, Zaragoza, Spain.

Development of silica filled thin film composite poly(1-trimethylsilyl-1-propyne) membranes for organophilic pervaporation.
Stan Claes, Pieter Vandezande, Steven Mullens, Roger Leysen, Roos Peeters, Inge Genné, Marlies K. Van Bael
1st International Workshop NanoPorous Materials in Energy and Environment (NAPEN), October 12-15, 2008, Chania, Greece

Development of silica filled thin film composite poly(1-trimethylsilyl-1-propyne) membranes for organophilic pervaporation.
Stan Claes, Pieter Vandezande, Steven Mullens, Roger Leysen, Roos Peeters, Inge Genné, Marlies K. Van Bael
12th Aachener Membran Kolloqium (AMK), October 29-30, 2008, Aachen, Germany.

Development of silica filled thin film poly[1-(trimethylsilyl)-1-propyne] membranes for organophilic pervaporation.
Stan Claes, Pieter Vandezande, Steven Mullens, Roger Leysen, Roos Peeters, Marlies K. Van Bael
BMG/NMG membrane symposium: 12th poster day membrane technology, November 26, 2008, Antwerpen, Belgium

The development of silica-filled thin film poly[1-(trimethylsilyl)-1-propyne] membranes for organophilic pervaporation.
Stan Claes, Pieter Vandezande, Steven Mullens, Roger Leysen, Roos Peeters, Marlies K. Van Bael
PERMEA 2009, June 7-11, 2009, Prague, Czech Republic

The development of silica-filled thin film poly[1-(trimethylsilyl)-1-propyne] membranes for organophilic pervaporation.
Stan Claes, Pieter Vandezande, Steven Mullens, Roger Leysen, Roos Peeters, Marlies K. Van Bael
Euromembrane 2009, September 6-10, 2009, Montpellier, France

Synthesis of thin film composite silica-filled PTMSP membranes and their application in pervaporation for the separation of ethanol/water mixtures.
Pieter Vandezande, **Stan Claes**, Steven Mullens, Frans H. J. Maurer, Marlies K. Van Bael
NanoMemCourse on Food Applications of Nanostructured Materials, September 15-24, 2010, Cetraro (CS), Italy

Thin film composite silica-filled PTMSP membranes for pervaporation of ethanol/water mixtures.
Pieter Vandezande, **Stan Claes**, Steven Mullens, Marlies K. Van Bael
13th Aachener Membran Kolloquium (AMK), October 27-28, 2010, Aachen, Germany

Synthesis and optimization of high flux thin film composite PTMSP-silica membranes for pervaporation of EtOH/water mixtures.
Stan Claes, Pieter Vandezande, Steven Mullens, Marlies K. Van Bael
International Congress on Membranes and Membrane Processes (ICOM 2011), July 24-29, 2011, Amsterdam, The Netherlands

Supercritical CO2 treatment: An alternative way of enhancing the free volume, flux and selectivity of PTMSP membranes.
Stan Claes, Pieter Vandezande, Steven Mullens, Marlies K. Van Bael, Frans H. J. Maurer
International Congress on Membranes and Membrane Processes (ICOM 2011), July 24-29, 2011, Amsterdam, The Netherlands

List of abbreviations

ABE	acetone – butanol – ethanol
Amoco	American oil company
BuOH	butanol
CL	Crosslinker, *in casu* 3,3'-diazido-diphenylsulfone
COD	Chemical Oxygen Demand
Da	Dalton
DCM	dichloromethane
DMF	N,N-dimethylformamide
DSC	Differential Scanning Calorimetry
EA	ethylacetate
ECN	Energy research Centre of the Netherlands
EG	ethylene glycol
EOS	equation of state
EtOH	ethanol
GPC	Gel Permeation Chromatography
IPA	isopropyl alcohol
J	flux
k	mass transfer coefficient
KF	Karl-Fisher
MEK	methyl ethyl ketone
MeOH	methanol
ML	mass loss
MSE	Molecular Surface Engineering
MTBE	methyl-*tert*-butyl ether
MTR	Membrane Technology and Research
MWCO	Molecular Weight Cut-Off
M_n	number average molecular weight
M_w	weight average molecular weight
NMP	N-methyl-2-pyrrolidone
o-Ps	*ortho*-positronium
PALS	positron annihilation lifetime spectroscopy

PAN	polyacrylonitrile
Pd	polydispersity
PDMS	polydimethylsiloxane
PEN	Poly(ethylene naphthalate)
PET	polyethylene terephthalate
P_i^G	permeability
PP	polypropylene
p-Ps	*para*-positronium
PS	polystyrene
Ps	positronium
PSI	pervaporation separation index
PTMSP	poly[1-(trimethylsilyl)-1-propyne]
PV	pervaporation
PVA	polyvinylalcohol
PVDF	polyvinylidene fluoride
PVT	pressure volume temperature
R	specific permeation rate
$scCO_2$	supercritical carbon dioxide
SD	swelling degree
SEM	scanning electron microscopy
Ta	tantalum
TFC	thin film composite
T_g	glass transition temperature
TGA	thermogravimetrical analysis
THF	tetrahydrofuran
TIPS	Topchiev Institute of Petrochemical Synthesis
UF	ultrafiltration
VITO	Flemish Institute for Technological Research
VOC	volatile organic compounds
XRF	x-ray fluorescence
τ	*ortho*-positronium lifetime
α_{A/H_2O}	A/H_2O separation factor
α_{ij}	i/j selectivity